약학박사 학위논문

Pharmacokinetics and pharmacodynamics of novel nanoformulations for the proteasome inhibitor drug carfilzomib:

Expanding its therapeutic utility against solid cancers

새로운 나노제형의 개발을 통한 프로테아좀 저해제약물 carfilzomib 의 약동학 및 약력학적 특성 개선

2019 년 2 월

서울대학교 대학원

약학과 약제과학 전공

박 지 은

Pharmacokinetics and pharmacodynamics of novel nanoformulations for the proteasome inhibitor drug carfilzomib:

Expanding its therapeutic utility against solid cancers

지도교수 이 우 인

이 논문을 약학박사 학위논문으로 제출함

2018 년 12 월

서울대학교 대학원

약학과 약제과학 전공

박 지 은

박지은의 박사 학위논문을 인준함

2018 년 12 월

위 원 장 정 석 재 (인)

부 위 원 장 김 대 덕 (인)

위 원 이 우 인 (인)

위 원 신 소 영 (인)

위 원 이 재 영 (인)

ABSTRACT

Pharmacokinetics and pharmacodynamics of novel nanoformulations

for the proteasome inhibitor drug carfilzomib:

Expanding its therapeutic utility against solid cancers

박지은 (Ji Eun Park)

약학대학 약학과 약제과학 (Pharmaceutics, College of Pharmacy)

The Graduate School

Seoul National University

Over two decades ago, the proteasome was considered a risky or even untenable therapeutic target. Today proteasome inhibitors (PIs) are a mainstay in the treatment of multiple myeloma (MM) and have sales in excess of three billion US dollars annually. More importantly, the availability of PIs has greatly improved the survival and quality of life for patients with MM. Carfilzomib (CFZ) is the second-in-class PI with much improved efficacy and safety profiles over bortezomib, the first-in-class PI, for MM therapy. Despite the remarkable efficacy of CFZ against MM, the clinical trials in patients with solid cancers yielded rather disappointing results with minimal clinical benefits. The potential for improvement remains and the development and optimal use of PIs for solid cancer therapy continues to be an active area of research. Rapid degradation of CFZ *in vivo* and its poor penetration to tumor sites is considered to be major factors limiting its efficacy against solid cancers. To expand the utility of CFZ to solid cancer therapy, the aim was to overcome the pharmaceutical limitations of CFZ, and current findings may provide important insights in the development of next-generation PIs. As one of approaches to improve the pharmacokinetic profiles of CFZ, a novel polymer micelle-based formulation of CFZ was developed. In the previous report, polymer micelles (PMs) composed of biodegradable block copolymers poly(ethylene glycol)-poly(caprolactone) (PEG-PCL) were shown to improve the metabolic stability of CFZ *in vitro*. In **Chapter I**, *in vivo* anticancer efficacy and pharmacokinetic

profiles were assessed using CFZ-loaded PM composed of PEG-PCL-deoxycholic acid (CFZ-PM). Despite *in vitro* metabolic protection of CFZ, CFZ-PM displayed *in vivo* anticancer efficacy in mice bearing human lung cancer xenograft (H460) comparable to that of the clinically used cyclodextrin-based CFZ (CFZ-CD) formulation. The plasma pharmacokinetic profiles of CFZ-PM were also comparable to those of CFZ-CD. The residual tumors that persisted in xenograft mice receiving CFZ-PM displayed an incomplete proteasome inhibition. In summary, these results showed that despite its favorable *in vitro* performances, CFZ-PM formulation did not improve *in vivo* anticancer efficacy and accessibility of active CFZ to solid cancer tissues over CFZ-CD. Thus, it seems to be necessary to consider potential confounding factors in translating *in vitro* results to *in vivo* settings and to develop another type of nanoformulation with an enhanced *in vivo* stability. In **Chapter II**, it was investigated whether a nanocrystal (NC) formulation enhances *in vivo* stability and anticancer efficacy of CFZ against breast cancer. The surface of NC was coated with albumin in order to enhance the formulation stability and drug delivery to tumors via interactions with albumin-binding proteins located in and near cancer cells. The novel albumin-coated NC formulation of CFZ (CFZ-alb NC) displayed improved metabolic stability and enhanced cellular interactions, uptake, and cytotoxic effects in breast cancer cells *in vitro*. CFZ-alb NC also showed greater anticancer efficacy in a murine 4T1 orthotopic breast cancer model than CFZ-CD. Overall, these results demonstrated the potential of CFZ-alb NC as a viable formulation for breast cancer therapy. These studies may provide valuable insights into the future efforts to validate the potential of CFZ-based therapy for breast cancer and to develop effective CFZ delivery strategies that can be used to treat solid cancers.

Keywords; proteasome inhibitor carfilzomib, nanoformulation, polymer micelle, nanocrystal, albumin, solid cancers

Student Number; 2016-30511

CONTENTS

ABSTRACT.....I

CONTENTS.....III

LIST OF TABLES.....VI

LIST OF FIGURES.....VII

INTRODUCTION: The review of next-generation proteasome inhibitors for cancer research.....1

1. Proteasomes.....2

2. Proteasome inhibitor drugs in clinical use for cancer therapy.....4

2.1. Bortezomib (BTZ, PS-341, Velcade®): Rise of proteasome inhibitors as an anticancer agent.....5

2.2. Carfilzomib (CFZ, PR-171, Kyprolis®): Novel mode of proteasome inhibition.....8

2.3. Ixazomib (IXZ, MLN9708, Ninlaro®): First oral proteasome inhibitor drug.....12

3. Drug resistance (acquired or *de novo*)*: Major hurdles in improving PI therapy*.....13

4. Development strategies for next-generation proteasome inhibitors.....14

4.1. Immunoproteasome-selective inhibitors.....15

4.2. Peptide-based proteasome inhibitors.....15

4.3. Non-peptide-based proteasome inhibitors.....15

4.4. Application of drug delivery system on proteasome inhibitors.....17

CHAPTER I. Polymer micelle formulation for the proteasome inhibitor drug carfilzomib: Anticancer efficacy and pharmacokinetic studies in mice.....19

1. Introduction……20

2. Material and methods……..21

3. Results……24

3.1. Physicochemical properties of CFZ-PM……24

3.2. In vivo anticancer efficacy of CFZ-PM in H460 xenograft mice……25

3.3. Proteasome inhibition in post-treatment xenograft tumor tissues and whole blood samples collected from mice that received CFZ-PM or CFZ-CD……25

3.4. Comparison of plasma PK profiles of CFZ-PM and CFZ-CD in ICR mice ……28

4. Discussion ……29

CHAPTER II. Expanding therapeutic utility of carfilzomib for breast cancer therapy by novel albumin-coated nanocrystal formulation……32

1. Introduction……33

2. Material and methods……35

3. Result and discussion……43

3.1. Preparation and characterization of CFZ-alb NC……43

3.2. Enhanced physical and metabolic stability of CFZ-alb NC……46

3.3. Enhanced cellular uptake and cytotoxic effects of CFZ-alb NC in breast cancer cell lines....48

3.4. Enhanced in vivo anticancer efficacy of CFZ-alb NC in BALB/C bearing 4T1 breast cancer cells……51

3.5. Comparison of PK and BD profiles of CFZ-alb NC with CFZ-CD……53

3.6. SPARC-dependent uptake of CFZ-alb NC to cancer cells……57

4. Supporting information……60

4.1. Supporting experimental methods……60

4.2. Supporting table……63

4.3. Supporting figures……64

CONCLUSION……70

REFERENCES……72

국문 초록……83

APPENDIX…,……85

LIST OF TABLES

INTRODUCTION

Table 1. Proteasome inhibitors in clinical use: Their interactions with the proteasome target……..6

Table 2. Clinically used dosing regimens and pharmacokinetic (PK) parameters reported for FDA-approved proteasome inhibitor drugs……..…..9

CHAPTER I

Table 1. Physicochemical characterization of drug-free and carfilzomib (CFZ)-loaded polymeric micelles (PM)…….25

Table 2. Pharmacokinetic parameters of carfilzomib after the intravenous administration of polymeric micelle formulation containing carfilzomib (CFZ-PM) and cyclodextrin-based carfilzomib formulation (CFZ-CD) to ICR mice……...……28

CHAPTER II

Table 1. Physicochemical properties of CFZ-alb NC and *CFZ-alb NC……45

Table 2. Pharmacokinetic (PK) parameters following the intravenous administration of CFZ-alb NC or CFZ-CD at an equivalent CFZ dose of 3 mg/kg to ICR mice……..…..54

LIST OF FIGIRES

INTRODUCTION

Figure 1. The structure and function of 26S proteasome in the ubiquitin-proteasome system (UPS).....3

Figure 2. Structures of proteasome inhibitors in clinical use……..……..4

CHAPTER I

Figure 1. Effects of polymeric micelle formulation containing carfilzomib (CFZ-PM) vs cyclodextrin-based carfilzomib formulation (CFZ-CD) on tumor growth in H460 xenograft mice…….……26

Figure 2. Proteasome activities in the post-treatment tumor tissue lysates and whole blood samples collected from H460 xenograft mice that received the intravenous injections of polymeric micelle formulation containing carfilzomib (CFZ-PM) or cyclodextrin-based carfilzomib formulation (CFZ-CD)…….……27

Figure 3. Immunoblotting analyses showing that the proteasome catalytic subunit β5, a primary target of carfilzomib remains unchanged in post-treatment tumor tissue lysates collected from the xenograft mice that received different treatments……..…….……27

Figure 4. Plasma concentration-time profiles of carfilzomib after the intravenous administration of polymeric micelle formulation containing carfilzomib (CFZ-PM) or cyclodextrin-based carfilzomib formulation (CFZ-CD) to mice…….……..……..28

CHAPTER II

Figure 1. Physicochemical properties of CFZ-alb NC…….……..…..…44

Figure 2. Physical and metabolic stability profiles of CFZ-alb NC……46

Figure 3. Cellular uptake of rhodamine B-labeled CFZ-alb NC (*CFZ-alb NC) in breast cancer cell lines……49

Figure 4. Cytotoxic effects of CFZ-alb NC in breast cancer cell lines……50

Figure 5. *In vivo* anticancer efficacy of CFZ-alb NC in BALB/C mice bearing 4T1 orthotopic xenograft tumors……52

Figure 6. Comparison of pharmacokinetic and biodistribution profiles between CFZ-alb NC and CFZ-CD following the intravenous administration (a single equivalent CFZ dose of 3 mg/kg)……..……55

Figure 7. Role of SPARC in the uptake of CFZ-alb NC into cancer cells……...……58

INTRODUCTION

The review of next-generation proteasome inhibitors for cancer research

***This chapter (section 1 to 4.3.) includes the introductory sections that were published as a review article 'Next-generation proteasome inhibitors for cancer research' in Translational Research (Volume 198, pages 1-16, August 2018) and the newly added section 4.4. that is focused on novel formulations and delivery systems for proteasome inhibitor drugs, pertinent to the current thesis work.**

1. Proteasomes

The proteasome is a large multi-protease complex and is responsible for the controlled degradation of more than 80% of cellular proteins [1]. As such, the proteasome plays a key role in maintaining cellular protein homeostasis and regulates numerous biological processes, such as cell survival, DNA repair, apoptosis, signal transduction, and antigen presentation. Structurally, the 20S mammalian proteasome consists of a cylinder made of four stacked rings: two identical outer α-rings and two identical inner β-rings, each containing seven distinct but related subunits (Figure 1). In mammalian proteasomes, each β-ring harbors three catalytic β-subunits (β1, β2 and β5) which display different substrate preferences, referred to as caspase-like (C-L), trypsin-like (T-L) and chymotrypsin-like (CT-L) activities, respectively [2]. The active sites of these catalytic subunits face inward, accepting peptide substrates from the proteasome's hollow inner chamber. By controlling which proteins enter its inner chamber, the proteasome is able to degrade proteins in a highly-regulated fashion [3]. Proteins targeted for proteasome-mediated degradation are typically tagged by the covalent attachment of polyubiquitin chains ("ubiquitination") before being recognized and degraded by the proteasome complex. The concerted action of ubiquitination by a series of enzymes and proteolysis by the proteasome complex is collectively known as the ubiquitin-proteasome system (UPS). Over the past three decades, the UPS has been extensively explored as a target for drug discovery [4, 5], culminating in the remarkable clinical success of proteasome inhibitor (PI) drugs in the treatment of hematological malignancies including multiple myeloma (MM). Although a great amount of effort has been made to develop agents which target other UPS components such as ubiquitin ligases and deubiquitinases, to date only the proteasome has been successfully exploited as a therapeutic target to treat human disease.

Following the clinical success of proteasome-targeted therapies for cancer treatment, much effort has been made to address the limitations associated with existing PI drugs. Like almost all cancer therapeutics, cancer resistance, either acquired or *de novo*, is a major hurdle for PI drugs. So far, various resistance mechanisms have been reported for PI drugs in preclinical and clinical settings [6, 7] but remain unsettled. In recent years, there have been increasing attempts to design novel PIs that can overcome resistance or bypass cross-resistance to existing PI drugs [8]. In addition, PI drugs have

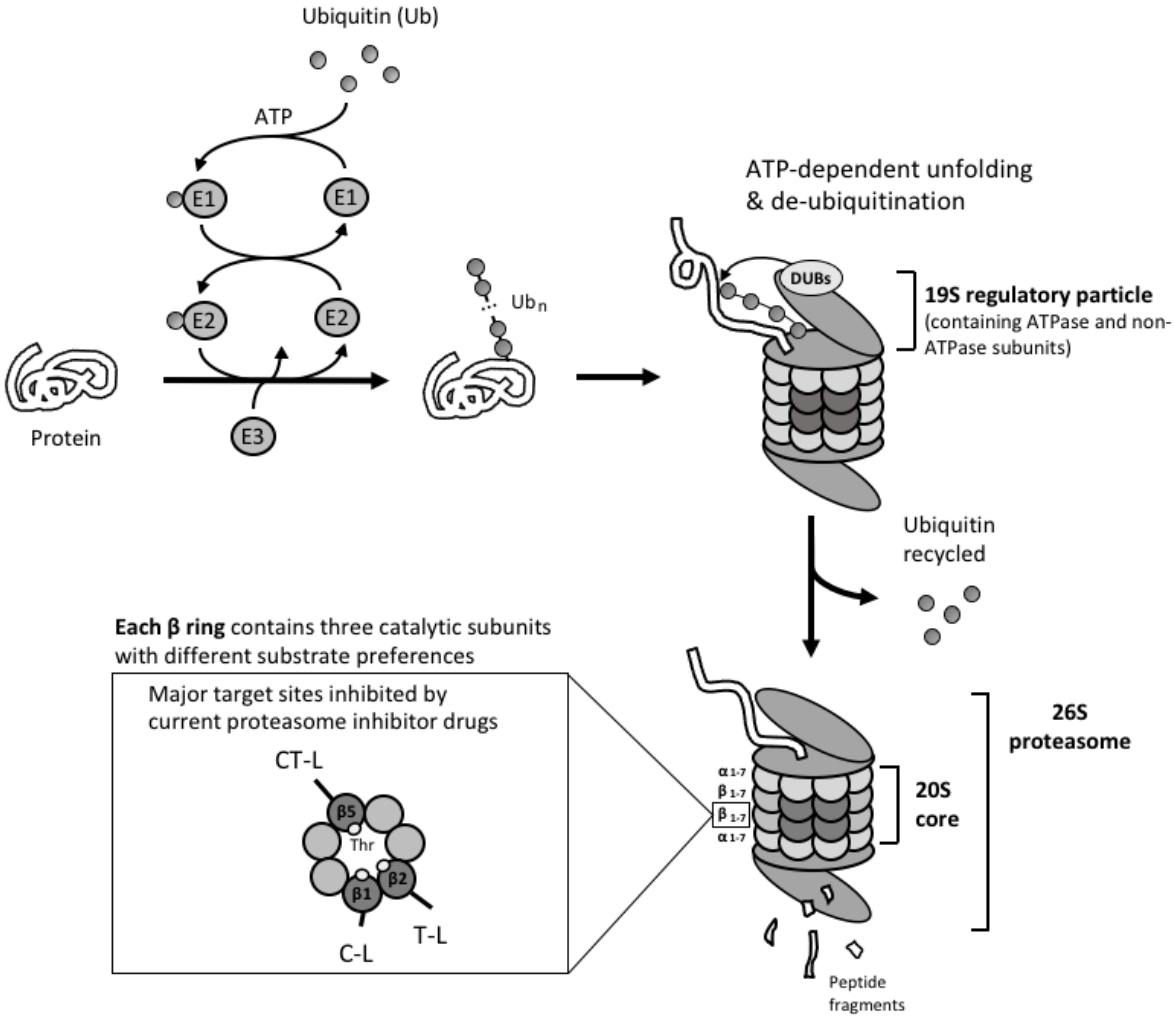

Figure 1. The structure and function of 26S proteasome in the ubiquitin-proteasome system (UPS). Proteins targeted for proteasome-mediated degradation are typically tagged by the covalent attachment of polyubiquitin chains of at least 4 ubiquitin (Ub) moieties ("ubiquitination"). This ubiquitination is carried out by the concerted action of three distinct enzymes, E1 (Ub activation), E2 (Ub conjugation), and E3 (Ub ligation). Subsequently, ubiquitinated proteins are recognized, unfolded and de-ubiquitinated by the lid of 26S proteasome (19S regulatory particles composed of ATPase and non-ATPase subunits). The proteolysis takes place at the inner chamber inside the 20S core, generating short peptide fragments of typically 2 to 24 amino acid residues. The 20S core consists of two outer α rings and two inner β rings, each containing seven distinct subunits. Each β ring harbors three catalytic β-subunits (β1, β2 and β5) which display different substrate preferences and their activities are commonly referred to as caspase-like (C-L), trypsin-like (T-L) and chymotrypsin-like (CT-L) activities, respectively. Among the three catalytic β-subunits, β5 subunit is the major target of current proteasome inhibitor drugs via their interactions with the catalytic threonine (Thr) residue.

shown exquisite efficacy in treating MM and other hematological malignancies, but not solid cancers [9]. The lack of therapeutic efficacy of PI drugs against solid cancers has often been attributed in part

to their poor pharmacokinetic (PK) profiles including their short circulation time and insufficient distribution to proteasome targets located in solid tumor tissues [10]. Moreover, our understanding remains limited on how the kinetics (both the magnitude and duration) and mode of proteasome inhibition can impact the pharmacodynamic (PD, such as efficacy and safety) profiles of PI drugs. Moving forward, an enhanced the understanding of the PKs and PDs of PI drugs and of the relationship between them is needed. Here, we provide a brief overview of three clinically used PI drugs for cancer therapy focusing on PK/PD considerations and also summarize current efforts to develop next-generation PI drugs and to improve the current PI therapy via novel drug delivery systems.

2. Proteasome inhibitor drugs in clinical use for cancer therapy

Currently, three PIs are in clinical use, bortezomib (BTZ, Velcade®, the first-in-class PI drug with US FDA approval in 2003), carfilzomib (CFZ, Kyprolis®, the second-in-class PI drug with US FDA approval in 2012) and ixazomib (IXZ, Ninlaro®, the first oral PI drug with US FDA approval in 2015) (Figure 2). Although these PI drugs have brought tremendous improvements to the treatment of MM, earlier efforts to develop therapeutics targeting the proteasome had received considerable skepticism. This skepticism was not unreasonable, given the fundamental roles and abundant presence of the proteasome in all types of cells. Despite such skepticism, early preclinical results in models of human cancer were very promising, especially for MM and other hematological malignancies [11, 12]. Propelled by exemplary academic-industrial partnerships, BTZ was successfully developed as the first-in-class PI drug with record efficiency in drug development and became a blockbuster drug in cancer therapy [13]. The clinical success of BTZ has prompted the development of CFZ and IXZ soon after. Below is a brief account of discovery and development efforts of these clinically used PI drugs.

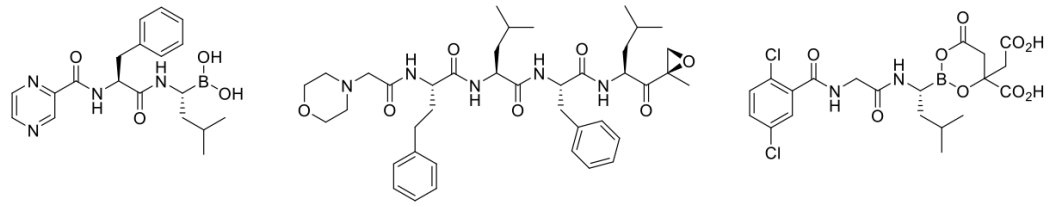

Bortezomib (PS-341, Velcade®) Carfilzomib (PR-171, Kyprolis®) Ixazomib (MLN9708, Ninlaro®)

Figure 2. Structures of proteasome inhibitors in clinical use.

2.1. Bortezomib (BTZ, PS-341, Velcade®): Rise of proteasome inhibitors as an anticancer agent

The earliest efforts to identify specific PIs began in the late 1980's [14, 15]. These early inhibitors were used to probe the function of the proteasome itself and to examine its biological role within the cell. The path towards PIs as therapeutic agents began with research into the role of the UPS in muscle wasting. Goldberg *et al.* proposed that upregulation of the UPS could explain the muscle wasting phenomenon observed in conditions such as sepsis, cancer, and burn injuries [16]. They further suggested that muscle wasting could be treated with PIs by suppressing excessive proteolysis of muscle proteins. In subsequent efforts, a highly potent PI, PS-341, now known as BTZ, was identified [17]. Pre-clinical studies soon revealed that BTZ is highly effective against various types of cancers [12, 18].

Structurally, BTZ is a dipeptide boronic acid that forms a coordinate covalent bond with the catalytic threonine residue of the proteasome's β5 and β1 subunits [19]. As a result, BTZ displays a potent inhibitory effect on the CT-L activity and to a lesser extent on the C-L activity of the 20S proteasome [20] (Table 1). In addition to its high affinity binding to the proteasome, BTZ also demonstrated nanomolar cytotoxic potencies against a variety of cancer cell lines, in particular, those derived from MM [12, 21]. These *in vitro* findings also translated into promising *in vivo* efficacies in mouse xenograft models of both hematological and non-hematological malignancies [12, 18, 22].

Prompted by strong preclinical data, several early phase clinical trials had investigated BTZ for its safety and tolerability in over 200 cancer patients by late 2001 [23]. BTZ was relatively well tolerated with adverse events consisting of low-grade fever, fatigue, thrombocytopenia, and in some patients, peripheral neuropathy. BTZ soon received US FDA fast-track approval for the treatment of relapsed and refractory MM in 2003, based on the outstanding efficacy results from the phase II open-label SUMMIT trial [24]. BTZ's clinical efficacy was further proven in combination with other therapeutic agents, leading to a full US FDA approval in 2005 as a second-line MM therapy [25] and in 2008 as a first-line therapy for patients with newly diagnosed MM [26]. BTZ also received approval for use in patients with previously-treated mantle cell lymphoma from the US FDA in 2014 and from the European Medicines Agency in 2012 [27]. Today BTZ is commonly used as a first-line agent in combination with other anti-myeloma agents, for example, immunomodulatory agents such as

Table 1. Proteasome inhibitors in clinical use: Their interactions with the proteasome target

Drug name	Pharmacophore	Binding mode	IC_{50} (nM)		
			CT-L	C-L	T-L
Bortezomib	boronic acid	reversible	2 ~ 3[1]	14.5 ~ 40[1]	1200[1]
			7.9[2]	53[2]	590[2]
Carfilzomib	epoxyketone	irreversible	5.1 ~ 5.7[3]	2,400[4]	3,600[4]
Ixazomib	boronic acid	reversible	5[5]	40[5]	> 10,000[5]
			2.8 ~ 4.1[1]	31[1]	3500[1]

[1] Calu-6 cells were treated with PIs for 1 hr. Proteasome-Glo assay [28]
[2] Purified human erythrocyte 20S proteasomes [29]
[3] Purified human 20S proteasomes [30]
[4] Purified human 20S proteasomes [31]
[5] MM.1S cells were treated with ixazomib for 3 h and harvested. Cell extracts were then analyzed for CT-L (Chymotrypsin-like), C-L (Caspase-like), and T-L (Trypsin-like) activity assay [32]

thalidomide or lenalidomide, cytotoxic drugs like melphalan, and glucocorticoids such as dexamethasone or prednisone. BTZ has also served as a proof-of-concept paving the way for two additional US FDA-approved PI drugs. While a number of clinical trials have investigated the possibility of extending the therapeutic effects of BTZ beyond MM, the results so far have been disappointing [10, 33].

BTZ is currently formulated for intravenous or subcutaneous injections (as a lyophilized powder with mannitol). An earlier study explored the possibility of oral administration [18], but this approach was not further pursued due to low bioavailability (~11% in mice [34]). BTZ was shown to have rapid and wide biodistribution profiles in preclinical studies [12]. Interestingly, a recent publication reported that the biodistribution of BTZ in various tissues is impacted by the tissue density of the proteasome which BTZ tightly and reversibly binds to [35]. This study further demonstrated that saturation of proteasome binding sites at high doses of BTZ can contribute to non-dose-proportional PK behaviors of BTZ. Similar to these preclinical findings, the results from a phase I clinical trial also indicated that BTZ displays a large volume of distribution (> 400 L) in patients with solid cancers [36]. Subsequent clinical trials reported similar findings on the PK profiles of BTZ (detailed reviews available [37], Table 2). When the metabolism of BTZ was investigated using human liver microsomes, BTZ was converted to pharmacologically inactive metabolites primarily via oxidative deboronation,

mediated by multiple cytochrome P450 enzymes (CYPs) with their relative contribution in the following order, CYP3A4, CYP2C19, CYP2D6, CYP1A2 and CYP2C9 [38, 39]. Consistent with these results, the systemic exposure of BTZ was increased and decreased with co-administration of ketoconazole (a CYP3A4 inhibitor) and rifampicin (a potent CYP3A4 inducer), respectively [40, 41]. On the other hand, co-administration of omeprazole (a CYP2C19 inhibitor) had only a minimal impact on the PK profiles of BTZ in patients with advanced solid cancers [42]. Given the importance of hepatic metabolism in the elimination of BTZ, patients with hepatic dysfunction may require dose adjustment, but no guideline or recommendation is available yet. In preclinical studies, the majority of the radio-labeled BTZ was excreted into bile duct (~66%) with the remainder excreted into the urine [12]. In a clinical study, patients with renal impairment responded to BTZ therapy similar to those with normal renal function [43].

Being the first-in-class PI drug, BTZ also became the first to be explored for the relationship between proteasomal inhibition (both the magnitude and duration) and anticancer efficacy *in vivo*. When the PK/PD profiles were compared in mouse xenograft models which responded differently to BTZ, the results indicated that both drug penetration and proteasome inhibition were much attenuated in mice carrying poorly perfused xenograft tumors which did not respond to BTZ treatment [44]. These findings were applied to the development of next-generation PI drugs as well as novel drug delivery systems. For example, in order to modulate the magnitude and duration of proteasome inhibition by BTZ, several groups investigated the potential utility of nanoformulations including the design of prodrugs or bone-targeting moieties [45-47]. However, the results from these efforts have yet to be translated into clinical application.

Despite the remarkable clinical success achieved by BTZ, several limitations have emerged. Like many other cancer therapies, a subset of patients responds to BTZ therapy while others do not. Even those who initially respond to BTZ therapy almost inevitably develop resistance over time [48]. The median duration of clinical response was typically about 12 months [49, 50]. The mechanisms underlying cancer resistance to BTZ have been actively investigated, yielding various potential strategies to overcome resistance including the development of PI drugs based on novel structural scaffolds [51]. In addition to drug resistance, BTZ therapy is associated with the severe adverse effect

of peripheral neuropathy, which was later attributed to its off-target interactions with a serine protease (HtrA2/Omi) involved in neuronal survival [52, 53]. This dose-limiting toxicity of BTZ was substantially alleviated by administering the drug via subcutaneous injection [54] or by implementing once-weekly dosing [55, 56]. These issues prompted the development of next-generation PIs with more favorable safety profiles and fewer off-target interactions.

2.2. Carfilzomib (CFZ, PR-171, Kyprolis®): Novel mode of proteasome inhibition

The second-in-class PI drug CFZ (Kyprolis®, developed by Proteolix/Onyx Pharmaceuticals and now available through Amgen) received its fast-track US FDA approval in 2012, based on its efficacy and safety results in patients with relapsed and refractory MM [57]. The development of CFZ was initiated by the identification of the proteasome as the major target of the natural product epoxomicin [58]. The design and synthesis of a biotinylated chemical probe led to the discovery that the epoxyketone group of epoxomicin covalently binds to the proteasome with an exceptional selectivity over other types of proteases. Subsequent efforts were made to build a library of epoxomicin analogs and identified a lead candidate, YU-101, based on their potent anticancer activities [59, 60]. Later, YU-101 was further modified to yield CFZ which displayed very promising preclinical results [31].

Structurally, CFZ is a tetrapeptide harboring an epoxyketone as its pharmacophore and it forms an irreversible, covalent bond with proteasome catalytic subunits, predominantly β5 (Table 1). The exquisite selectivity of CFZ toward the proteasome is achieved by the formation of two covalent bonds, one with the catalytic Thr1O$^{\gamma}$ nucleophile and a second with the adjacent Thr1N amino group. Based on high-resolution co-crystal structures between the proteasome and various epoxyketone-based inhibitors, the formation of a 1, 4-oxazepano adduct has been identified between the epoxyketone of these inhibitors and the catalytic threonine residue within the β5 active site [61, 62]. Due to this proteasome-selective mechanism of action, CFZ has afforded much improved safety profiles. Additionally, the irreversible nature of the interaction between CFZ and the proteasome allows it to achieve sustained and durable proteasome inhibition, which may contribute to its efficacy even in the presence of resistance to BTZ [63]. Of note, the irreversible modification of the proteasome target by CFZ or other peptide epoxyketones have also been exploited to develop activity-based probes (ABPs) that allow for covalent labeling of functional proteasomes or profiling of proteasome activity under

Table 2. Clinically used dosing regimens and pharmacokinetic (PK) parameters reported for FDA-approved proteasome inhibitor drugs.

Drug name	Current clinical dosing regimens	Tested dosing regimens and reported PK parameters			Ref.
		Tested dosing regimens	PK parameters	Notable characteristics	
Bortezomib (Velcade®, PS-341)	1.3 mg/m^2 IV on days 1, 4, 8 & 11 of 21-day cycles	1.45 mg/m^2, IV (C1D1)	CL, 75.3 (51.2) L/h; V_{ss}, 416 (158) L; $t_{1/2}$, 8.68 (4.16) h	Phase I trials in patients with advanced solid cancers; dose-proportionality in PK parameters not established	[36]
		1.6 – 2.0 mg/m^2, IV (C1D1)	CL, 63.7-112 (29.8-126) L/h; V_{ss}, 696-979 (357-473) L; $t_{1/2}$, 10.4-14.8 (4.96-10.4) h		
		1.3 mg/m^2, IV. single dose (C1D1) vs. multiple doses (C1D11, C1D3, & C3D11)	*single dose*: CL, 111.6 (73.6) L/h; V_{ss}, 1540 (2730) L; $t_{1/2}$, 11.5 (12.7) h *multiple doses*: CL, 18.2-28.0 (9.2-19.8) L/h; V_{ss}, 1613-2213 (1125-2730) L; $t_{1/2}$, 75.6-108.6 (34.6-64.8) h	Upon repeated dosing, CL decreased while the systemic exposure and $t_{1/2}$ increased.	[64]
		1.0 mg/m^2 IV (C1D11) vs. 2.5 mg/m^2 SC (C1D11)	*SC*: C_{max}, 20.4 (8.87) ng/mL; T_{max}, 30 (5-60) min; AUC_{last}, 155 (56.8) ng·h/mL *IV*: C_{max}, 223 (101) ng/mL; T_{max}, 2 (2-5) min; AUC_{last}, 151 (42.9) ng9·h/mL	Phase III study in patients with RRMM. Equivalent systemic exposure between SC and IV groups.	[54, 65]
Carfilzomib (Kyprolis®, PR-171)	20 mg/m^2 on days 1 & 2; if tolerated, escalated to 27 mg/m^2 (IV infusion, 2-10 min) or 56 mg/m^2 (IV infusion, 30 min) on day 8 of cycle 1; followed by tolerated dose on days 9, 15 & 16 of a 28-day cycle and next cycles (additional variations possible in subsequent cycles)	20 mg/m^2, IV (C1D1)	CL, 659 (353) L/h; V_{ss}, 108 (71) L; $t_{1/2}$, 0.66 (0.48) h	Phase I trial in patients with RRMM.	[66]
		20 mg/m^2, 2-10 min IV infusion on D1, 2, 8, 9, 15 & 16	*D1*: CL, 146 (22) L/h *D16*: CL, 136 (53) L/h	CL exceeded hepatic blood flow.	[67]
		2-10 min IV infusion. 20 mg/m^2 on D1 & 2 → 27 and 36 mg/m^2 on D8, 9, 15 & 16	*20 mg/m^2 (D1)*: CL, 263 (398) L/h; V_{ss}, 27.7 (48.6) L; $t_{1/2}$, 0.44 (0.15-2.20) h *20 mg/m^2 (D16)*: CL, 136 (52.8) L/h; V_{ss}, 7.75 (3.77) L; $t_{1/2}$, 1.10 (1.00-1.13) h *27 mg/m^2 (D16):* CL, 150 (30.9) L/h; V_{ss}, 11.1 (4.45) L; $t_{1/2}$, 0.35 (0.26-0.92) h	Phase I/II trials in patients with advanced solid cancers. Rapid systemic CL, large V_{ss} and very short elimination half-lives.	[68]
		30 min IV infusion. 20 mg/m^2 on D1 & 2 → 36, 45, 56 or 70 mg/m^2 on D8, 9, 15 & 16	*20 mg/m^2 (C1D1):* CL, 143 (56.6†) L/h; $t_{1/2}$, 0.837 h *27 mg/m^2 (C2D16):* CL, 102 L/h; $t_{1/2}$, 0.973 h *56 mg/m^2 (C2D16):* CL, 118 (27.7†) L/h; $t_{1/2}$, 0.875 h	Phase I trial in patients with RRMM. Comparable PK properties between 30 min and 2-10 min infusion.	[69]
		30-min IV infusion. 20 mg/m^2 on D1 → 45, 56, 70 or 88 mg/m^2 on D8 & 15	*20 mg/m^2 (D1):* CL, 146 (30.4†) L/h; $t_{1/2}$, 0.64 (0.193-1.29) h; AUC_{last}, 260 (27.6†) ng·h/mL *70 mg/m^2 (D15*): CL, 131 (28.6†) L/h; $t_{1/2}$, 0.95 (0.572-1.29) h; AUC_{last}, 1030 (20.5†) ng·h/mL *88 mg/m^2 (D15):* CL, 138 (34.3†) L/h; $t_{1/2}$, 0.848 (0.648-0.952) h; AUC_{last}, 1190 (29.1†) ng·h/mL	Phase I/II trials in patients with RRMM. Dose-proportional increase in AUC.	[70]

Ixazomib (Ninlaro®, MLN9708)	4 mg orally administered on days 1, 8, & 15 of 28-day cycles	0.24-3.95 mg/m^2 on D1, 8 & 15	*D1:* T_{max}, 1 (0.5-8.0) h *D15*: $t_{1/2}$, 3.6- 11.3 days	Rapid absorption and long terminal half-lives.	[71]
		0.24-2.23 mg/m^2 on D1, 4, 8 & 11 of 21-d cycles	*2 mg/m^2 (D1)*: T_{max}, 0.65 (0.25-3.97) h *2 mg/m^2 (D11):* T_{max}, 1 (0.5-23.6) h; $t_{1/2}$, 3.3- 7.4 days	2.23 mg/m^2 is equivalent to 4.0 mg	[72]
		4 mg on D1, 8 & 15	CL, 2.0 (4.9‡) L/h; BA, 60%; T_{max}, 1.5 (0.3-8) h	Results from population PK modelling.	[73]
		4 mg on D1, 8 & 15	Model parameter: CL, 1.86 L/h; BA, 58%;	Combination treatment with lenalidomide & dexamethasone in RRMM	[74]

Abbreviations: IV, intravenous; SC, subcutaneous; CL, clearance; V_{ss}, volume of distribution at steady-state; $t_{1/2}$, terminal half-life; C_{max}, maximum plasma concentration; T_{max}, time to C_{max}; AUC_{last}, area under the concentration–time curve from time 0 to the last time point; BA, bioavailability; RRMM, refractory or relapsed multiple myeloma; D, Day(s); C, cycle(s)

Values reported as means (standard deviation, % coefficient of variation (†) or % standard error (‡)) except for T_{max} and $t_{1/2}$, which are expressed as median (range).

diseased conditions or in response to cellular stimuli [75]. Such ABPs may be potentially used as diagnostics to detect disease or monitor response to therapy [76-78].

In 2005, phase I clinical trials with CFZ began and successfully identified the phase II recommended doses and dosing schedules that were further investigated in subsequent clinical trials [66, 79]. From early on, it was observed that a subset of patients who did not respond to BTZ-based therapy could still benefit from CFZ. Recently completed phase III clinical trials provided further evidence that CFZ-containing regimens can be effective against relapsed MM, including those patients who relapsed after receiving prior therapies including BTZ [80, 81]. In particular, the phase III ENDEAVOR trial was a head-to-head comparison of CFZ and BTZ in patients with relapsed or refractory MM [81]. In this trial, CFZ was shown to be superior to BTZ in extending overall survival of patients in the relapsed setting. In addition to its superior efficacy, the CFZ-containing regimen showed much improved safety profiles, especially in terms of peripheral neurotoxicity. While cardiovascular events were observed in CFZ-treated patients, no evidence was found of cumulative cardiac injury or ventricular dysfunction in the CFZ group. With these outstanding outcomes, CFZ is now part of a standard of care for relapsed or refractory MM and will likely evolve as part of frontline therapy in the near future.

When the PK profiles of CFZ were initially assessed in rats, the results indicated very rapid clearance, short circulation time (plasma half-lives less than 1 h) and wide biodistribution [31, 82]. At all dose levels tested, the clearance of CFZ exceeded rat hepatic flow. In line with these *in vivo* results, CFZ was found to be rapidly metabolized in rat hepatocytes, but also in rat blood and in homogenates prepared from other tissues [82]. The major metabolites of CFZ were peptide fragments and the diol of CFZ, formed via peptidases and epoxide hydrolases, respectively. Similar to these preclinical results, early phase clinical trials also indicated that CFZ displays very short half-lives (12 ~ 40 min), rapid systemic clearance (116 ~ 263 L/h) and large volumes of distribution at steady state (9 ~ 28 L) at all dose levels tested (11, 15, 20, and 27 mg/m^2) [66, 68] (Table 2). Plasma clearance of CFZ in humans also exceeded hepatic blood flow, further indicating a considerable contribution of extrahepatic mechanism to the overall elimination of CFZ [67]. Consistent with *in vitro* results showing only minor roles of CYP-mediated metabolism or renal excretion in the overall disposition of CFZ, the PK profiles

of CFZ were not impacted by co-administration with CYP inhibitors or inducers [67] or by renal impairment [83, 84].

Along with its structural and mechanistic differences from BTZ, CFZ offers a treatment option with greatly reduced risk of peripheral neuropathy. CFZ treatment is associated with different types of adverse effects including cardiovascular complications, hypertension, and heart failure, but overall these adverse effects are reversible and manageable with careful monitoring [85]. CFZ shares several adverse events with BTZ such as anemia, fatigue, and diarrhea. One potential downside of CFZ is its poor aqueous solubility. Despite the incorporation of a *N*-terminal morpholine ring to improve solubility, CFZ remains practically insoluble and the current formulation requires the use of a 50-fold excess of a β-cyclodextrin derivative to prepare an injectable solution. As with BTZ, CFZ is not suitable for oral administration and is susceptible to drug resistance in clinical use. These problems have prompted the development of additional next-generation PIs.

2.3. Ixazomib (IXZ, MLN9708, Ninlaro®): First oral proteasome inhibitor drug

With both BTZ and CFZ being administered only via intravenous or subcutaneous injection, there has been an unmet need for orally available PI drugs. In 2015, IXZ (Ninlaro®, Takeda Pharmaceuticals Limited) received its US FDA approval as the first orally bioavailable PI drug. Based on the promising efficacy observed in preclinical studies, IXZ rapidly advanced to clinical trials [28, 32]. IXZ, orally administered once a week (4 mg on days 1, 8, and 15 of 28-day cycles) in combination with lenalidomide plus dexamethasome, has now been approved in 40 countries including USA and the EU for the treatment of MM patients who have received one prior therapy, based on the superior results in clinical trials [72, 86]. IXZ also displayed a good safety profile with no significant inhibitory effect on HtrA2/Omi, a non-proteasomal target of BTZ previously linked to peripheral neuropathy [32, 86, 87]. IXZ is currently being investigated in several clinical trials as a single agent and in combination with other agents against multiple types of cancer (https://clinicaltrials.gov).

Structurally, IXZ is a capped dipeptide boronic acid and preferentially and reversibly inhibits the CT-L activity of the proteasome as well as the C-L and T-L activities at high concentrations with potencies similar to BTZ [32]. However, the dissociation half-life of IXZ was significantly shorter than

that of BTZ (18 *vs.* 110 min), which may account for the faster recovery of proteasome activity (IXZ *vs.* BTZ, 69 *vs.* 20%) in cell-based assays and its larger volume of distribution in mice (IXZ *vs.* BTZ, 20.2 *vs.* 4.3 L/kg) [28]. Although not examined, some of these differences may have contributed to the improved safety profiles of IXZ over BTZ, despite sharing the boronic acid residue as their pharmacophore.

For oral administration, IXZ is formulated as a citrate ester prodrug (MLN9708) which is rapidly hydrolyzed to the pharmacologically active form (MLN2238) under physiological conditions [28]. In phase I clinical trials, orally administered IXZ was rapidly absorbed (mean T_{max}, 0.5 ~ 1 h) and had a long terminal half-life (mean $T_{1/2}$, 3.3 ~ 7.4 days in twice-weekly dosing; 3.3 ~ 11.3 days in weekly dosing) [71, 72] (Table 2). When tested using recombinant CYP enzymes *in vitro*, IXZ was metabolized by multiple CYPs at concentrations exceeding those observed clinically and deemed unlikely to incur potential drug-drug interactions [88]. Yet, co-administration with rifampin, a strong CYP3A inducer, led to substantial changes in the PK profiles of IXZ (C_{max} and AUC decreased by 54% and 74%, respectively) [88]. Overall, the PK profiles of IXZ showed dose-proportional behaviors. Using the compiled clinical data from 755 patients treated with IXZ, Gupta *et al.* conducted population PK analyses and reported the following average estimates for PK parameters: absolute bioavailability (58%), volume of distribution (543 L), terminal phase half-life (9.5 days), and systemic clearance (1.86 L/h) [74]. Systemic exposure to IXZ was affected by moderate or severe hepatic impairment [89], but not by renal impairment [74]. While IXZ has the potential to greatly improve the quality of life for patients with MM, its therapeutic advantages over BTZ or CFZ have yet to be investigated in randomized clinical trials.

3. Drug resistance (acquired or *de novo*): Major hurdles in improving PI therapy

Common in many cancer therapies, the issues of drug resistance also pose major hurdles for PI therapies. MM patients who initially respond to PI therapy almost inevitably develop resistance over time (acquired resistance). Once patients relapse with MM refractory to PI-based therapy, there are currently few effective treatment options left. While a subset of MM patients responds well to PI

therapy, others do not (*de novo* resistance). Several potential mechanisms for resistance to PI therapy have been proposed using cell-based model systems. Yet, those mechanisms await further validation in patients with MM and also in patients with solid cancers. For the lack of clinical benefits of PI therapy for solid cancers, it has been postulated that active PI drugs may have insufficient access to the proteasome target located in solid cancer cells (related to the PK issues). This possibility was supported in part by the preclinical results showing effective tumor growth suppression following direct intratumoral injection of PI drugs [12, 90]. In addition, intravenous dosing of BTZ was effective in mice harboring highly perfused xenograft tumors, but not poorly perfused ones [44]. Alternatively, it was also proposed that solid cancer cells may be inherently less sensitive to PI therapy than MM cells known for their elevated levels of proteotoxic stress or ER stress [91, 92]. To tease out why patients with solid cancers do not benefit from PI therapy, it would be necessary to develop PI drugs that can afford sufficient access to the proteasomes in solid cancer cells and/or to develop targeted drug delivery systems.

Current understanding of resistance mechanisms for PI drugs, although not complete, has provided important platforms to screen for PI drugs that can potentially overcome resistance to existing PI drugs. Several reports observed the presence of mutations in the *PSMB5* gene encoding the β5 catalytic subunit from cancer cell line models resistant to BTZ and low levels of Xbp1, a key regulator of one arm of the unfolded protein response (UPR), in primary cells isolated from MM patients following BTZ therapy [93-96]. For cancer cell line models resistant to CFZ and epoxomicin, the upregulation of P-glycoprotein was reported to be causally linked to drug resistance [97, 98]. This information provided important guidance during the development of another epoxyketone-based PI, OPZ [30, 93]. The screening and optimization processes for OPZ and related compounds included the testing in cell lines expressing P-glycoprotein.

4. Development strategies for next-generation proteasome inhibitors

As discussed above, the discovery of next-generation PIs with improved PK/PD profiles could improve clinical outcomes for MM patients (especially those with resistance to existing PI therapy) and extend

therapeutic benefits to patients with solid cancers where existing PI drugs have proved largely ineffective. To achieve this goal, the following development strategies have been actively explored. Given that comprehensive reviews are already available on the first two strategies, we focused on the recent efforts to develop non-peptide-based PIs and drug delivery system.

4.1. Immunoproteasome-selective inhibitors

The immunoproteasome (iP) is a variant of the constitutive proteasome in which the constitutive catalytic subunits β1, β2 and β5 are replaced by their respective inducible counterparts β1i, β2i and β5i, under inflammatory conditions and certain pathological states including cancer. By targeting the iP, it may achieve more selective inhibition of the proteasomal activity in cancer cells, thereby widening the therapeutic window. Although iP inhibitors have been studied in the preclinical setting, to date none have entered clinical trials [99]. As the iP is strongly implicated in inflammatory pathways, iP-selective inhibitors are currently being investigated as potential anti-inflammatory agents. Detailed reviews on iP inhibitors are already available [100-102].

4.2. Peptide-based proteasome inhibitors

The vast majority of existing PIs utilize a peptide backbone and an active warhead that interacts with the catalytic Thr residues of β-subunits with different mechanisms of action (e.g., aldehydes, vinyl sulfones or esters, boronates, epoxyketones, β-lactones). With the successful clinical development of the peptide boronates (BTZ and IXZ) and epoxyketone (CFZ), intense efforts have been underway to further refine the structure-activity relationship (SAR) and to identify compounds with optimal pharmacological profiles among peptide-based proteasome inhibitors. For further information on peptide-based PIs, comprehensive reviews are already available [103, 104].

4.3. Non-peptide-based proteasome inhibitors

From one of the earliest efforts to identify structurally-novel PIs via high-throughput screening, PI-083 was identified as a non-peptide PI [105]. Utilizing a 2-chloro-1,4-naphthoquinone scaffold, PI-083 preferentially inhibited the CT-L activity of the 20S proteasome (IC_{50}: 1.0 μM) and inhibited T-L and C-L activities at slightly higher concentrations (IC_{50}: 4.5 μM for both). When tested against a panel of 10 solid cancer cell lines, PI-083 exerted cytotoxic effects with IC_{50} values ranging from 1.7 to 11 μM.

PI-083 was also effective in suppressing *in vivo* tumor growth in mouse xenograft models at a dose of 1 mg/kg twice weekly. Based on docking results and the compound's SAR, it is postulated that PI-083 may act as a covalent PI with the chlorinated 2-carbon undergoing nucleophilic attack by the proteasome's catalytic threonine residue [106]. Recovery of proteasome activity following incubation with PI-083 was slow, with only partial recovery of activity after 18 h. Attempts to improve PI-083's inhibitory potency were generally unsuccessful and the SAR was highly sensitive to modification.

A subsequent report from the same group identified PI-1840, a structurally-unrelated non-peptide compound which potently and selectively inhibited the CT-L activity of the 20S constitutive proteasome (IC_{50}: 27 nM) [107]. PI-1840 showed no appreciable inhibition of 20S proteasome T-L or C-L activity and had an IC_{50} value of greater than 1 μM against the CT-L activity of the iP. Analysis via mass spectrometry and dialysis confirmed that PI-1840 acts as a fully-reversible inhibitor. A panel of solid cancer cell lines displayed varying degrees of sensitivity to PI-1840 (IC_{50}: 2.2 ~ 45.2 μM), and the cytotoxic potency appeared to correlate with the degree of proteasome inhibition achieved by PI-1840. When tested in mice bearing MDA-MB-231 human breast cancer xenografts, PI-1840 (150 mg/kg daily via intraperitoneal injection) effectively suppressed tumor growth, in contrast to no appreciable suppression in the control groups that received either BTZ (1 mg/kg twice weekly via intraperitoneal injection) or the vehicle only. No observable toxicity was noted in animals receiving high doses of PI-1840. The safety profiles observed with PI-1840 may be related to its high degree of selectivity for the constitutive β5 subunit relative to the iP subunit β5i and its lack of inhibition of T-L or C-L activities. Given that the existing PI drugs tend to target both β5 and β5i subunits with relatively low selectivity, it awaits further investigations to determine whether the selective inhibition of β5 by PI-1840 may be advantageous or disadvantageous in terms of anticancer efficacy. The PK profiles of PI-1840 have not yet been published.

Another non-peptide PI dubbed G4-1, based on a tri-substituted pyrazole scaffold, was reported by our own research group [108]. Identified via the combination of structure-based virtual screening and *in vitro* kinetic assays, G4-1 inhibits both β5 and β5i catalytic activities with IC_{50} values of 1.6 and 2.4 μM, respectively. β1 and β1i subunits (C-L activity) were also inhibited at low micromolar concentrations, with minimal inhibition of T-L activity. G4-1 exerted cytotoxic effects against a variety

of solid cancer and MM cell lines, regardless of acquired resistance to BTZ and CFZ. Further structural analyses indicated that G4-1 is a reversible, non-covalent inhibitor. As expected from its non-peptide-based structure, G4-1 displayed much improved *in vitro* metabolic stability over BTZ or CFZ when tested using mouse and human liver microsomes. In a mouse xenograft model of human prostate cancer, G4-1 (5 mg/kg, twice-weekly) was effective in suppressing tumor growth with no overt signs of toxicity. Additional PK or PD profiles of G4-1 have not yet been published.

In addition to those described above, there have been several other recent reports of efforts to develop non-peptide PIs but further investigations are still needed to validate their mode of interaction with the proteasome, their extent of interaction with non-proteasomal targets and their *in vivo* efficacy. While there is also a body of research covering peptide-based non-covalent PIs, such as those described by Blackburn *et al*. [109, 110], it is expected that these compounds will be susceptible to the same rapid, often extrahepatic, clearance as existing peptide-based PIs. Peptide-based PIs may also be less likely to penetrate poorly-perfused tumors due to either their physiochemical properties or their interactions with efflux transporters [111]. Moving forward, significant research efforts will be required to identify non-peptide PIs which display optimal PK/PD profiles and suitability for clinical use.

4.4. Application of drug delivery system on proteasome inhibitors

In improving the PK profiles of the existing PIs, the nanoparticle-based drug delivery systems (NDDS) may prove useful by prolonging the circulation time and changing the biodistribution profile, thereby enhancing the delivery of PIs to solid cancer tissues and reducing the toxicity in normal tissues. In cancer therapy, there exist several examples of successfully applying NDDS: doxorubicin (Doxil™, Janssen, liposomal formulation), irinotecan (Onivyde™, Merrimack Pharmaceuticals, liposomal formulation), paclitaxel (Genexol-PM™, Samyang Biopharmaceuticals, polymeric micelle formulation; Abraxane™, Celgene, albumin bound nanoparticle) [112].

For the first-in-class PI drug BTZ, there have been a number of attempts to apply novel NDDS and extend the therapeutic utility of BTZ. Polymeric micelle-based formulation of BTZ showed an improved tolerability and efficacy against triple negative breast cancer [46]. In another report, BTZ-containing polymeric micelles were prepared using poly(D,L-lactic-co-glycolic acid) (PLGA) and polyethylene glycol with a bone-targeting ligand alendronate. The results showed an extended

circulation time as well as enhanced survival and decreased tumor burden in the MM mouse model [47]. A similar approach was attempted using PLGA-based nanoparticles conjugated with transferrin as a tumor-targeting ligand and the results showed an enhanced delivery of BTZ to pancreatic cancer cells [113]. Taking advantage of slightly acidic tumor microenvironment compared to normal tissues, pH-sensitive polymer carriers were used to design novel delivery options for BTZ (where the drug release is triggered under acidic condition) [114-116]. The liposomal nanoparticles were also explored and the encapsulation of a BTZ prodrug in the liposomal nanoparticles demonstrated tumor growth suppression with reduced toxicity compared to BTZ in the mice carrying MM xenografts [45]. Another report used a liposomal BTZ formulation conjugated with NGR peptides and showed improvements in terms of toxicity and survival in the orthotopic mouse model of neuroblastoma [117]. Other types of NDDS applied to BTZ include hollow mesoporous silica nanospheres [118] and solid-lipid nanoparticles [119]. However, the NDDS for BTZ reported so far await further validation and careful examination for their clinical translation.

For CFZ, the NDDS may offer potential benefits of extending the therapeutic utility beyond MM, but also of developing an alternative, cyclodextrin-free formulation (the current CFZ formulation contains 16-fold molar excess of sulfobutyl ether β-cyclodextrin (Captisol®) to CFZ). During the past several years, our laboratory and others have made efforts to develop the NDDS to CFZ. Tethered polymer nanoassemblies were prepared for CFZ, but the results showed a modest improvement in the cytotoxic effects against human lung cancer cells [120]. Another study examined a dual drug-loaded liposomal formulation to deliver CFZ and doxorubicin [121]. The dual drug-loaded liposomes were more effective in suppressing tumor growth in a mouse model of MM xenograft than co-administration of single drug-loaded liposomes [121]. A more recent report developed CFZ nanoparticles coated with neutrophil membranes [122]. The results showed quite promising suppression of early metastasis, but the limitations included the multi-step preparatory processes that may not be cost-effective and amenable for scale-up [122]. Thus, there is a clear need for novel, cost-effective NDDS which can expand the therapeutic utility of CFZ.

CHAPTER I.

Polymer Micelle Formulation for the Proteasome Inhibitor Drug Carfilzomib:

Anticancer efficacy and pharmacokinetic studies in mice

*** The work from Chapter I was published in PLoS ONE 12(3):e0173247 on March, 2017.**

1. Introduction

The proteasome, a multisubunit protease complex, is an anticancer target validated by remarkable clinical successes of proteasome inhibitor drugs. Since its fast-track FDA approval in 2003, the first-in-class proteasome inhibitor drug bortezomib (Velcade^{TM}) has become a mainstay of multiple myeloma (MM) therapy, despite drawbacks including severe neurotoxicity caused by off-target interactions with neuronal proteases [123]. In 2012, the second-in-class proteasome inhibitor drug carfilzomib (Kyprolis^{TM}, CFZ) received an accelerated FDA approval for patients who have relapsed/refractory MM after receiving at least two prior therapies including bortezomib. CFZ in combination with other immunomodulatory agents such as lenalidomide and dexamethasone demonstrated good response profiles and several clinical trials are ongoing for its use as frontline therapies [124-126]. Compared to BTZ, CFZ is well tolerated with acceptable toxicity profiles and few instances of dose-limiting neurotoxicity, likely due to the selective interactions of its epoxyketone pharmacophore with the proteasome target [127].

Despite the notable benefits with CFZ, there remains much room for improvement. CFZ is practically insoluble in aqueous media and the current formulation contains 60 mg of lyophilized CFZ powder with 3,000 mg of sulfobutylether-β-cyclodextrin (Captisol®). Additionally, CFZ is rapidly inactivated *in vivo*; the majority (> 95%) of CFZ is eliminated from systemic circulation within 30 min following intravenous injection due to its peptide backbone cleavage and epoxide hydrolysis [128]. The poor *in vivo* stability and short half-lives of CFZ have been considered major culprits for its lack of efficacy in patients with solid cancers by limiting the access of the active drug to proteasome targets within solid tumor tissues [129, 130]. Thus, novel drug delivery strategies that can improve solubility, *in vivo* stability of CFZ and the accessibility of active drug to targeted tumor sites may potentially extend its therapeutic benefits in patients with solid cancers.

Polymeric micelles (PMs) composed of amphiphilic block copolymers have gained much attention for their application in drug delivery, especially due to their biocompatibility and utility in improving drug solubility and stability in the biological system and achieving passive tumor targeting, commonly referred to as enhanced permeability and retention (EPR) effect [131, 132]. In the case of

CFZ, it was previously reported that several CFZ-loaded PM formulations composed of biodegradable block copolymers poly(ethylene glycol)-poly(caprolactone) (PEG-PCL) displayed improved metabolic stability and anticancer efficacy profiles *in vitro* [133]. Given these results, the logical next step was to examine whether these *in vitro* improvements achieved by CFZ-loaded PM formulations would be recapitulated *in vivo*.

In this report, we examined the anticancer efficacy and plasma pharmacokinetic (PK) profiles of the CFZ-loaded PM formulation (CFZ-PM, composed of PEG-PCL 5-5.5 KDa with deoxycholic acid added) *in vivo*. Despite our previous results showing *in vitro* metabolic protection with CFZ-PM [133], its *in vivo* performances in terms of anticancer efficacy, plasma PK profiles and proteasome inhibition in residual tumor tissues did not show notable improvements over the cyclodextrin (CD)-based CFZ formulation (CFZ-CD). Careful consideration of these results and confounding factors may provide valuable insights into the future efforts to validate the potential of CFZ-based therapy for solid cancer and to develop effective CFZ delivery strategies that can be used to treat solid cancers.

2. Materials and Methods

2.1. Cell lines and reagents

A human lung adenocarcinoma cell line H460 was obtained from Korean Cell Line Bank (KCLB, Seoul, Korea) and maintained according to the KCLB-recommended culture conditions. CFZ was purchased from LC laboratories (Woburn, VA, USA). Block polymer PEG-PCL with molecular weight 5-5.5 kDa was purchased from Polymer Source (Montreal, QC, Canada). 2-hydroxypropyl-β-cyclodextrin, EDTA, chloropropamide, deoxycholic acid (DCA) and formic acid were purchased from Sigma-Aldrich (St. Louis, MO, USA). The fluorogenic substrate, *N*-Succinyl-Leu-Leu-Val-Tyr-7-amino-4-methylcoumarin (Suc-LLVY-AMC), was purchased from Bachem (Torrance, CA, USA). All solvents for HPLC were obtained from Burdick & Jackson Company (Morristown, NJ, USA).

2.2. Preparation and characterization of CFZ-PM formulation

The CFZ-PM formulation was prepared using PEG-PCL 5-5.5 KDa with DCA through the thin film method as previously described [133]. The particle size distribution and zeta potential values were

measured for CFZ-PM or empty PM (prepared without CFZ) using an electrophoretic light scattering method (DLS, Zetasizer Nano ZS, Malvern, UK). Critical micelle concentrations (CMCs) of CFZ-PM and empty PM were determined using the pyrene I_3/ I_1 method [134]. Briefly, pyrene solution in acetone (2 μM) was added to PM solution in water at varying PM concentrations and left to equilibrate at 37 °C overnight. The fluorescence signal intensities of pyrene in the solution were measured at the first (I_1 at 372 nm) and third (I_3 at 383 nm) peaks following excitation at 334 nm using a SpectraMax M5 microplate reader in order to determine the encapsulation of pyrene corresponding to micelle formation (SpectraMax M5, Molecular Devices, CA, USA).

2.3. Anticancer efficacy of CFZ-PM in NOD/SCID mice harboring human lung cancer (H460) xenografts

Animal procedure was performed using the protocol approved by the Seoul National University Institutional Animal Care and Use Committee (approval No. SNU-151127-3). NOD/SCID mice were obtained from Japan SLC, Inc. (Hamamatsu, Japan). Briefly, H460 cells (3×10^6 cells/spot) were subcutaneously injected into the flank of mice (NOD/SCID, 6-7 weeks old). After the tumor volume reached 50 – 150 mm^3, the mice were randomized into 6 different treatment groups (n=4-5) as follows; CFZ-PM at the dose of 3 or 6 mg/kg, CFZ-CD (complexed with 20% (v/w) 2-hydroxypropyl-β-cyclodextrin in 10 mM citrate buffer, pH 3) at the dose of 3 or 6 mg/kg, vehicle (10 mM citrate buffer, pH 3), and empty PM. Drug was dosed via tail vein injection (two consecutive days/week for 3 weeks). Tumor growth was assessed by measuring the short and long diameters of the tumor with a caliper and using the following formula: tumor volume (mm^3) = 0.5 × (short diameter, mm)^2 × (long diameter, mm). Mice were sacrificed on day 18 and tumor tissues and whole blood samples were collected for proteasome activity assay and immunoblotting analysis.

2.4. Assessment of proteasome target inhibition/modification in excised xenograft tumor tissues from mice that received drug treatment

In order to assess whether CFZ-PM improved the accessibility of the active drug to tumor tissues, the proteasome target inhibition was measured in excised tumor tissues and whole blood samples from mice that received drug treatment. Tumor tissues and whole blood samples were collected 48 h after

the injection of the respective treatments on the last day of the *in vivo* efficacy experiment. The excised tumor tissues were homogenized with passive lysis buffer (Promega, WI, USA) using a hand-held tissue grinder on ice. The homogenates were centrifuged at 3,000g for 20 min at 4°C and the resulting supernatant was used for proteasome activity assay and immunoblotting analysis. The proteasome activity was determined by monitoring the cleavage rate of fluorescent 7-amino-4-methylcoumarine (AMC) from Suc-LLVY-AMC. Briefly, lysates of excised tumor tissues (10 μg of total protein) or whole blood (1 μL) were incubated with Suc-LLVY-AMC (100 μM dissolved in 20 mM Tris-Cl buffer (pH 8.0) containing 500 μM EDTA). Fluorescence signals of liberated AMC were monitored for a period of 60 min using excitation and emission wavelengths of 360 and 460 nm on a SpectraMax M5 microplate reader (Molecular Devices, CA, USA).

Since CFZ irreversibly inhibits the proteasome via covalent modification, the presence of covalently modified catalytic subunit β5 can also be used to assess the extent of the proteasome inhibition. Briefly, tumor tissue lysates (10 μg of total protein) were resolved using 12.5% SDS-PAGE and transferred onto a PVDF membrane (Bio-Rad Laboratories). Membranes were blocked in 5% milk in Tris-buffered saline containing 0.05% Tween-20 (TBST) and probed with the following antibodies; for β5 (dilution 1:1000, Abcam) and β-actin (dilution 1:1000, Cell Signaling). Membranes were washed with TBST and probed with the corresponding secondary antibodies conjugated with horseradish peroxidase. Bound antibodies were visualized using an enhanced chemiluminescence substrate (Thermo Fisher Scientific).

2.5. Assessment of plasma PK profiles of CFZ-PM in mice

PK studies in mice were carried out following the protocol approved by the Seoul National University Institutional Animal Care and Use Committee (approval No. SNU-160512-5). The CFZ-PM and CFZ-CD were injected via tail vein into ICR mice obtained from Samtako (Gyeonggido, Korea) at doses of 3 or 6 mg/kg (n=4-5 per group), respectively. At the pre-determined time points (2, 5, 20, 60, 120, 360, 600 and 1,440 min), whole blood samples were collected from the retro-orbital plexus of the mice using microhematocrit tubes. To minimize blood loss due to sampling, approximately 50 μL of whole blood was drawn at each sampling time and individual mice did not have more than 6 times of blood sampling.

Plasma samples (20 μL) separated from whole blood were quenched with acetonitrile (60 μL) containing chlorpropamide (2 μg/mL, an internal standard) and mixed by vortexing for 15 min. After the mixture was centrifuged at 9,000 g for 15 min at 4°C, the concentration of CFZ in the supernatant was measured using an HPLC interfaced with mass spectrometry (Shimadzu LCMS-8050). Briefly, 10 μL of the resulting supernatant was injected and separation of CFZ and chlorpropamide was achieved using a Phenomenex C18 column and the mobile phase composed of H_2O:acetonitrile (40:60, v/v) containing 0.1% formic acid (flow rate = 0.35 mL/min). CFZ and chlorpropamide were detected in the ESI mode (positive ion mode, CFZ: 720.20→100.15 *m/z*; chlopropamide: 277.05→175.10 *m/z*). The detailed report on analytical conditions and assay validation parameters including accuracy and precision is currently in preparation. PK parameters were calculated using non-compartmental methods (WinNonLin version 5.0.1, Pharsight).

2.6. Statistical analyses

The results were expressed as the mean with standard deviation. Statistical significance between groups was determined using ANOVA followed by Dunnett's or Tukey's *post hoc* test (GraphPad Prism, GraphPad Software Inc., CA, USA). *P* values less than 0.05 were considered to indicate statistical significance.

3. Results

3.1. Physicochemical properties of CFZ-PM

The particle size distribution and zeta potential of CFZ-PM and empty drug-free PM were determined using dynamic light scattering. The mean diameters of CFZ-PM and empty PM were comparable (56.0 ± 6.1 vs 41.2 ± 5.7 nm) and so were zeta potential values (-0.1 ± 0.4 vs -0.5 ± 0.3 mV) (Table 1). These results indicated that both size distribution and zeta potential were not substantially altered by CFZ drug loading. In addition, particle sizes did not show substantial changes in cell culture media containing fetal bovine serum compared to phosphate-buffered saline (data not shown). These results suggest that PEGylation of micelles may have decreased the tendency for nanoparticles to aggregate. The critical

micelle concentration (CMC) values measured by fluorescence spectrophotometry with pyrene were also comparable between empty PM and CFZ-PM with 0.18 and 0.14 mg/mL, respectively (Table 1).

Table 1. Physicochemical characterization of drug-free and carfilzomib (CFZ)-loaded polymeric micelles (PM).

Group	Size (nm)	Zeta potential (mV)	CMC (mg/mL)
Drug-free PM	41.2 ± 5.7	-0.5 ± 0.3	0.18
CFZ-PM	56.0 ± 6.1	-1.0 ± 0.4	0.14

Data are shown as means ± S.D. (n=3). CMC, critical micelle concentration

3.2. In vivo anticancer efficacy of CFZ-PM in H460 xenograft mice

The doses and dosing schedules of CFZ-PM and CFZ-CD (3 or 6 mg/kg, intravenous administration on two consecutive days per week) were based on clinically used regimens and available information in the literature [135]. The tumor size was substantially smaller in the groups that received CFZ-PM or CFZ-CD than in the control groups that received empty PM or vehicle only, but no difference was observed between the groups that received CFZ-PM and CFZ-CD at the dose of 3 mg/kg (Fig 1A). It was unable to compare tumor growth suppression of CFZ-PM to that of CFZ-CD at the dose of 6 mg/kg since 4 out of 6 mice that received 6 mg/kg of CFZ-CD died during the treatment period. The mice that received 6 mg/kg of CFZ-PM survived with no sign of substantial toxicity, at least based on body weight changes (Fig 1D). The tumor growth suppression by CFZ-PM was not however dose-dependent; tumor growth curves for 3 and 6 mg/kg doses overlapped and weights of excised tumors for both doses were similar (Figs 1B and 1C).

3.3. Proteasome inhibition in post-treatment xenograft tumor tissues and whole blood samples collected from mice that received CFZ-PM or CFZ-CD

In order to probe possible reasons for no enhancement of anticancer efficacy with CFZ-PM over CFZ-CD, we compared the extent of proteasome inhibition in the excised xenograft tumor tissues and whole blood samples collected from the xenograft mice receiving different drug treatments (collected 48 h following the last injection). In the groups that received CFZ-PM (3 or 6 mg/kg) or CFZ-CD (3 mg/kg), the inhibition of the proteasome activity in tumor lysates was modest (and not reaching statistical

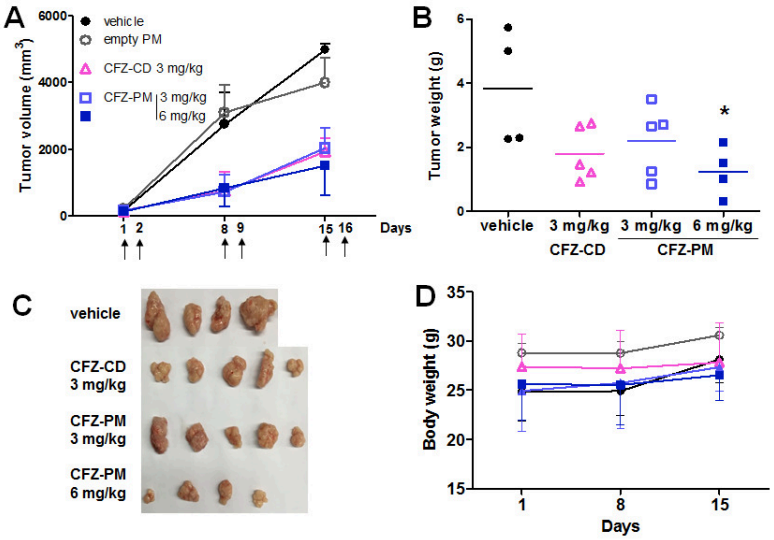

Figure 1. Effects of polymeric micelle formulation containing carfilzomib (CFZ-PM) vs cyclodextrin-based carfilzomib formulation (CFZ-CD) on tumor growth in H460 xenograft mice. NOD/SCID mice harboring H460 xenograft tumors were randomized to 5 different groups and received respective intravenous injections on two consecutive days per week; CFZ-PM at the dose of 3 (□) or 6 (■) mg/kg, CFZ-CD at the dose of 3 (△) mg/kg, vehicle (citrate buffer ●) and empty PM (dissolved in saline ○). The upper arrow symbol (↑) indicates the day of drug injection. (A) Tumor growth curves. (B, C) Weights and images of excised tumor tissues on day 18. (D) Body weights. Data are shown as means ± S.D. (n=4-5). *, $p < 0.05$ vs. vehicle control using ANOVA followed by Dunnett's *post hoc* test.

significance), with more than 50% of the activity remaining relative to the control group (Fig 2A). It should be noted that these results were obtained from the residual tumor tissues collected 48 h after last injection of the respective treatments. Thus, the measured proteasome activity in tumor lysates may represent that from tumor cells where active CFZ did not reach. Alternatively, the measured proteasome activity may come from the recovery following the initial inhibition. For instance, the previous report by Demo et al. [31] showed that the proteasome activity in major organs can substantially recover 24 h after intravenous injection of the single CFZ dose of 5 mg/kg. However, these results differ from those obtained by other investigators. With a repeated dosing schedule (clinically used and same as our current study), the proteasome activity in patients displayed only a minimal recovery [136]. The slow recovery of proteasome activity is also in line with rather slow proteasome *de novo* biogenesis rates taking at least several days [137-140]. Given the irreversible nature of proteasome inhibition by CFZ and a relatively long time for *de novo* proteasome biogenesis to replace the covalently modified proteasomes, the observed proteasome activity in residual xenograft tissues is unlikely from the recovery following initial inhibition [141]. In contrast, the proteasome activities in whole blood samples

collected 48 h after the last injection of the respective treatments showed an almost complete inhibition in all three tested groups, CFZ-PM (3 or 6 mg/kg) and CFZ-CD (3 mg/kg) (Fig 2B, $p < 0.001$, each treatment different from the control).

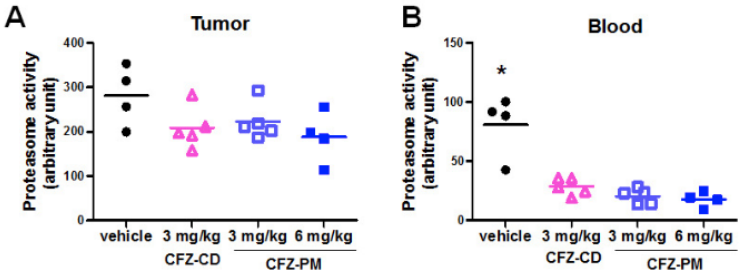

Figure 2. Proteasome activities in the post-treatment tumor tissue lysates (A) and whole blood samples (B) collected from H460 xenograft mice that received the intravenous injections of polymeric micelle formulation containing carfilzomib (CFZ-PM) or cyclodextrin-based carfilzomib formulation (CFZ-CD). The tumor tissues and whole blood samples were collected 48 h after the last injection of the respective treatments. Proteasome activities in tumor tissue lysates or whole blood lysates were assessed by measuring the cleavage rate of the fluorogenic substrate Suc-LLVY-AMC. *, $p < 0.001$ vs. all other groups using ANOVA followed by Dunnett's *post hoc* test.

In addition to measuring post-treatment proteasome activities, we also probed the extent of CFZ-induced covalent modification of the major proteasome catalytic subunit β5. This assay takes advantage of the altered electrophoretic mobility of the covalently modified β5 protein by CFZ as previously described [142]. The band of the positive control (tumor lysates incubated with 50 nM CFZ for 2 h *in vitro*) showed a mobility shift compared to the negative control (tumor lysates incubated with the vehicle DMSO for 2 h) (Fig 3). No detectable β5 band shift was observed in the post-treatment tumor lysates collected 48 h after the last drug treatment in either CFZ-PM or CFZ-CD groups. Altogether, these results suggest that CFZ-PM did not enhance the access of active CFZ to cancer cells in xenograft tumors and the extent of proteasome inhibition *in vivo*.

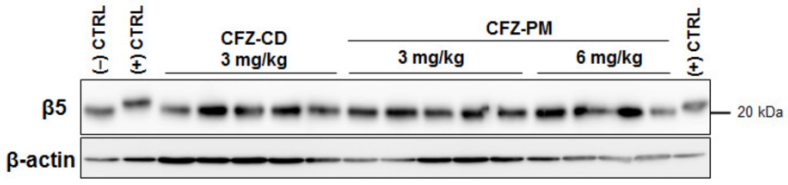

Figure 3. Immunoblotting analyses showing that the proteasome catalytic subunit β5, a primary target of carfilzomib remains unchanged in post-treatment tumor tissue lysates collected from the xenograft mice that received different treatments. (CFZ-CD: cyclodextrin-based carfilzomib formulation; CFZ-PM: polymeric micelle formulation containing carfilzomib) The tumor tissues were collected 48 h after the last injection of the respective treatments.

3.4. Comparison of plasma PK profiles of CFZ-PM and CFZ-CD in ICR mice

Given that CFZ-PM did not suppress tumor growth more effectively than CFZ-CD (Fig 2), it was examined whether the plasma PK profiles differ between CFZ-PM and CFZ-CD. Following the intravenous injection of CFZ-PM or CFZ-CD to ICR mice, the plasma concentration-time curves for both groups displayed a rapid decline. During early time points (up to 2 h), the mice that received CFZ-PM (either 3 or 6 mg/kg) showed higher drug concentrations than those that received CFZ-CD (Fig 4). However, this trend was reversed in later time points (6, 12 and 24 h after injection); the mice that received CFZ-PM injection (3 or 6 mg/kg) showed lower CFZ concentrations in plasma than those that received CFZ-CD.

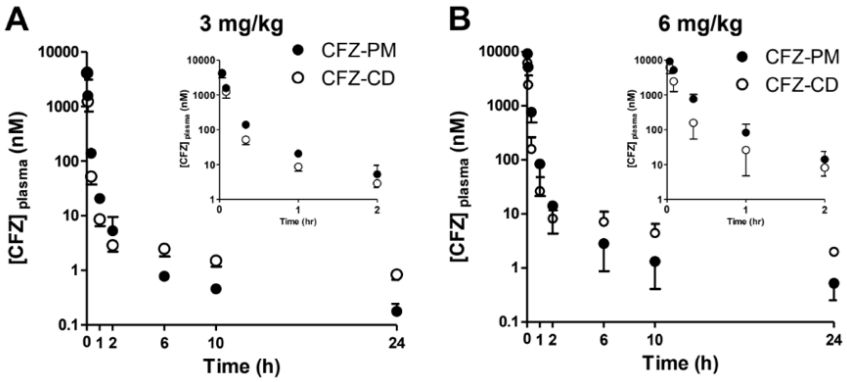

Figure 4. Plasma concentration-time profiles of carfilzomib after the intravenous administration of polymeric micelle formulation containing carfilzomib (CFZ-PM) or cyclodextrin-based carfilzomib formulation (CFZ-CD) to mice (A, 3 mg/kg and B, 6 mg/kg). Data are shown as means ± S.D. (n=4-5). The inset figures show the plasma concentration-time profiles up to 2 h.

Table 2. Pharmacokinetic parameters of carfilzomib after the intravenous administration of polymeric micelle formulation containing carfilzomib (CFZ-PM) and cyclodextrin-based carfilzomib formulation (CFZ-CD) to ICR mice.

Pharmacokinetic Parameters	CFZ-PM		CFZ-CD	
	3 mg/kg	6 mg/kg	3 mg/kg	6 mg/kg
$AUC_{0\text{-}2h}$ (nmol×min/mL)	38.6 ± 1.2	118.1 ± 25.3	33.3 ± 7.7	55.2 ± 21.1
$AUC_{0\text{-}24h}$ (nmol×min/mL)	39.8 ± 0.8	121.4 ± 27.2	35.4 ± 8.0	58.8 ± 21.8
AUC_{INF} (nmol×min/mL)	39.9 ± 0.8	121.8 ± 27.4	36.4 ± 8.0	62.6 ± 22.9
CL (mL/min/kg)	105 ± 2	71 ± 15	119 ± 29	152 ± 71*

Data are shown as means ± S.D. (n=4-5). $AUC_{0\text{-}2h}$, Area under the plasma concentration-time curve (AUC) from time 0 to 2 h; $AUC_{0\text{-}24h}$, AUC from time 0 to 24 h; AUC_{INF}, AUC extrapolated to infinity; CL, clearance. *, $p < 0.05$ vs. all other groups using ANOVA followed by Tukey's *post hoc* test.

For detailed comparison, the PK parameters were obtained using non-compartmental methods (Table 2). As expected from the rapid initial decline in the plasma concentration-time curves, the $AUC_{0\text{-}2h}$ values accounted for approximately 96.7% and 97.0% of the AUC_{INF} values in the CFZ-PM groups at the doses of 3 and 6 mg/kg, respectively. In the case of the CFZ-CD groups, the $AUC_{0\text{-}2h}$ values accounted for approximately 91.4% and 88.1% of the AUC_{INF} values at the doses of 3 and 6 mg/kg, respectively. The CL values of CFZ in all four groups exceeded the average hepatic blood flow in mice, suggesting substantial extrahepatic metabolism of CFZ. These results are in line with the previous reports in rats and humans [128, 130]. The systemic exposure of CFZ-PM and CFZ-CD at the dose of 3 mg/kg appeared to be comparable based on the similar AUC_{INF} and CL values between the two groups. When the AUC_{INF} values of 3 and 6 mg/kg doses were compared, the CFZ-PM group displayed approximately 3-fold increases (39.9 ± 0.8 vs 121.8 ± 27.4) while the CFZ-CD group displayed approximately 1.7-fold increases (36.4 ± 8.0 vs 62.6 ± 22.9). These differences in the AUC_{INF} values led to a slower CFZ clearance in the CFZ-PM group at the dose of 6 mg/kg than the other groups ($p < 0.05$).

4. Discussion

The proteasome is well accepted as a critical player in several traditional hallmarks of cancer, defined by Hanahan and Weinberg [143]. More recently, proteotoxic stress triggered by imbalances in protein homeostasis has been annotated as another hallmark of cancer [144]. In this regard, CFZ with improved efficacy and safety profiles merits further investigations to extend its therapeutic utility beyond MM. In particular, recent reports suggested that certain solid cancers render proteasome addiction as vulnerability, thereby a potential target for therapeutic interventions. Using genome-wide siRNA screening, the knockdown of proteasome genes was found to cause lethality in basal-like triple-negative breast cancer cells [145]. This particular study examined the effectiveness of bortezomib administered via different dosing routes in suppressing *in vivo* tumor growth and metastasis. Only intratumoral injection, but neither intraperitoneal nor intravenous route, displayed an efficient proteasome inhibition associated with enhanced anticancer efficacy [145]. An early report with bortezomib also indicated that intratumoral injection of the drug leads to an effective proteasome inhibition and growth suppression

in mice harboring prostate cancer xenografts [146]. Altogether, these findings provide an impetus to develop novel delivery strategies that can effectively target proteasomes in solid cancer tissues and validate the potential of CFZ-based therapy for solid cancer patients.

Previously, we developed several CFZ-loaded PM formulations displaying improved metabolic stability and anticancer efficacy *in vitro* [133]. In this study, we investigated *in vivo* anticancer efficacy and PK profiles of CFZ-PM (CFZ-loaded PEG-PCL 5-5.5 KDa with DCA) in mice. In the tumor xenograft model, CFZ-PM did not show substantial improvements in the anticancer efficacy and proteasome inhibition at the tumor sites over CFZ-CD (Figs 2 and 3). In addition, the plasma PK profiles of CFZ-PM were for the most part comparable to those of CFZ-CD at the dose of 3 mg/kg except showing slightly higher drug concentrations at early time points (Fig 4). These results indicated an incomplete proteasome inhibition in the post-treatment tumor tissues collected from H460 xenograft mice 48 h after the last injection of CFZ-PM (Figs 2 and 3). In further probing possible reasons for the lack of improvements with CFZ-PM over CFZ-CD, it would be important to examine whether the xenograft model employed in the current study allowed for sufficient passive targeting effect. The particle size distribution of CFZ-PM (56.0 ± 6.1 nm, Table 1) is sufficiently small to pass through the pore size of vascular membranes (60 ~ 100 nm) [147, 148]. However, these results suggest that CFZ-PM was not more effective in providing the access of active CFZ into tumor sites than CFZ-CD. It is increasingly recognized that tumor types, tumor vascular heterogeneity, abnormal tumor blood vessels or high interstitial fluid pressure may influence the access of chemotherapy to cancer cells [149, 150]. To overcome such variability, various pharmacological and physical strategies including focal radiation and sonoporation have been exploited in the field [151-153]. It would be important to obtain more detailed biodistribution data and to consider combining approaches to improve tumoral penetration of active CFZ in future investigations.

The extent and rate of CFZ release from CFZ-PM *in vivo* may also be a factor influencing anticancer efficacy. The plasma PK profiles of CFZ-PM after a single intravenous administration displayed higher drug concentrations during the initial phase (up to 2 h) than those of CFZ-CD at the dose levels of both 3 and 6 mg/kg (Fig 4). When the plasma PK parameters were compared, mice that

received CFZ-PM (6 mg/kg) displayed a greater systemic exposure and a slower CFZ clearance than those that received CFZ-CD (6 mg/kg) (Table 2). However, the systemic toxicity appeared to be more severe in xenograft mice treated with CFZ-CD (6 mg/kg) than those treated with CFZ-PM (6 mg/kg); four out of six mice receiving 6 mg/kg repeated doses of CFZ-CD died. Although these results need to be interpreted with caution due to the small sample size, these results suggest that CFZ-PM may have the potential to increase maximum tolerated dose levels and possibly CFZ release kinetics and biodistribution profiles different from CFZ-CD. Given the relatively low drug loading efficiency (2.3%) of the current CFZ-PM [133], the initial micelle concentrations (upon immediate dilution of the CFZ-PM 3 mg/kg dose in an average mouse blood volume of approximately 2 mL) are estimated to be well above the measured CMC value (0.14 mg/mL, Table 1). However, as polymers are cleared from blood, micelle concentration will decrease and micelles could degrade and release CFZ. Thus, it might be necessary to explore polymer-based nanoparticles stabilized with various structural/functional modifications [132, 147]. For the docetaxel-loaded PM formulation composed of the same block copolymer, PEG-*b*-PCL, the CMC value of 0.02 mg/mL was reported in *in vitro* conditions [154]. Thus, it may be feasible to lower CMC values for CFZ-loaded PM formulations by carefully optimizing various factors (e.g., drug-to-polymer ratios, addition of excipients stabilizing hydrophobic cores) using the current block copolymer or by using different types of block copolymers.

In summary, the results in this study showed that the current CFZ-PM does not enhance anti-cancer efficacy *in vivo*. Careful consideration of these results and confounding factors may provide valuable insights into the future efforts to validate the potential of CFZ-based therapy for solid cancer and to develop effective CFZ delivery strategies that can be used to treat solid cancers.

CHAPTER II.

Expanding Therapeutic Utility of Carfilzomib for Breast Cancer Therapy by Novel Albumin-coated Nanocrystal Formulation

*** The work from Chapter II is currently under revision in Journal of Controlled Release (Manuscript number: JCR-D-18-01200).**

1. Introduction

Breast cancer is ranked first in the incidence of disease and second in cancer-related deaths in women worldwide [1, 2]. Among different subtypes of breast cancer, triple-negative breast cancer (TNBC), which lacks the expression of estrogen receptor, progesterone receptor, and human epidermal growth factor receptor 2 (HER2), is notorious for its aggressive behavior and resistance to endocrine and anti-HER2 therapies (e.g., tamoxifen, trastuzumab) [3, 4]. Thus, novel and effective therapies for TNBC are urgently needed. A growing body of preclinical evidence supports that the proteasome is an effective therapeutic target against breast cancers including TNBC [5, 6]. Bortezomib, the first-in-class proteasome inhibitor, reversibly inhibits the proteasome with its boronic acid pharmacophore. While bortezomib has shown remarkable successes in multiple myeloma therapy, it has brought only marginal therapeutic benefits to patients with solid cancers including breast cancer [7]. The lack of clinical efficacy of bortezomib is attributed in part to its poor penetration into the targeted solid tumor tissues and the narrow therapeutic window due to dose-limiting toxicities arising from proteasomal inhibition in normal tissues and off-target interactions with non-proteasomal targets [5, 8].

Carfilzomib (CFZ, Kyprolis®) is the second-in-class proteasome inhibitor and has received the FDA approval a decade after the approval of bortezomib. Unlike bortezomib, CFZ covalently and irreversibly inhibits the proteasome with its epoxyketone pharmacophore and displays minimal interactions with non-proteasomal targets, thereby improving safety profiles over bortezomib [9]. Due to the poor solubility of CFZ (log P = 4.13, ~ 10 μM in PBS [10]), the current injectable formulation of CFZ contains 16-fold molar excess of sulfobutyl ether *β*-cyclodextrin (Captisol®) as a solubilizer. When administered as the current cyclodextrin (CD)-based formulation, CFZ has a very short circulation time (plasma half-lives of 0.5 – 1 h in humans and preclinical species) due to the extensive hepatic and extra-hepatic metabolism and wide tissue distribution [11]. As an alternative formulation, previous studies have surveyed the feasibility of CFZ nanoformulations including liposomes, polymer micelles, tethered polymer nanoassemblies, and neutrophil membrane-coated nanoparticles [12-15]. The shortcomings of these approaches however include the low drug loading efficiency, burst release of the drug in blood circulation, and no-to-marginal improvement in *in vivo* anticancer efficacy. Thus, there is a clear need

for a new nanoformulation of CFZ with improved pharmacokinetic (PK) and biodistribution (BD) profiles as well as pharmacodynamics, such as anticancer efficacy and proteasome target modulation.

To develop a cost-effective nanoformulation with an improved circulation time and anticancer efficacy *in vivo*, we designed a CD-free, nanocrystal (NC)-based formulation of CFZ. NC formulations exploit poor water solubility of anticancer drugs to produce injectable nanoparticles with a high drug content [16-18]. NCs with sufficiently high lattice energy can circulate for a prolonged period and may gain selective access to solid tumors via leaky vasculature. To facilitate favorable interactions of NCs with cancer cells (thereby enhancing the delivery of NCs to cancer cells), the surface of NCs can be modified with various molecules. In particular, albumin has gained considerable interest as a potential surface modifier, due to low toxicity, biocompatibility, and the ability to reduce interactions with phagocytes in the reticuloendothelial system (RES) [19-21]. Moreover, albumin can interact with cancer cells based on its increased use as an energy source in rapidly proliferating cancer cells [22]. It has been reported that nano-albumin-bound-drugs (nab-drugs) can aid drug permeation across tumor vessels [23, 24]. Albumin-bound paclitaxel (nab-paclitaxel) displayed promising efficacy and safety profiles in patients with breast cancers including TNBC [25]. Although the exact mechanisms by which nab-drugs reach cancer cells are not fully understood, it is suggested that albumin facilitates the movement across the endothelial cell membrane by binding to the gp60 receptor and sequentially interacting with other albumin-binding proteins such as SPARC (Secreted Protein Acidic and Rich in Cysteine) abundantly expressed in and near cancer cells [26]. Importantly, our previous studies support that albumin coating helps deliver paclitaxel and docetaxel NCs to solid tumors through the interaction with those albumin-binding proteins [27, 28].

In this study, we examined whether NCs with albumin coating could enhance the delivery of CFZ to breast cancers. Using albumin-coated CFZ NCs (CFZ-alb NC), we observed that CFZ-alb NC enhanced cytotoxic effects in breast cancer cell lines and tumor growth suppression in a murine 4T1 orthotopic breast cancer model, compared to the CD-based formulation of CFZ (CFZ-CD). We also observed the improved BD profiles of CFZ-alb NC in 4T1 orthotopic breast cancer model and investigated potential involvement of SPARC in the enhanced tumoral accumulation of CFZ-alb NC.

2. Material and methods

2.1. Materials

CFZ was purchased from Shenzhen Chemical Co. Ltd. (Shanghai, China). Pluronic F127 (F127) was a gift from BASF (New York, NY, USA). Human serum albumin (HSA; ≥ 96% purity assessed by agarose gel electrophoresis, Cat. No. A1653) and (2-hydroxypropyl)-β-cyclodextrin were from Sigma-Aldrich (St. Louis, MO, USA). All other reagents were from Thermo Fisher Scientific (Waltham, MA, USA).

2.2. Preparation of CFZ-alb NC

CFZ-alb NC was prepared by crystallizing CFZ in the presence of F127 and coating the resulting CFZ-NC with HSA, as reported previously [28]. Briefly, 6 mg of CFZ and 48 mg of F127 were dissolved in a mixture of 3 mL of chloroform and 1 mL of methanol and dried in a round-bottom flask by rotary evaporation at 40 ˚C for 10 min. The dry drug-polymer film was hydrated with 6 mL of water and sonicated in a water bath for 10 s. The NC suspension was further probe-sonicated for 5 min with an amplitude of 40% and a 4:1 duty cycle every 5 s in an ice bath. Subsequently, the suspension was incubated with 48 mg of HSA for 24 h at room temperature on a rotating shaker. Excess surfactant and albumin were removed by centrifugation at 135,700 g for 15 min at 4 ˚C.

Optionally, CFZ-alb NC was fluorescently labeled by adding rhodamine B as 0.1 mg/mL aqueous solution during the film hydration step. The rhodamine B-labeled CFZ-alb NC was called *CFZ-alb NC. To quantify the incorporated rhodamine B, the fluorescence intensity ($\lambda_{ex}/\lambda_{em}$= 540 nm/625 nm) of a known amount of CFZ-alb NC dissolved in acetonitrile (ACN) was measured with a SpectraMax M3 microplate reader (Molecular Devices, CA, USA). Most *in vitro* studies were performed with freshly prepared CFZ-alb NC. For *in vivo* studies, CFZ-alb NC was lyophilized with trehalose as a cryoprotectant (CFZ-alb NC:trehalose = 1:5 (w/w)) (Fig. S1). The lyophilized product of CFZ-alb NC was dissolved in PBS before administration. The concentration of trehalose in the dosing solution (containing 0.8 mg/ml of CFZ) was estimated to be around 4.3 mOsm/L, which is unlikely to compromise the isotonicity (approximately 300 mOsm/L).

2.3. Characterization of CFZ-alb NC

2.3.1. Size, surface charge, and morphology

The size and surface charge of CFZ-alb NC diluted in phosphate buffer (1 mM, pH 7.4) were measured with a Zetasizer Nano-ZS90 (Malvern Instruments, Westborough, MA, USA). The morphology of CFZ-alb NC was examined with a FEI Tecnai G2 20 Transmission Electron Microscope (FEI Company, Hillsboro, OR, USA) at 200 keV. Samples were mounted on a 400-mesh Cu grid with Formvar/carbon supporting film, followed by negative staining with 1% uranyl acetate. Images were captured with a SIA L3-C2 megapixel CCD camera (Scientific Instruments and Application, Duluth, GA, USA). The length of CFZ-alb NC was analyzed from TEM images with ImageJ (National Institutes of Health, Bethesda, MD, USA).

2.3.2. Powder X-ray diffraction (PXRD)

CFZ and CFZ-alb NC were analyzed with a Rigaku SmartLab diffractometer (Rigaku Americas, The Woodlands, TX, USA) equipped with a Cu-Kα radiation source. The powder samples were placed on glass holder, and diffraction patterns were obtained from 5 to 40° 2θ at a scan speed of 4° per min and a step size of 0.02°. The voltage and current used were 40 kV and 44 mA, respectively.

2.3.3. Contents of CFZ and albumin in CFZ-alb NC

The CFZ content in CFZ-alb NC was determined by HPLC. CFZ-alb NC with a pre-measured mass was dissolved in a 50:50 mixture of ACN and water and filtered with 0.45 μm syringe filter. HPLC was performed with an Agilent 1100 HPLC system (Agilent, Palo Alto, CA, USA), equipped with Ascentis C18 column (25 cm × 4.6 mm, particle size: 5 μm). The column was initially equilibrated with 40% of ACN, followed by a linear gradient of ACN from 40% to 80% over 10 min and from 80% to 40% over the next 10 min at a flow rate of 0.7 mL/min. CFZ was detected with a UV detector at a wavelength of 210 nm.

The albumin content in CFZ-alb NC was quantified with SDS-PAGE. CFZ-alb NC with a known mass or albumin standard solutions were mixed with 4× Laemmli sample buffer and heated at 95 °C for 5 min to separate albumin from CFZ-alb NC. The samples were resolved in a 12%

polyacrylamide gel and stained with QC Colloidal Coomassie Stain (Bio-Rad, Hercules, CA, USA). The stained gel was imaged with Azure C300 (Azure Biosystems, Dublin, CA, USA), and albumin bands were subjected to densitometric analysis using the AzureSpot Analysis Software (Azure Biosystems, Dublin, CA, USA). The albumin content was determined by comparing the band intensity of CFZ-alb NC and albumin standards.

2.4. Stability of CFZ-alb NC

2.4.1. Physical stability

To predict the physical stability of CFZ-alb NC, we resorted to a linear relationship between the number of particles and light scattering intensity [29]. The derived count rate (i.e., absolute light scattering) of CFZ-alb NC suspension with a concentration equivalent to CFZ 7.2 – 72 μg/mL was measured in phosphate-buffered saline (PBS) or undiluted fetal bovine serum (FBS) at 37 ˚C over 24 h with a Zetasizer Nano-ZS90 (Malvern Instruments, Westborough, MA, USA). The derived count rate of FBS was subtracted from each measurement made in FBS. In a separate experiment, the dissolution of CFZ-alb NC in FBS was monitored by measuring the count rate continuously over 20 min at the final concentration equivalent to 7.2 or 30 μg/mL of CFZ. Measurements were made twice every two seconds at the measurement position of 4.65 nm and with an attenuator setting of 10.

2.4.2. *In vitro* metabolic stability

To compare the *in vitro* metabolic stability in CFZ formulations (CFZ solution, CFZ dissolved in dimethyl sulfoxide (DMSO); CFZ-CD, CFZ dissolved in 10 mM citrate buffer (pH 3.1) containing 20% (w/v) 2-hydroxypropyl-β-cyclodextrin); and CFZ-alb NC dissolved in PBS), the whole blood and the liver were collected from a male Sprague Dawley rat. The whole blood was treated with heparin (25 IU/mL) and kept on ice until the assay was performed. The isolated liver was washed and homogenized in ice-cold PBS (pH 7.4, a 1:5 ratio of liver weight (g) to PBS volume (mL)). Each of CFZ formulations (4 μL) was added to the whole blood (396 μL) or liver homogenates (396 μL) to result in the final CFZ concentration equivalent to 1 μM. A reaction mixture (40 μL) was taken at 0, 5, 10, 30, and 60 min at 37 °C, and snap-frozen in liquid nitrogen until the measurements of the remaining CFZ concentration.

2.5. Cell cultures and treatments

Human breast cancer cell lines (MDA-MB-231, MCF-7, HCC1943, and HCC1937) were obtained from Korean Cell Line Bank (KCLB, Seoul, Korea). Mouse breast cancer cell line 4T1 was purchased from ATCC (Manassas, VA, USA). All cell lines were maintained in RPMI-1640 medium supplemented with 10% FBS and penicillin-streptomycin (100 IU/mL-100 μg/mL) at 37 °C in a humidified incubator operating at 5% CO_2.

2.5.1. Cellular uptake study for rhodamine B-labeled CFZ-alb NC (*CFZ-alb NC)

Cells were seeded in a 35 mm glass bottom dish (MatTak, Ashland, MA, USA) at a density of 50,000 cells per dish. After 24 h, the medium was replaced with fresh medium, and the cells were incubated with *CFZ-alb NC equivalent to 30 μg/mL CFZ or free rhodamine B solution at a comparable level for 2 h in complete medium. After washing twice with PBS, the cells were fixed with 4% paraformaldehyde in PBS for 10 min. Following nuclear staining with Hoechst 33342 (2 μg/mL; Cat. No. H1399), cells were imaged with a Nikon A1R confocal microscope (Nikon America Inc., Melville, NY, USA). Hoechst 33342 and *CFZ-alb NC or free rhodamine B were detected with $\lambda_{ex}/\lambda_{em}$ of 407 nm/425 – 475 nm and 561 nm/570 – 620 nm, respectively. For quantitative analysis, cells were prepared in the same manner and analyzed with an Accuri C6 flow cytometer (BD Biosciences, San Jose, CA, USA). At least 10,000 gated events were acquired, and FL-2 channel ($\lambda_{ex}/\lambda_{em}$ 488 nm/585 nm) was monitored to determine the cellular level of rhodamine B.

2.5.2. Cell viability assay

Cancer cells were seeded on 96-well plates (4T1, 2000 cells/well; MDA-MB-231 and MCF-7, 5000 cells/well; HCC1640, HCC1937, and U87MG, 8000 cells/well) 24 h prior to drug treatment. For the continuous drug treatment condition, cells were continuously exposed to CFZ solution or CFZ-alb NC for 72 h. For the pulse treatment condition, cells were treated with CFZ solution or CFZ-alb NC for 2 h, then washed twice with PBS, and grown in drug-free media for 72 h. Viable cells were measured with the CellTiter 96® AQ_{ueous} One Solution Cell Proliferation Assay (Promega, Madison, WI, USA) using Synergy HT plate reader (BioTek, Winooski, VT, USA).

2.6. Animal experiments

BALB/c mice (female, 5 – 6 weeks of age, 19 – 21 g), ICR mice (male, 8 weeks of age, 35 – 38 g), and Sprague Dawley rats (male, 8 weeks of age, 250 – 260 g) were obtained from Nara Biotech Co., Ltd. (Seoul, Korea) or Envigo (Indianapolis, IN, USA), and were acclimatized at the animal research facility in Seoul National University (SNU) or Purdue University (PU) for at least one week. All animal experiments were performed in accordance with the protocols approved by the Institutional Animal Care and Use Committee of SNU and PU (SNU-161205-2-1, SNU-170424-2-1, and PU-1503001212).

2.6.1. *In vivo* anticancer activity

To establish an orthotopic breast cancer mouse model, 4T1 cells (1.5×10^5 cells suspended in 50 μL of complete media) were inoculated into the inguinal mammary fat pad on both left and right sides of BALB/c mice (on day 0). When the palpable knob with a similar size appeared on day 4, the mice bearing 4T1 xenograft were randomly assigned to different groups (n= 5 – 6 per group) as follows: vehicle only group (10 mM citrate buffer (pH 3.1)), CFZ-CD at a dose of 3 mg CFZ/kg, and CFZ-alb NC at a dose of 3 mg CFZ/kg. The drug was administered two consecutive days a week for three weeks via tail vein injection. Tumor size was measured using a digital caliper; tumor volume = length×$(\text{width})^2/2$. The body weight of mice was monitored every 2 – 3 days until day 22. Whole blood samples and harvested major organs were snap-frozen and stored at -80 °C until analysis or fixed in 4% paraformaldehyde and embedded in paraffin for histological examination.

2.6.2. Plasma pharmacokinetic study

CFZ-alb NC and CFZ-CD were injected via tail vein into ICR mice at the dose of 3 mg/kg (n = 3 – 4 per group). At the pre-determined time points (2, 5, 20, 60, 120, 360, 600, and 1,440 min), blood samples (10 – 20 μL) were collected from the retro-orbital plexus of the mice using microhematocrit tubes. The detailed analytical conditions and assay validation parameters were previously reported [30]. PK parameters were calculated by non-compartmental method using WinNonlin software (Pharsight Corp., Version 5.0.1).

2.6.3. Biodistribution study

CFZ-alb NC and CFZ-CD were injected via tail vein into BALB/c mice harboring orthotopic xenografts (described in 2.6.1.) at an equivalent dose of 3 mg/kg when the tumor size became approximately 200 – 300 mm^3. After 0.5, 2, and 6 h, the mice were anesthetized with isoflurane/oxygen mixture (3 – 5%:95 – 97%; v/v). At least 800 µL of blood was collected with a heparinized syringe via cardiac puncture. Tumor and major organs were harvested, weighed, and snap-frozen until analysis. To measure the CFZ amount accumulated in tissues, the tissue homogenates were prepared on ice by adding the following proportion of PBS; 0.2 g tissue per mL PBS for all tissues except the lung (0.17 g tissue per mL PBS) and adrenal glands (0.1 g tissue per mL PBS). Tissue homogenates (100 µL) were extracted with cold *tert*-butyl methyl ether (600 µL) containing an internal standard (carfilzomib-d_8 250 ng/mL; Cayman Chemical, Ann Arbor, MI, USA) by vortex mixing. After centrifugation at 3,724 g for 10 min, 400 µL of organic phase was transferred to a new tube, and evaporated. The samples were reconstituted in 100 µL of ACN and transferred to a new vial for LC-MS/MS analysis. To measure the CFZ concentration remaining in plasma, 5 µL of plasma was mixed with H_2O (15 µL) and ACN (40 µL) containing an internal standard (carfilzomib-d_8 250 ng/mL; Cat. No. 22558). After vortex mixing, samples were centrifuged at 13,000 *g* for 10 min. The supernatant (50 µL) was transferred to a new vial for LC-MS/MS analysis.

2.6.4. Quantification of CFZ in tissue homogenates

Samples were analyzed by the HPLC system coupled to Agilent 6460 QQQ LC-MS/MS (Agilent, Palo Alto, CA, USA) equipped with an electrospray ionization interface operated in a positive ion mode. The chromatographic separation was performed on a C18 column (50 × 2.0 mm id, 3 mm) with a mobile phase that consisted of 0.1% formic acid in water (A)-0.1% formic acid in ACN (B) at a flow rate of 0.3 mL/min. The gradient was set up as follows: 0.5 min 85% A, 15% B; 3 min 100% B; 4 min 100% B; 5.5 min 85% A, 15% B; 6 min 85% A, 15% B. The autosampler temperature was set at 4 °C, and the injection volume was 10 µL. The optimized source-dependent mass parameters were set as follows: nebulizing gas 45 psi; gas flow, 9 L/min; sheath gas flow, 7 L/min; capillary voltage, 4 kV; gas temperature, 330 °C. The compound-dependent parameters, fragment voltage and collision energy,

were set at 180 V and 60 V for CFZ and carfilzomib-d_8 with the dwell time of 50 ms. Quantification was performed in the selected reaction monitoring (SRM) mode. The SRM transitions were as follows: for CFZ, m/z 720.3 > 100.1 (quantifier) and m/z 720.3 > 289.1 (qualifier); for the internal standard, m/z 728.3 > 108.1 (quantifier) and m/z 728.3 > 297.1 (qualifier).

2.6.5. Proteasome activity measurement in tissue homogenates from mice that received drug treatment

The homogenized tissue samples in PBS (prepared as described in the section 2.6.3.) were mixed with the same volume of ice-cold passive lysis buffer (Promega, Madison, WI, USA; Cat. No. E1941). After centrifugation of tissue mixtures at 3,000 *g* for 10 min at 4 °C, the supernatant was collected and used for proteasome activity assay (50 – 150 μg total protein/μL verified to be within the linear range of the assay using serial diluted samples). For blood samples, the whole blood (0.2 μL) was mixed with ice-cold passive lysis buffer (1.8 μL), and used for proteasome activity assay. To assess the proteasome activity, the tissue supernatant or blood mixture (2 μL) was incubated with 100 μM Suc-LLVY-AMC (Bachem, Bubendorf, Switzerland) in the assay buffer (48 μL; 20 mM Tris-Cl buffer (pH 8.0) and 500 μM EDTA). The proteasome activity was determined by monitoring the initial cleavage rate of fluorescent 7-amino-4-methylcoumarine from Suc-LLVY-AMC. Fluorescence signals were detected every min for 60 min using a SpectraMax M3 microplate reader (Molecular Devices, CA, USA) at the wavelengths of $\lambda_{ex}/\lambda_{em}$ = 360/460 nm with the cut-off filter set at 420 nm.

2.7. Involvement of SPARC in the cellular uptake of CFZ-alb NC

2.7.1. Quantification of mRNA expression of h*SPARC*

Total RNA of breast cancer cells was isolated using PureLink RNA Mini Kit and transcribed to cDNA using SuperScript III First-Strand Synthesis kit. The mRNA level of h*SPARC* was assessed by quantitative real-time PCR using TOPreal™ qPCR 2X PreMIX (Enzynomics, Seoul, Korea), the primer pair (forward, 5′-tcgacagtcagccgcatct-3′; reverse, 5′-ccgttgactccgaccttca-3′), and StepOnePlus™ Real-Time PCR system (Applied Biosystems, Foster city, CA, USA). The h*GAPDH* level was similarly measured as a house-keeping control (forward primer, 5′-gggacttcgagaagaac-3′; reverse primer, 5′-agaggtacccgtcaatg-3′), and the relative h*SPARC* levels were then calculated using the ΔΔCt method.

2.7.2. Immunoblotting analysis for hSPARC

Cell lysates were prepared in RIPA buffer, mixed with 4× Laemmli sample buffer, and heated at 95 °C for 5 min. Cell lysates containing the equivalent protein amount of 30 μg were resolved using 10% SDS-PAGE and transferred onto PVDF membranes (Bio-Rad, Hercules, CA, USA). After blocking using 5% milk in Tris-buffered saline containing 0.05% Tween-20 (TBST), the membranes were probed with the antibodies for hSPARC (1:200; R&D Systems, Minneapolis, MN, USA; Cat. No. AF941) and β-actin (Cell Signaling Technology, Danvers, MA, USA; Cat. No. 4970). After washing with TBST, the membranes were incubated with the corresponding secondary antibodies conjugated with horseradish peroxidase. Bound antibodies were visualized with an enhanced chemiluminescence substrate using ImageQuant^{TM} LAS4000 (GE Healthcare, Little Chalfont, United Kingdom).

2.7.3. Immunohistochemical analysis for mSparc

Tissue antigen was retrieved by boiling deparaffinized slides in 10 mM Tris, 1 mM EDTA, and 0.03% Tween 20 (pH 9.0) using a pressure cooker. After washing with water and blocking with 4% bovine serum albumin in PBS Tween-20 (PBST), slides were incubated with the mSparc antibody (1:20; R&D Systems, Minneapolis, MN, USA; Cat. No. AF942) for 60 min at room temperature. After washing slides with PBST, a streptavidin-biotin system was used according to the manufacturer's instructions (BioGenex, San Ramon, CA, USA). The slides were counterstained with Mayer's Hematoxylin (Sigma-Aldrich, St. Louis, MO, USA). All sections were examined under a Vectra imaging system (PerkinElmer, Waltham, MA, USA).

2.7.4. Association between h*SPARC* expression and overall survival in the TCGA dataset

To explore a potential association between the h*SPARC* expression and the outcomes in breast cancer patients, the datasets available from the ONCOMINE (www.oncomine.org) were analyzed; the datasets were sorted based on the gene name (h*SPARC*), the analysis type (cancer *vs* normal analysis), and the cancer type (breast cancer). The case dataset containing the h*SPARC* expression levels and overall survival of breast cancer patients was downloaded from a breast cancer meta-data set (reported in TCGA, The Cancer Genome Atlas) [31, 32].

2.7.5. Impact of h*SPARC* knockdown on cellular uptake of CFZ-alb NC in U87MG cells

To achieve the stable knockdown of h*SPARC*, U87MG cells were transduced using a lentiviral vector-based shRNA system targeting hSPARC (obtained from Santa Cruz Biotechnology, Dallas, TX, USA) (Detailed experimental methods were reported in the thesis of JH Jo and will soon be published; the thesis available at [http://hdl.handle.net/10371/138009]. To assess the cellular uptake of CFZ-alb NC, U87MG cells with hSPARC knockdown or wildtype control were seeded on a poly-L-lysine-coated 12-well plate (at a density of 1×10^5 cells/well) in complete media containing FBS. After 24 h, cells were rinsed with Opti-MEM media, exposed to unformulated CFZ or CFZ-alb NC in Opti-MEM media for 2 h, and then washed 3 times with PBS. After harvesting cells with 50% methanol (200 μL), aliquots of cell lysates were transferred to separate tubes for the measurement of CFZ via LC-MS/MS analysis (100 μL) or the protein quantitation assay (30 μL). For LC-MS/MS analysis, cell lysates (100 μL) were subject to probe sonication and extracted with ice-cold ACN (100 μL) containing an internal standard by vortex mixing. After centrifugation at 3,000 g for 10 min, 150 μL of supernatant was transferred to a new vial for LC-MS/MS analysis.

2.8. Statistical analysis

All data are presented as mean ± standard deviation (SD) of the replicates from independent experiments unless stated otherwise. Student's *t*-test or ANOVA with a *post-hoc* test was performed to determine statistical significance using GraphPad Prism (GraphPad Software, version 7.0.3.). A p-value < 0.05 was considered significant.

3. Results and discussion

3.1. Preparation and characterization of CFZ-alb NC

CFZ-alb NC was prepared following the two-step method as reported previously [28]. In the first step, CFZ and F127 (an amphiphilic triblock co-polymer of poly(ethylene oxide)-poly(propylene oxide)-poly(ethylene oxide)) were dissolved in a mixture of chloroform and methanol and subsequently evaporated to form a dry film. Incipient CFZ nanocrystal (CFZ-NC) was formed by hydration of the

film. F127 played dual roles: it helped hydrate and retrieve the film from the container (without F127, a dry film of CFZ resisted hydration and only 0.02 wt% of CFZ was retrieved from the film) and prevented excessive crystal growth of CFZ-NC by binding to the NC surface [17, 33]. In the second step, the incipient CFZ-NC was further functionalized with HSA, and the excess HSA and F127 were removed by multiple washing.

The TEM images of CFZ-alb NC showed a rod-like structure with an average length and width of 352 ± 195 nm and 58 ± 15 nm, respectively (n=135, analyzed using the Image J software) (Fig. 1A). When measured with a dynamic light scattering (DLS), the size and polydispersity index of CFZ-alb NC were 270.8 ± 21.5 nm and 0.27 ± 0.06, respectively (n = 10 independently prepared batches) (Fig. 1B and Table 1). Although the average size of CFZ-alb NC is relatively large compared to other nanoformulations, the current size may still be sufficient for extravasation through peritumoral vasculature with the reported cut-off size in the range of 200 – 1,200 nm [34-36]. Even if CFZ-alb NC

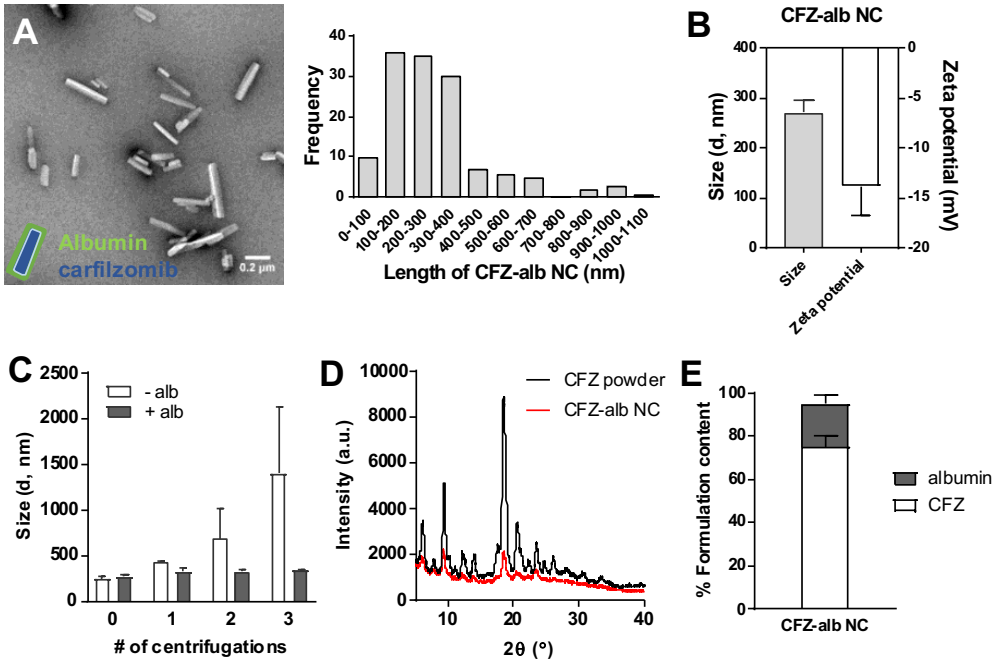

Figure 1. Physicochemical properties of CFZ-alb NC. (A) Representative TEM image of CFZ-alb NC and size distribution (analyzed from TEM images, n=135). (B) The average size and zeta potential of CFZ-alb NC, measured by DLS. Mean values ± SD (n=10 identically prepared batches). (C) The particle size of CFZ NC with or without human serum albumin added during the three repeated procedures of centrifugation and washing, measured by DLS. (D) Powder X-ray diffraction of CFZ powder (black) and CFZ-alb NC (red). Arbitrary unit (a.u.). (E) Content (%) of CFZ and albumin in CFZ-alb NC. Mean values ± SD (n = 6 – 10 independently prepared batches).

Table 1. Physicochemical properties of CFZ-alb NC and *CFZ-alb NC.

Formulation	Size (nm)	Polydispersity Index	Zeta potential (mV)	Formulation content (wt%)		
				CFZ	albumin	rhodamine B
CFZ-alb-NC	270.8 ± 21.5	0.27 ± 0.06	-13.7 ± 3.2	74 ± 6	20 ± 4	-
*CFZ-alb NC	328.0 ± 48.6	0.21 ± 0.09	-8.5 ± 1.1	82 ± 4	16 ± 3	0.34 ± 0.11

Mean values ± SD from different batches for CFZ-alb NC (n = 10) and *CFZ-alb NC (n = 3).

does not freely traverse the tumor interstitium, CFZ-alb NC may undergo gradual disintegration and release CFZ near cancer cells. The shape of NC appears to depend on the drug itself rather than process parameters. In the previous reports, docetaxel and paclitaxel form crystals with sheet- and rod-like structures, respectively, even with similar procedural methods [27, 28]. The elongated shape of CFZ-alb NC is also considered advantageous for transvascular flux as compared to the spherical shape at an equivalent volume [37, 38] and for resisting uptake by macrophages [39]. CFZ-alb NC was lyophilized with trehalose as a cryoprotectant for a long-term storage of the formulation and verified to redisperse to the original size (Fig. S1).

The zeta potential of CFZ-alb NC was -13.7 ± 3.2 mV, likely due to the HSA present on the surface of NCs (Fig. 1B and Table 1). The surface-bound HSA protected F127-coated CFZ-NC from aggregation (Fig. 1C). In the absence of HSA, CFZ-NC aggregated upon repeated centrifugation and washing procedures, as F127 was gradually removed from the NC surface [40]. Under the same conditions of multiple centrifugation and washing, the size of CFZ-alb NC did not increase. When PXRD patterns were assessed, CFZ powder displayed multiple sharp peaks, indicative of crystalline solids, while CFZ-alb NC showed much attenuated peak intensities, indicative of surface-bound HSA (Fig. 1D) [28]. The contents of CFZ and albumin in CFZ-alb NC were 74 ± 6 % (w/w) and 20 ± 4 % (w/w), respectively (n = 6 independently prepared batches) (Fig. 1E and Table 1). When the weight ratio of CFZ to albumin is considered, it is estimated that the albumin content corresponds to approximately 1.5 continuous layers of albumin covering the NC surface (Table S1).

3.2. Enhanced physical and metabolic stability of CFZ-alb NC

We next examined whether CFZ-alb NC can display the physical and metabolic stability. In assessing the physical stability of NCs in aqueous media, light scattering intensity can serve as a convenient and reliable indicator [28, 29]. Stable NCs maintain the light scattering capability, thereby a constant derived count rate, whereas disintegrating or dissolving NCs show a decreasing derived count rate. When tested in PBS, CFZ-alb NC maintained a linear relationship between the derived count rates the concentration within the tested range (7.2 to 72 μg/mL CFZ) up to 24 h (Fig. S2A). In undiluted FBS, similar trends were observed with comparable slopes up to 4 h and slightly decreasing slopes at 7 or 24 h (Fig. 2A). When the derived count rates were continuously monitored over 20 min, CFZ-alb NC (7.2 μg/mL CFZ, Fig. 2B; 30 μg/mL CFZ, Fig. S2B) yielded the signals consistently greater than those of FBS alone. These results support the physical stability of CFZ-alb NC at its concentrations as low as

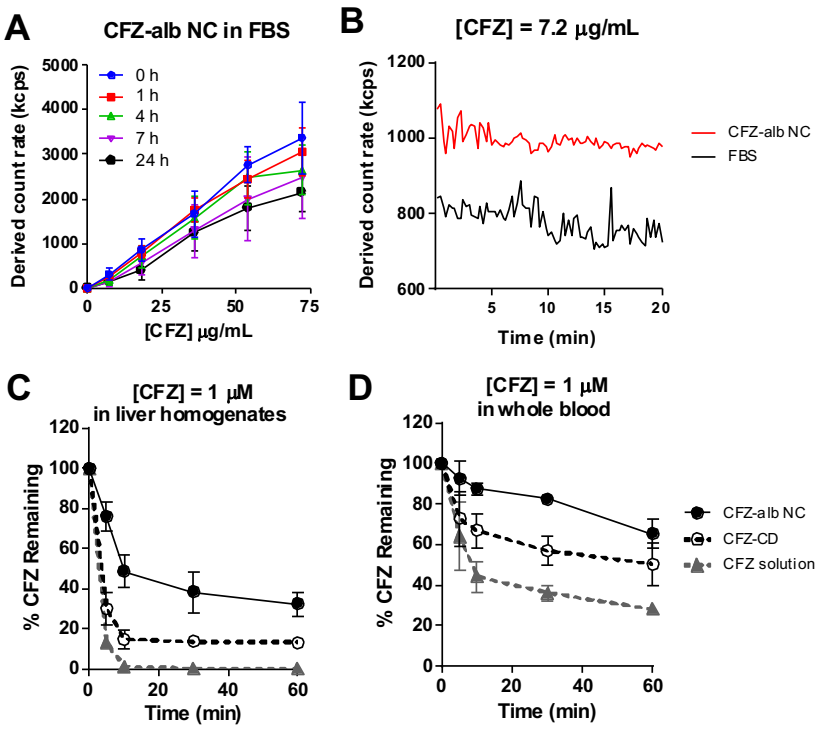

Figure 2. Physical and metabolic stability profiles of CFZ-alb NC. (A) In the presence of undiluted FBS, the derived count rates of CFZ-alb NC maintained linear relationships over the concentrations ranges tested (7.2 to 72 μg/mL CFZ) for 24 h. (B) The derived count rates of CFZ-alb NC (equivalent to 7.2 μg/mL CFZ, in the presence of undiluted FBS) were obtained by continuous monitoring for the first 20 min. (C and D) Remaining amount of CFZ following the incubation with CFZ-alb NC, cyclodextrin-based CFZ formulation (CFZ-CD), and unformulated CFZ solution in rat liver homogenates (C) and whole blood (D). Mean values ± SD (n=3 independently prepared batches of CFZ-alb NC).

7.2 μg/mL CFZ, even in the presence of serum proteins. When CFZ-alb NC (3 mg/kg, based on the CFZ content) is administered to a mouse with a typical blood volume of 1.5 – 2.5 mL [41], the initial blood concentration of CFZ-alb NC can be roughly estimated to be 24 – 40 μg/mL CFZ. If the current *in vitro* results measured in undiluted serum were to reflect the physical stability of CFZ-alb NC *in vivo*, one may expect CFZ-alb NC to circulate as intact particulate forms in blood, especially during the early hours after drug administration.

CFZ displays a very short circulation time due to its rapid metabolic inactivation by epoxide ring opening and peptide hydrolysis [42]. To assess whether CFZ-alb NC can improve metabolic stability, CFZ-alb NC was incubated with rat liver homogenates. As a control, separate reactions were performed with CFZ solution (dissolved in DMSO) or clinically used CD-based CFZ formulation (CFZ-CD, CFZ dissolved in 10 mM citrate buffer (pH 3.1) containing 20% (w/v) 2-hydroxypropyl-β-cyclodextrin). At a concentration equivalent to CFZ 1 μM, both CFZ solution and CFZ-CD displayed very rapid disappearance of CFZ (<10% remaining after 10 min) in the presence of rat liver homogenates (Fig. 2C). These results are consistent with the previous reports showing the half-lives of CFZ in various rat tissue homogenates in the ranges of 4 – 39 min [41]. On the other hand, CFZ-alb NC displayed much improved stability with approximately 40% of the active drug remaining even at 60 min in the liver homogenates (Fig. 2C). The disappearance of CFZ after addition of CFZ-alb NC and CFZ-CD was quite rapid at early time points and became slower at later time points. The rapid disappearance of CFZ at early time points may arise from the readily available portion of CFZ near the outer layer of NC formulation. At later time points, the drug release from the disintegration of NC formulation may take longer time. Given the results were obtained using liver homogenates (containing a variety of metabolizing enzymes and proteins including the proteasome), it is unknown what contributes to this biphasic pattern of CFZ disappearance and further investigations are warranted. The metabolic stability profiles in whole blood displayed similar trends, finding CFZ-alb NC most stable (Fig. 2D). These results indicate that CFZ-alb NC can confer both physical and metabolic stability, rendering a promising potential to extend the circulation time of CFZ *in vivo*.

3.3. Enhanced cellular uptake and cytotoxic effects of CFZ-alb NC in breast cancer cell lines

In order to assess its cellular uptake, CFZ-alb NC was fluorescently labeled using a small quantity of rhodamine B. The rhodamine B-labeled CFZ-alb NC (*CFZ-alb NC) was comparable to the unlabeled CFZ-alb NC in terms of the average size, zeta potential, and morphology (Table 1 and Figs. S3A and S3B), similar to the previous reports with other drugs and nanoformulations [43, 44]. The content of incorporated rhodamine B in *CFZ-alb NC was 0.34 ± 0.11 wt% (n = 3). Established breast cancer cell lines (murine, 4T1; human, MCF7, HCC1937) were incubated with *CFZ-alb NC (30 μg/mL) for 2 h and observed by confocal microscope imaging (Fig. 3A and Fig. S3C). Little signal was obtained from the incubation of *CFZ-alb NC in the dish without cells (data not shown), ruling out the possibility that the signal obtained with 4T1 cells may come from protein adsorption and subsequent fixation of protein. The incubation with *CFZ-alb NC yielded red fluorescence signals localized in the cytoplasm (Fig. 3A, d-f), indicating cellular uptake of *CFZ-alb NC (merged images shown in Fig. 3A, f). As a control, free rhodamine B solution was tested at an equivalent dye concentration (0.1 μg/mL). As shown in Fig. 3A (g-i), the treatment of free rhodamine B showed little signal in all three cell lines (Fig. 3A and S3C). No signal from the incubation of *CFZ-alb NC in the dish without cells (data not shown) ruled out the plausible signal from protein adsorpition and subsequent fixation of protein. In quantitative analysis by flow cytometry, the fluorescent signal intensities were higher in cells treated with *CFZ-alb NC than those in the control groups (no treatment or free rhodamine B) for all three cell lines (Fig. 3B). Of the *CFZ-alb NC-treated cell lines, HCC1937 cells showed the highest fluorescence signal intensity, followed by 4T1 and MCF-7 cells.

Next, we tested whether the enhanced cellular uptake of CFZ-alb NC leads to greater cytotoxic effects in breast cancer cells. When treated with unformulated CFZ, five breast cancer cell line models (human: MCF7, MDA-MB-231, HCC1143, and HCC1937; murine: 4T1) displayed IC_{50} values of low nano-molar ranges for CFZ (Fig. S4A). With regard to the expression levels of the proteasome catalytic subunits (β1, β2, and β5), the four human breast cancer cell lines tested were comparable to human multiple myeloma RPMI8226 cells (well-known for its abundant expression of the proteasome and sensitivity to proteasome inhibitor drugs) (Fig. S4B). In addition, the four human breast cancer cells

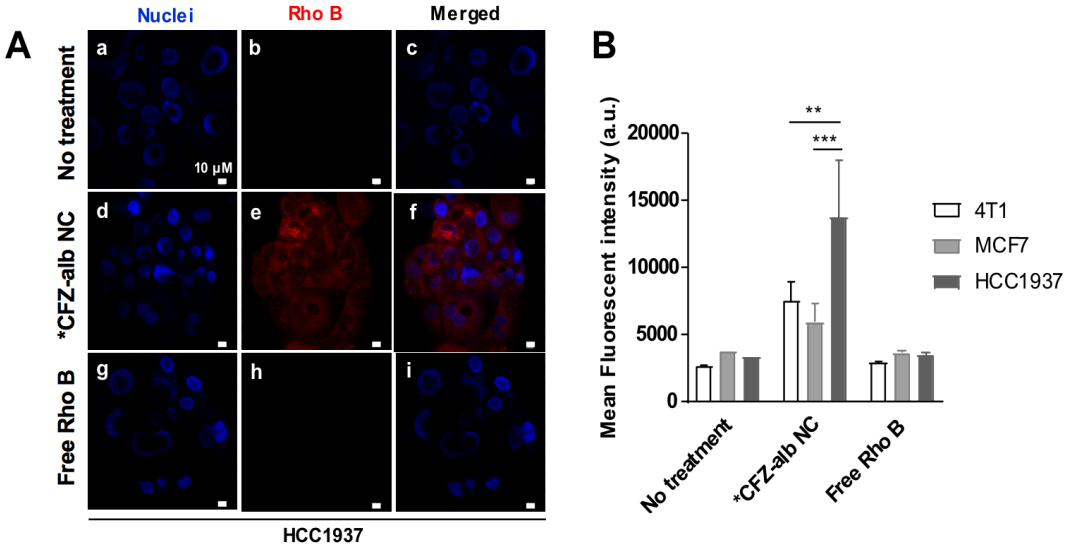

Figure 3. Cellular uptake of rhodamine B-labeled CFZ-alb NC (*CFZ-alb NC) in breast cancer cell lines. (A) Representative confocal microscopy images of HCC1937 cells following 2 h incubation with *CFZ-alb NC (30 µg/mL CFZ) (d, e, and f). Free rhodamine B (Rho B) was used as a negative control (g, h, and i). Scale bar = 10 µm. (B) Intensities of fluorescent signals associated with breast cancer cells (4T1, MCF7, HCC1937) after 2 h incubation with *CFZ-alb NC, measured by flow cytometry. Arbitrary unit (a.u.). Two-way ANOVA followed by Tukey's *post hoc* test. $^{**}p < 0.0021$, $^{***}p < 0.0002$. Mean values ± SD (n= 3 independently and identically performed experiments).

displayed comparable proteasome activities (chymotrypsin-like, trypsin-like, and caspase-like activity, typically attributed to β5, β2, and β1 subunits, respectively) to the RPMI8226 cells (Fig. S4C). Although the expression and activity of proteasomes were similar across the tested cell lines, MCF7 cells were least sensitive to CFZ based on 2D colony formation assay (Fig. S4E). MCF7 cells were also shown to be resistant to bortezomib [5]. The mechanism of MCF7 resistance to proteasome inhibitors remains unclear. Since CFZ is a known substrate of P-glycoprotein (P-gp) [44], the P-gp mediated drug efflux was initially suspected as a possible resistance mechanism in MCF7 cells, but this was excluded given the lack of P-gp expression (Fig. S4D). Cells under 3D spheroid culture conditions are known to enrich stem-like cancer cells [45, 46], and the 3D spheroid formation was highest with CFZ-treated MCF7 cells (Fig. S4F). These results can be cautiously interpreted that a sub-population of stem-like cancer cells existing in MCF7 cells may play a role in the resistance to proteasome inhibitors.

The cytotoxic effects of CFZ-alb NC was tested with either continuous or pulse treatment. Upon continuous exposure at low CFZ concentrations (equivalent to 20 and 50 nM for 72 h), CFZ-alb NC and unformulated CFZ solution (dissolved in DMSO) displayed similar cytotoxic effects (Fig. 4A).

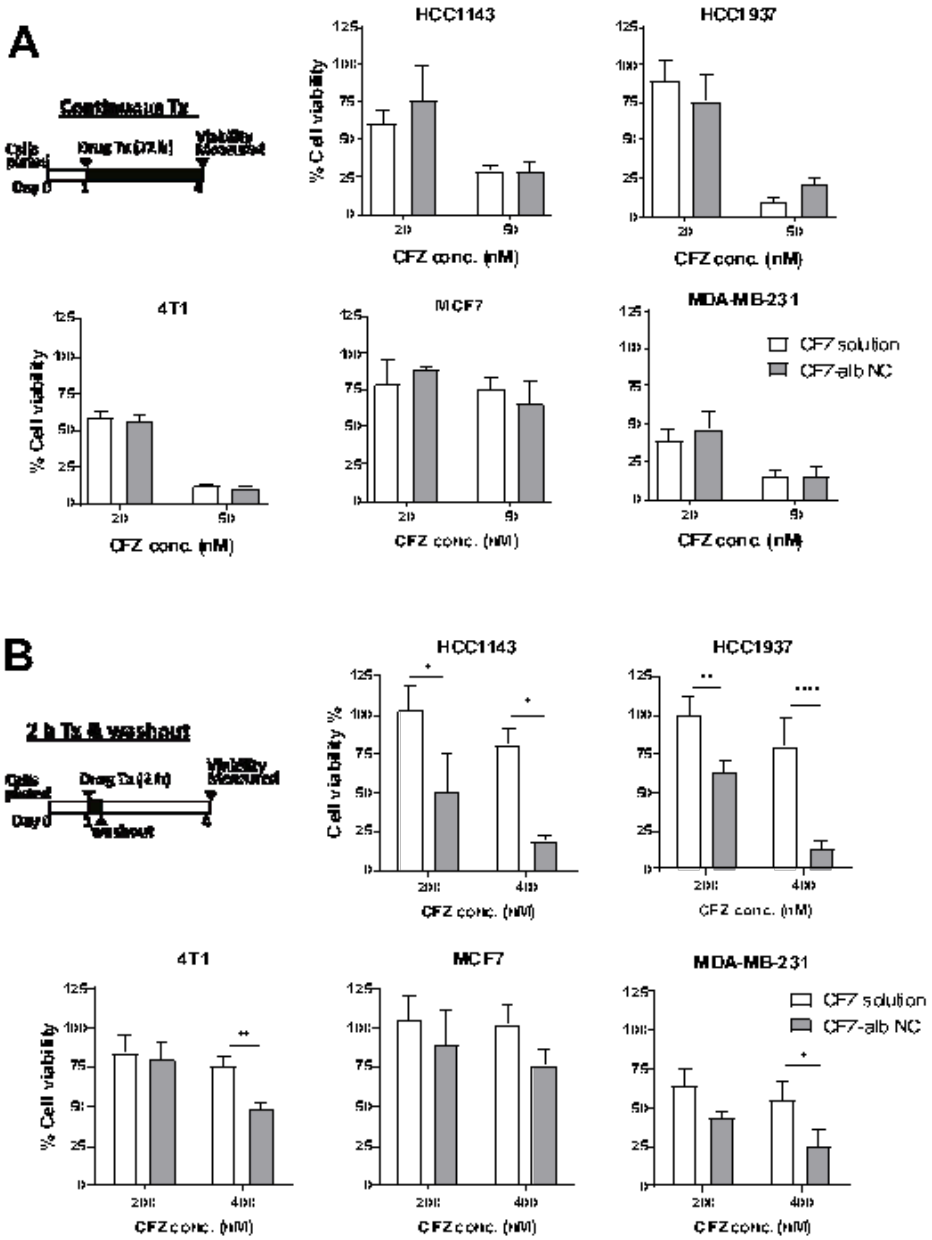

Figure 4. Cytotoxic effects of CFZ-alb NC in breast cancer cell lines. Cell viability was measured following the treatment of human breast cancer cell lines with CFZ-alb NC or unformulated CFZ solution under continuous treatment (Tx) conditions for 72 h (A) or pulse Tx conditions for 2 h followed by washout (B). Two-way ANOVA followed by Sidak's *post hoc* test. $*p < 0.0332$, $**p < 0.0021$, $****p < 0.0001$. Mean values ± SD (n= 4~5 independently and identically performed experiments).

These results were expected in that CFZ-alb NC would dissolve over time at sufficiently low CFZ concentrations. Upon intravenous injection, however, CFZ-alb NC will be present initially at high concentrations and rapidly decline, featuring more dynamic changes over time [47, 48]. To mimic such conditions, cells were subject to a pulse treatment at high CFZ concentrations (equivalent to 200 or 400 nM) and grown without CFZ: cells were initially exposed to CFZ-alb NC or CFZ solution for 2 h, rinsed,

and grown in drug-free medium for 72 h prior to the measurement of cell viability. Upon a pulse-treatment, CFZ-alb NC displayed a greater cytotoxic effect than unformulated CFZ solution (Fig. 4B). When the intracellular CFZ content was determined by LC-MS/MS after a pulse treatment in HCC1937 cells, CFZ-alb NC led to a greater amount of CFZ than unformulated CFZ solution (Fig. S7E; CFZ-alb NC vs unformulated CFZ solution; 12.7 *vs* 7.0 pmol/mg protein). These results collectively suggest that CFZ-alb NC gains cellular entry during the initial short exposure to a greater extent than unformulated CFZ solution and possibly serves as an intracellular drug reservoir during the incubation in drug-free medium.

3.4. Enhanced in vivo anticancer efficacy of CFZ-alb NC in BALB/c bearing 4T1 breast cancer cells

The *in vivo* anticancer efficacy of CFZ-alb NC was assessed using the murine 4T1 orthotopic breast cancer model established by the transplantation of 4T1 cells in the mammary fat pad of BALB/c mice , which mimic human cancer pathology with tumors growing at the location of human disease in the presence of the proper stromal environment compared to the subcutaneous model [49]. Similar to the clinical dosing schedule of CFZ [50], intravenous injections of CFZ-alb NC and CFZ-CD (at the equivalent CFZ dose of 3 mg/kg) were carried out on two consecutive days per week for three weeks (Fig. 5A). CFZ-alb NC or CFZ-CD suppressed tumor growth compared to the vehicle only (Fig. 5B). On day 19, the tumor volumes of the mice receiving CFZ-alb NC were smaller than those receiving CFZ-CD ($p = 0.0024$) or the vehicle only ($p < 0.0001$), while the vehicle- and CFZ-CD-treated groups did not show statistical difference. On day 22, all three groups showed difference from each other: CFZ-CD ($p < 0.0001$ *vs* the vehicle only; $p < 0.0001$ *vs* CFZ-alb NC) and CFZ-alb NC ($p < 0.0001$ *vs* the vehicle only; $p < 0.0001$ *vs* CFZ-CD). Similar results were obtained for the weight of dissected tumor tissues (Figs. 5C and S5A) and specific tumor growth rates (Fig. S5B). During the span of experiment, the body weight of mice showed no major difference among the three groups (the overall changes from the initial weight was ± 10%, Fig. 5D), suggesting no signs of gross toxicity. The weight loss observed near the end of experiment (in all three groups) are likely due to distant metastasis commonly occurring in 4T1 tumor models (Fig. S5C). Histological examination of major organs (liver and lung) also showed no signs of major toxicities in three groups (Fig. S5D).

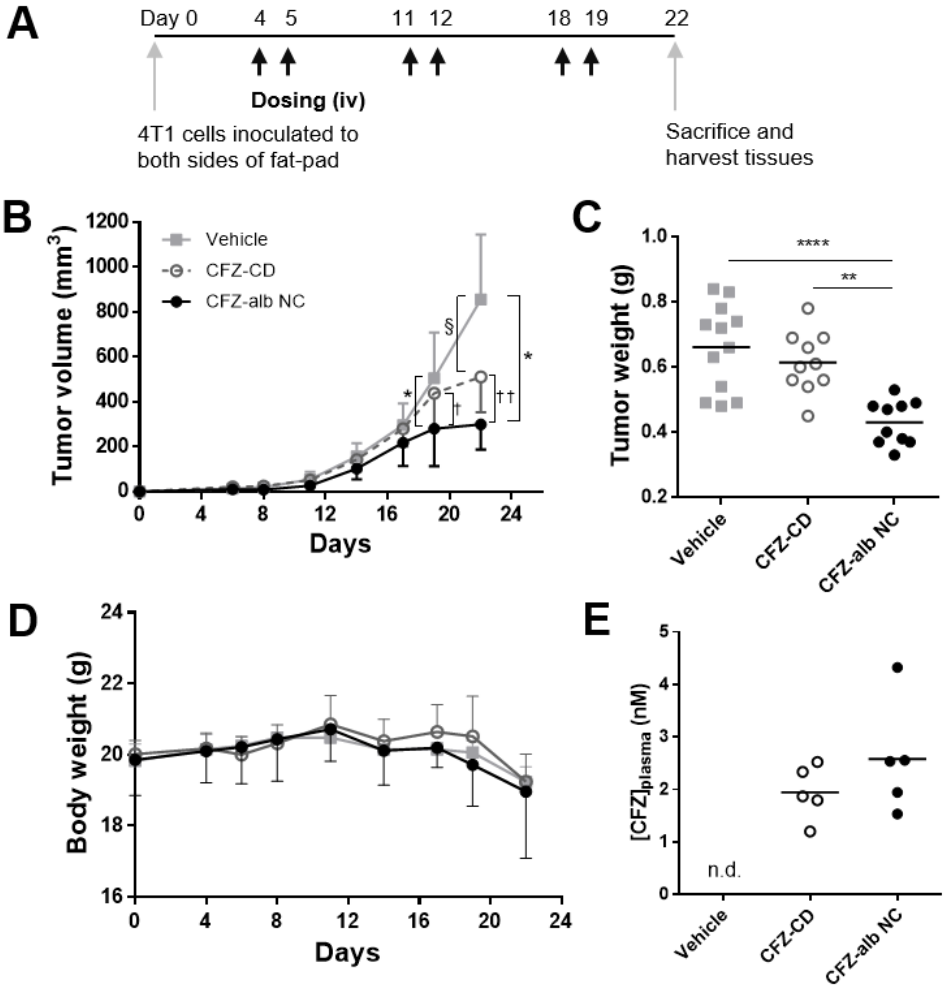

Figure 5. *In vivo* anticancer efficacy of CFZ-alb NC in BALB/c mice bearing 4T1 orthotopic xenograft tumors. (A) Experiment schedule including drug treatments. Mice received intravenous injections of CFZ-alb NC (n = 5; 3 mg/kg), CFZ-CD (n = 5; 3 mg/kg), or vehicle control (n = 6) on two consecutive days per week for three weeks. (B) Tumor growth curves. Two-way ANOVA followed by Tukey's *post hoc* test. On day 19: CFZ-alb NC *vs* vehicle, *$p < 0.0001$; CFZ-alb NC *vs* CFZ-CD, †$p = 0.0024$. On day 22: CFZ-alb NC *vs* vehicle, *$p < 0.0001$; CFZ-CD *vs* vehicle, §$p < 0.0001$; CFZ-alb NC *vs* CFZ-CD, ††$p < 0.0001$ (C) The weight of tumor tissues harvested on day 22. One-way ANOVA followed by Tukey's *post hoc* test. **$p < 0.0021$, ****$p < 0.0001$. (D) The body weight of mice during the span of experiment. (E) The concentration of CFZ from plasma collected on day 22 (n.d.; not detected). Mean values ± SD.

At the end of the *in vivo* anticancer efficacy experiments described above, we collected the tumor tissues and blood samples on day 22 (3 days following the last drug dosing on day 19) and attempted to quantify the CFZ levels by LC-MS/MS. The levels of CFZ in tumor tissues were below the lower limit of quantitation (< 1 ng/mL), but those of CFZ in plasma samples were higher in mice receiving CFZ-alb NC than CFZ-CD (Fig. 5E). Because CFZ is a covalent modifier, which forms an

irreversible CFZ-proteasome complex undetectable by LC-MS/MS [51, 52], the drug amount measured by LC-MS/MS may not accurately represent the total amount of CFZ reaching a particular tissue (as depicted in Fig. 6B). The recovery of the proteasome activity following inhibition is known to take at least several days due to the slow *de novo* biogenesis rates of proteasomes [53]. Thus, we examined the inhibitory extent of the proteasomal activity in tissues as another indicator of the CFZ distribution. In whole blood samples, the inhibitory extent of the proteasome activity was greater in the CFZ-alb NC group than in the CFZ-CD group ($p < 0.0001$) (Fig. S5B), consistent with the blood levels of CFZ (Fig. 5E). These results suggest that CFZ-alb NC increased the formation of the irreversible, long-lasting complex between CFZ and the proteasome in whole blood (mainly located in red blood cells), likely from the enhanced stability and cellular uptake of CFZ-alb NC over CFZ-CD.

3.5. Comparison of PK and BD profiles of CFZ-alb NC with CFZ-CD

In the previous study, albumin-coated paclitaxel NC was superior in anticancer efficacy and showed more favorable plasma PK and BD profiles compared to Abraxane® at the equivalent paclitaxel dose level [21]. To examine whether CFZ-alb NC confers similar advantages, we first examined the plasma PK profiles of CFZ-alb NC relative to those of CFZ-CD (an equivalent CFZ dose of 3 mg/kg) in ICR mice. Following a single intravenous administration, the plasma CFZ concentrations declined very rapidly in both groups (Fig. 6A). The PK parameters obtained via non-compartmental analysis did not show major differences between the two groups (Table 2). The volume of distribution at steady-state (V_{ss}, 19.85 ± 0.04 L/kg and 17.01 ± 9.40 L/kg for CFZ-alb NC and CFZ-CD, respectively) and the plasma half-lives ($t_{1/2,\ terminal}$, 387 ± 49 min and 796 ± 393 min; $t_{1/2,\ initial}$, 21 ± 4 min and 19 ± 5 min for CFZ-alb NC and CFZ-CD, respectively). The V_{ss} and $t_{1/2,\ initial}$ values of CFZ-CD were comparable to the previously reported values [11, 41, 48]. The $t_{1/2,\ terminal}$ values tended to be longer with CFZ-alb NC than with CFZ-CD, but the differences did not reach statistical significance due to large variability. The systemic exposure of CFZ (assessed by AUC_{inf}) was slightly greater with CFZ-alb NC (57.5 ± 14.0 min·nmol/mL) than with CFZ-CD (45.4 ± 6.9 min·nmol/mL), although the difference did not reach statistical significance. Likewise, the systemic clearance was slightly slower with CFZ-alb NC than with CFZ-CD but did not show statistical significance (76 ± 21 mL/min/kg and 94 ± 15 mL/min/kg for

CFZ-alb NC and CFZ-CD, respectively). Similar to the previous reports [11, 41], the clearance of both CFZ-alb NC and CFZ-CD was considerable fast, almost approximating to the hepatic blood flow in mice [54]. These results suggest that the extrahepatic metabolism likely plays an important role in the elimination of CFZ in both groups. Overall, CFZ-alb NC appeared to have a modest improvement over CFZ-CD with regard to the plasma PK profiles.

Table 2. Pharmacokinetic (PK) parameters following the intravenous administration of CFZ-alb NC or CFZ-CD at an equivalent CFZ dose of 3 mg/kg to ICR mice.

PK parameter (unit)	CFZ-alb NC (n = 3)	CFZ-CD (n = 4)
AUC_{inf} (min×nmol/mL)	57.5 ± 14.0	45.4 ± 6.9
CL (mL/min/kg)	76 ± 21	94 ± 15
V_{ss} (L/kg)	19.85 ± 0.04	17.01 ± 9.40
$t_{1/2,\ terminal}$ (min)	387 ± 49	796 ± 393
$t_{1/2,\ initial}$ (min)	21 ± 4	19 ± 5
MRT (min)	192 ± 125	274 ± 67

AUC_{inf}, area under the concentration-time curve from time 0 to infinity; *V_{ss}*, volume of distribution at steady state; *$t_{1/2,\ terminal}$*, half-life from the terminal phase; *$t_{1/2,\ initial}$*, half-life from the initial decline phase (0 – 120 min); *MRT, mean residence time; CL*, clearance. Student's *t*-test indicated no significant difference. Mean values ± SD.

To examine whether CFZ-alb NC can enhance tumor distribution of CFZ, BALB/c mice bearing 4T1 tumors were injected with a single intravenous dose of CFZ-alb NC or CFZ-CD (an equivalent CFZ dose of 3 mg/kg). Tumor tissues and major organs were harvested at 0.5, 2, or 6 h post-injection, processed to make tissue homogenates, and subsequently analyzed with respect to the CFZ levels by LC-MS/MS (the remaining CFZ quantity as either NC or released CFZ) and the proteasome activity by the enzyme kinetics assay (likely representing the cumulative CFZ access to a given tissue and the formation of the CFZ-proteasome complex in a given tissue). In tumor tissues, the CFZ-alb NC group displayed significantly higher CFZ levels than the CFZ-CD group at 0.5 h post-dosing (9.2 ± 1.7 *vs* 6.8 ± 1.1 nM CFZ/g tissue, $p = 0.028$) (Fig. 6C). However, this trend was reversed at 2 and 6 h post-dosing, where CFZ-alb NC group displayed lower CFZ levels than the CFZ-CD group (at 2 h, 4.3 ± 0.4 *vs* 8.2 ± 2.2 nM CFZ/g tissue, $p = 0.0003$; at 6 h, 1.4 ± 0.5 *vs* 7.0 ± 1.2 nM CFZ/g tissue, $p < 0.0001$). When we compared the extent of proteasomal activity inhibition (by forming the irreversible CFZ-proteasome complex) in tumor tissues, the CFZ-alb NC group displayed a greater or comparable extent

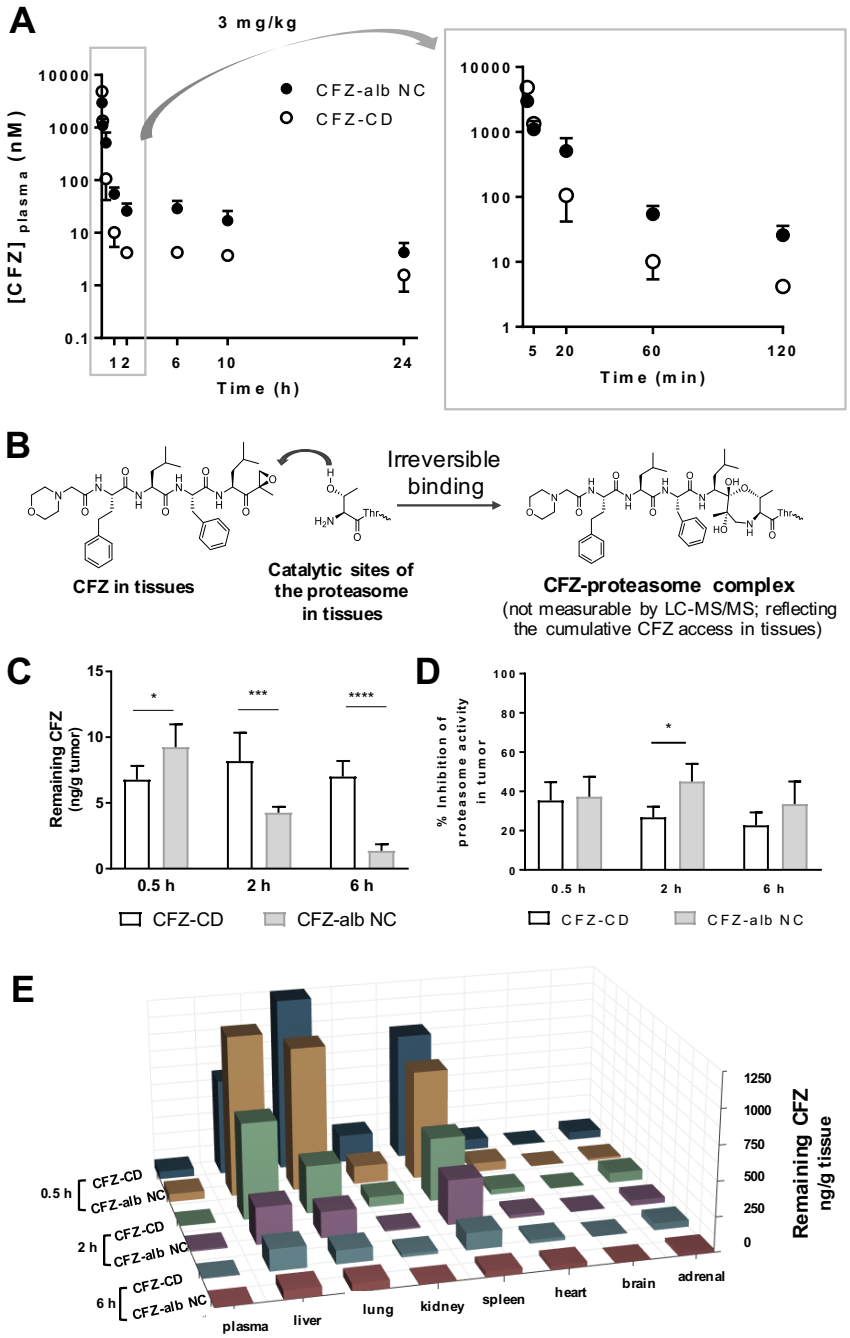

Figure 6. Comparison of pharmacokinetic and biodistribution profiles between CFZ-alb NC and CFZ-CD following the intravenous administration (a single equivalent CFZ dose of 3 mg/kg). (A) The plasma concentration-time profiles of CFZ after the administration of CFZ-alb NC (n = 3) or CFZ-CD (n = 4) in ICR mice. Inset, plasma concentration-time profiles of CFZ for the first 2 h. (B) Diagram depicting the irreversible biding of CFZ with the proteasome in tissues. The resulting CFZ-proteasome complex is not measurable by LC-MS/MS, but can be indirectly assessed by measuring the inhibitory extent of the proteasomal activity. (C, D, and E) The results showing the measured amount of CFZ and the inhibitory extent of the proteasome activity in tumor tissues and major organs in BALB/c mice harboring 4T1 xenograft at 0.5, 2, and 6 h following the administration of CFZ-alb NC or CFZ-CD (n = 4 – 5 per group). The measured amount of CFZ (C) and the inhibitory extent of the proteasomal activity (D) in tumor tissues. (E) The measured amount of CFZ in major organs. Two-way ANOVA followed by Sidak's *post hoc* test. *$p < 0.0332$, ***$p < 0.0002$, ****$p < 0.0001$. Mean values ± SD.

of the proteasomal inhibition than the CFZ-CD group (2 h post-dosing, 27% ± 5% for CFZ-CD *vs* 45% ± 9% for CFZ-alb NC, $p = 0.0112$) (Fig. 6D). The CFZ levels and proteasome activity in tumors, taken together, suggest that CFZ-alb NC was rapidly entrapped into tumor tissues after administration, subsequently releasing CFZ, and forming the CFZ-proteasome complex.

In both CFZ-alb NC and CFZ-CD groups, CFZ was predominantly distributed to the liver, the lung, and the spleen at 0.5 h post-dosing with a minor distribution into the kidney, the heart, adrenal glands, and the brain (Figs. 6E and S6A). CFZ-alb NC recognized and sequestered by mononuclear phagocytic system (MPS) as exogenous materials likely to be accumulated in MPS-rich organs, such as the liver, the lung, and the spleen [18]. Similar to the plasma PK profiles, CFZ levels in various tissues rapidly declined within 6 h post-injection. At 2 and 6 h post-injection, the CFZ-CD group resulted in CFZ levels in the liver, lung, and spleen comparable to or even higher than CFZ-alb NC group (Figs. 6E and S6A). In the liver (at 2 and 6 h post-dosing), the CFZ-alb NC group showed more pronounced inhibition of the proteasome activity than the CFZ-CD group (Fig. S6B). CFZ-alb NC group had lower CFZ levels than CFZ-CD group in the liver, reminiscent of the results obtained in tumor tissues (Figs. 6C and 6D). No apparent organ toxicity of CFZ-alb NC was observed based on histological examinations (Fig. S5D). For CFZ-alb NC, the initial accumulation in the RES organs and very limited distribution to the brain were observed as expected from typical nanoparticle interactions and uptake by liver sinusoidal endothelial cells and Kupffer cells, mechanical filtration [55, 56], and poor penetration through the blood brain barrier [57].

The results in CFZ-CD group were rather surprising. Currently, the quantitative data of CFZ BD profiles by LC-MS/MS is limited. An early study used whole-body autoradiogram in rats after an intravenous injection of [^{3}H]-CFZ (a total CFZ dose of 2 mg/kg, prepared as an injectable CFZ-CD solution) and found predominant distribution of the radioactivity in the liver and lung [58]. It is unknown whether these observed profiles are attributable to the intrinsic properties of CFZ or CD itself. CD derivatives are generally assumed to have a minimal impact on the PK profiles of drugs [59]. However, there are cases where the complexation with CD alters the systemic exposure of certain compounds, especially those with high affinity for CD derivatives [60]. It remains to be determined whether the complexation with CD enhanced the distribution of CFZ to the liver and lung.

3.6. SPARC-dependent uptake of CFZ-alb NC to cancer cells

In line with the proposed role of SPARC present in the tumor microenvironment facilitating tumor accumulation of nab-drugs [23, 61], a positive association was reported between SPARC expression and response to nab-paclitaxel in multiple types of cancers (e.g., human head-and-neck cancer, non-small cell lung cancer, HER2-positive breast cancer) [62-64]. However, SPARC-independent pathways may also play a role in delivering nab-drugs to cancer cells [65, 66]. The relative importance of SPARC and non-SPARC pathways may well vary depending on cellular context and cancer types. In the case of breast cancer, the results from publicly available databases indicated that the h*SPARC* expression was higher in breast cancer tissues than in non-malignant control tissues (Fig. 7A). From the dataset collected from 498 breast cancer patients, the sub-groups with high and low h*SPARC* levels (top 10% and bottom 10% in the SPARC expression levels, respectively; n = 50 each) were identified and compared for their median survival. The higher h*SPARC* expression level was associated with poorer outcomes (median survival times of 23 and 31 months in the high and low h*SPARC* expression groups, respectively) (Fig. 7B; Fig. S7A showed similar trend in another dataset (n = 418)).

To investigate the potential involvement of SPARC in the delivery of CFZ-alb NC to cancer cells, we first compared the SPARC level among four human breast cancer cell lines used in our study. HCC1937 cells were highest in the mRNA and protein level of hSPARC, followed by HCC1143, MDA-MB-231, and MCF7 cells (Figs. 7C and 7D). hSPARC showed an apparent positive correlation with cellular uptake of CFZ-alb NC (HCC1937 taking up a greater amount of CFZ-alb NC than MCF7) (Fig. 3B) and also with cytotoxicity of CFZ-alb NC (HCC1937 displaying the greatest enhancement of cytotoxicity by CFZ-alb NC over the unformulated CFZ solution, followed by HCC1143, MDA-MB-231, and MCF7) (Figs. 4B and S7B). hSPARC expression was detected mainly on the plasma membrane of HCC1937 cells (Fig. S7C), and mSparc was abundantly expressed in the 4T1 tumor tissue sections (Fig. 7E). Based on these results, it was postulated that the SPARC expressed in or near cancer cells may facilitate cellular interactions and internalization of CFZ-alb NC, potentially accounting for the enhanced inhibition of the proteasome activity shown *in vivo* (Figs. 5B and 5C).

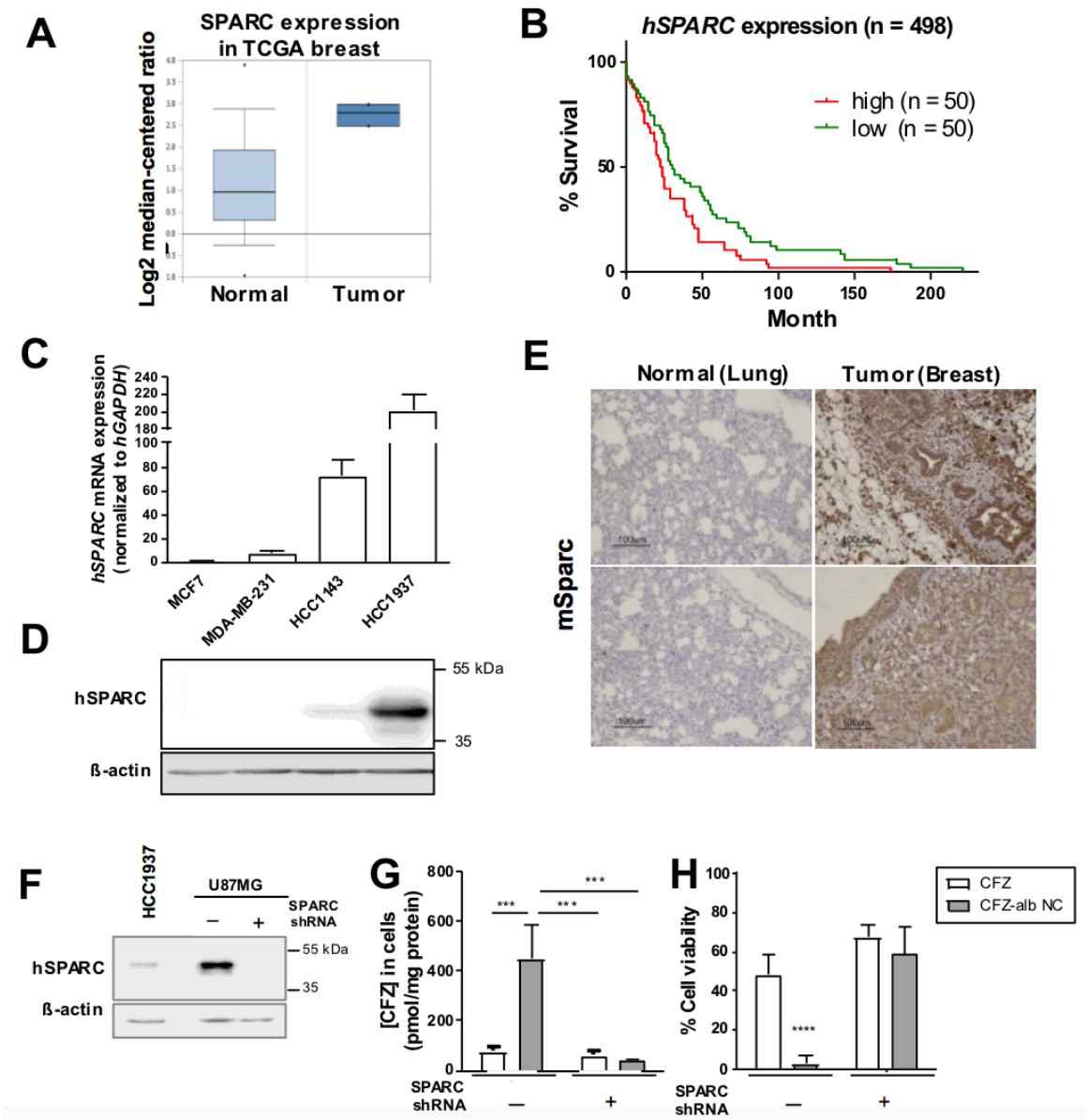

Figure 7. Role of SPARC in the uptake of CFZ-alb NC into cancer cells. (A) The relative expression of h*SPARC* gene in normal *vs* cancerous breast tissues (from a dataset in the TCGA database, n = 64; the detailed description provided in the methods). (B) The Kaplan-Meier curves depicting overall survival for breast cancer patients with a high and low levels of h*SPARC* (n = 498, the dataset from the previous report [31]). (C and D) The mRNA (C) and protein (D) expression level of hSPARC in breast cancer cell lines. (E) Immunohistochemical staining of mSPARC (positive staining visualized as brown colors using 3,3'-diaminobenzidine) in 4T1 tumor tissue sections. Normal lung tissue section showed a weak staining signal for mSparc under the same experimental condition (representative images, scale bar = 100 µm). (F) The protein levels of hSPARC in HCC1937 and U87MG cells following the lentiviral transduction of SPARC-targeting shRNA. (G and H) Comparison of the cellular uptake of CFZ (G) and cell viability (H) in U87MG cells where SPARC was completely knocked down following exposure to CFZ-alb NC or unformulated CFZ solution. Two-way ANOVA followed by Tukey's *post hoc* test. ***$p < 0.0002$, ****$p < 0.0001$. Mean values ± SD.

To obtain experimental evidence on the involvement of SPARC in the cellular uptake of CFZ-alb NC, we examined changes in cellular uptake and cytotoxicity of CFZ-alb NC in breast cancer cells by modulating their SPARC levels. When SPARC was partially knocked down by transient siRNA transfection in HCC1937 cells (Fig. S7D), no appreciable change was observed in cellular uptake (Fig. S7E) or cytotoxicity (Fig. S7F) of CFZ-alb NC. Boosting SPARC levels using decitabine (Fig. S7G) [63] also did not change the cellular uptake (Fig. S7H) and cytotoxic effects (Fig. S7I) of CFZ-alb NC. In order to obtain more conclusive evidence on the involvement of SPARC in the cellular uptake of CFZ-alb NC, we employed a model system that allows for a complete knockdown of SPARC from its high basal expression level. High levels of endogenous SPARC have been reported in glioma [67, 68], especially in U87MG cell lines derived from human glioblastoma. Upon lentiviral transduction of SPARC-targeting shRNA, U87MG cells showed an almost complete knockdown of SPARC at the protein level (Fig. 7F), making it suitable for the proof-of-concept study. When the cellular uptake and cytotoxicity of CFZ-alb NC were assessed in U87MG cells with complete SPARC knockdown, CFZ-alb NC displayed dramatic increases in both the cellular uptake (Fig. 7G) and cytotoxicity (Fig. 7H) compared to the control U87MG cells. These results provide clear evidence supporting the important role of SPARC in delivering albumin-containing nanoparticles to cancer cells and may warrant further exploration of albumin coating for the therapy of SPARC-overexpressing tumors including gliomas.

Taken together, our results support that CFZ-alb NC enhances pharmacodynamics of CFZ compared to CFZ-CD formulations by improving its physical and metabolic stability and enhancing cellular uptake by cancer cells. The extent by which CFZ-alb NC improved the anticancer efficacy compared to CFZ-CD was not as pronounced as albumin-coated paclitaxel NC (reported as Cim-F-alb [21, 28]). Possible reasons include the followings: (a) The size of CFZ-alb NC was larger than Cim-F-alb (270 *vs* 198 nm). It was previously shown that the cellular uptake of paclitaxel NCs significantly decreased as the particle size increased [28]. (b) The conformational status of surface-bound albumin was shown to be an important factor to determine the efficacy of NCs [21]. When the extent of proteolysis by thermolysin was compared using the pulse proteolysis method [28], the surface-bound albumin in CFZ-alb NC was comparable to native albumin ($23.9 \pm 3.9\%$ vs $15.8 \pm 5.1\%$, n=3), whereas denatured albumin (boiled at 95 °C for 10 min as a positive control) showed significantly higher extent

of proteolysis than native albumin (42.0 ± 9.5% vs 15.8 ± 5.1%, n=3). Given the slightly elevated proteolysis, the possible impact of albumin conformation changes on the performance of CFZ-alb NC may not be completely ruled out, but the majority of albumin in CFZ-alb NC appears to maintain its native conformation. (c) Different levels of albumin-interacting proteins including SPARC may impact the extent by which the surface-bound albumin facilitates cellular uptake. Cim-F-alb was tested in C57BL/6 mice harboring xenografts of B16F10 melanoma cells [21], which showed much greater SPARC expression level than 4T1 cells used in our current study [69]. (d) The improvement in the circulation time might have been less with CFZ-alb NC than albumin-coated paclitaxel nanocrystal. Given that paclitaxel has aqueous solubility even lower than CFZ, albumin-coated paclitaxel nanocrystal may have had a longer circulation time as NCs than CFZ-alb NC. Moreover, albumin-coated paclitaxel nanocrystal was administered at 30 mg/kg, much higher than 3 mg/kg for CFZ-alb-NC. Consideration of these possibilities may assist in optimizing CFZ formulations containing albumin for the treatment of breast cancer and other types of solid cancer. Nonetheless, our results indicate a promising potential for CFZ-alb NC as an alternative, CD-free formulation which can improve *in vivo* anticancer efficacy.

4. Supporting information

4.1. Supporting experimental methods

4.1.1. Cytotoxic effects of CFZ solution

Breast cancer cells were seeded onto 96-well plates 24 h prior to drug treatment. Cells were treated with CFZ solution (dissolved in DMSO; CFZ concentrations ranging from 1 to 500 nM; the DMSO content did not exceed 0.5% v/v) for 72 h and the cell viability was measured with the CellTiter 96® AQ_{ueous} One Solution Cell Proliferation Assay (Promega, Madison, WI, USA) using Synergy HT plate reader (BioTek, Winooski, VT, USA). The IC_{50} (half maximal inhibitory concentration) value was obtained using GraphPad Prism software 7.0.3.

4.1.2. Immunoblotting analysis

Cell lysates were prepared in the RIPA buffer, mixed with 4× Laemmli sample buffer, and heated at 95 °C (for the proteasome subunits) or 50 °C (for P-glycoprotein, P-gp) for 5 min. Cell lysates containing the equivalent protein amount (10 μg for proteasome subunits, 60 μg for P-gp) were resolved using 7.5 – 12% SDS-PAGE and transferred onto PVDF membranes (Bio-Rad, Hercules, CA, USA). After blocking using 5% milk in Tris-buffered saline containing 0.05% Tween-20 (TBST), the membranes were probed with the following antibodies: β1 (1:1,000 dilution; #PW8140; Enzo Biochem, Farmingdale, NY, USA), β2 (1:1,000 dilution; #PW8145; Enzo Biochem, Farmingdale, NY, USA), β5 (1:1,000 dilution; #PA1-1962; Thermo Fisher Scientific) and P-gp (1:200 dilution; #903701; BioLegend, San Diego, CA, USA).

4.1.3. Proteasome activity measurement in breast cancer cell lines

Cell lysates were prepared in the ice-cold passive lysis buffer (Promega, Madison, WI, USA). After centrifugation of cell lysates at 3,000 *g* for 10 min at 4 °C, the resulting supernatant was collected and used for the proteasome activity assay (10 μg total protein). To assess the proteasome activities, the supernatant (2 μL) was incubated in the assay buffer (48 μL) with the following fluorogenic substrates: 100 μM Suc-LLVY-AMC (Bachem, Bubendorf, Switzerland) for the chymotrypsin-like activity, 100 μM Ac-nLPnLD-AMC (Bachem, Bubendorf, Switzerland) for the caspase-like activity, and 20 μM Ac-RLR-AMC (BostonBiochem, Cambridge, MA, USA) for the trypsin-like activity. The proteasome activities were monitored as described in section 2.6.5.

4.1.4. 2-dimensional (2D) colony formation assay

Breast cancer cells were seeded onto a 6-well plate at a density 1,000 – 2,000 cells per well. After treated with CFZ solution for 2 h and subsequently washed twice with DPBS, cells were maintained in drug-free complete media for 11 – 14 days. After the removal of media, cell plates were placed on ice, washed twice with ice-cold DPBS and fixed with cold methanol for 10 min. The fixed cells were strained with crystal violet solution.

4.1.5. 3-dimenstional (3D) spheroid formation assay

Cells were seeded onto a 6-well plate at a density 5×10^4 cells per well in complete media. Cell were treated with CFZ (50 nM) and doxorubicin (100 nM) for 16 h, and then washed twice with DPBS. Cells were collected using trypsin and 500 – 2,000 cells were re-plated per well in ultra-low attachment 96 well plates (Corning, New York, USA). Cells were maintained in HuMEC Ready Medium supplemented with B-27 Supplement, epidermal growth factor (20 ng/mL; Sigma-Aldrich, St. Louis, MO, USA), basal fibroblast growth factor (20 ng/mL), heparin (4 μg/mL; Sigma-Aldrich, St. Louis, MO, USA), and penicillin-streptomycin at 37 °C in a humidified incubator operating at 5% CO_2. After 10 – 14 days, spheroids were visualized using Operetta imaging system (PerkinElmer, Waltham, MA, USA) and the number of spheroids with their size > 500 nm was counted.

4.1.6. hSPARC imaging in HCC1937 cells

HCC1937 cells were seeded in 35 mm petri dish at 1×10^5 cells per dish and incubated overnight. The cells were fixed in 4% paraformaldehyde at 4 ˚C for 15 min, rinsed twice with PBS, and incubated with 10 μg/mL of polyclonal goat anti-human SPARC antibody (R&D Systems, Minneapolis, MN, USA) overnight at 4 ˚C in 5% milk in TBST. After washing, the primary antibody was visualized with Alexa Fluor 488 conjugated-polyclonal rabbit anti-goat IgG (10 μg/mL; Invitrogen, Carlsbad, CA, USA) by incubating for 1 h at 4 ˚C. The stained cells were imaged with a Nikon A1R confocal microscope (Nikon America Inc., Melville, NY, USA), and Hoechst 33342 and Alexa Fluor 488 were detected with $\lambda_{ex}/\lambda_{em}$ of 407 nm/425 – 475 nm and $\lambda_{ex}/\lambda_{em}$ of 488 nm/500 – 550 nm, respectively.

4.1.7. siRNA-based h*SPARC* knockdown in HCC1937 cells

HCC1937 cells at the confluency of approximately 60% were transfected with h*SPARC*-targeting siRNAs (25 picomole; OriGene, Rockville, MD, USA) or scrambled siRNAs using Lipofectamine® RNAiMAX Reagent following the recommended protocol. At 48 h post-transfection, cells were harvested for the immunoblotting analysis of SPARC protein. To assess the cytotoxicity and cellular uptake of CFZ-alb NC, the transfected HCC1937 cells were treated with CFZ-alb NC or CFZ solution

for 2 h. After washing 2 – 3 times with PBS, cells were either grown for 72 h in drug-free media (cytotoxicity) or harvested with 50% methanol (uptake assay).

4.1.8. SPARC upregulation in HCC1143 cells

HCC1143 cells (confluency of approximately 50%) were pre-treated with decitabine solution in DMSO (5 μM; Shenzhen Chemical Co. Ltd., Shanghai, China) or DMSO (as a control) for three consecutive days. After 24 h, cells were either harvested for verifying the upregulation of hSPARC (by immunoblotting analysis) or re-plated on 96-well-plates. After 24 h, the HCC1143 cells were treated with CFZ-alb NC or CFZ solution for 2 h. After washing 2 – 3 times with PBS, cells grown for 72 h in drug-free media were accessed cytotoxicity.

4.2. Supporting table

Table S1. Theoretical calculation of the amount of human serum albumin (HSA) needed for coating CFZ NCs.

Surface area of occupying HSA molecule [1]	39 nm^2
Total surface area of each NC particle	(352 nm × 58 nm) × 4 + (58 nm × 58 nm) × 2 = 8.84×10^4 nm^2
Theoretical maximum number of HSA on each NC particle	approximately 2,267
Volume of each NC particle	352 nm × 58 nm × 58 nm = 1.18×10^6 nm^3
Density of CFZ	1.2 g/cm^3
For CFZ-alb NC	
74% CFZ	(74 g/1.2 g cm^{-3}) × (10^{21} nm^3 cm^{-3}) / (1.18 x 10^6 nm^3) = $5.23x10^{16}$ NC
20% HSA	(20 g/66,437 g mol^{-3}) × (6.022 x 10^{23} molecules/mol) = $1.81x10^{20}$ HSA molecules
Numbers of HSA per NC particle	3,468 (**153% coverage**)

4.3. Supporting figures

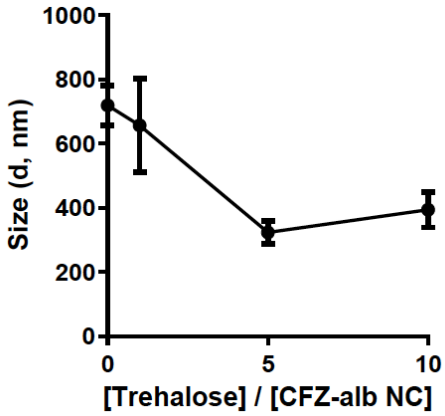

Figure S1. (related to Figure 1) The particle size of CFZ-alb NC reconstituted after lyophilization, measured by DLS. Trehalose was added at varying weight ratios prior to lyophilization.

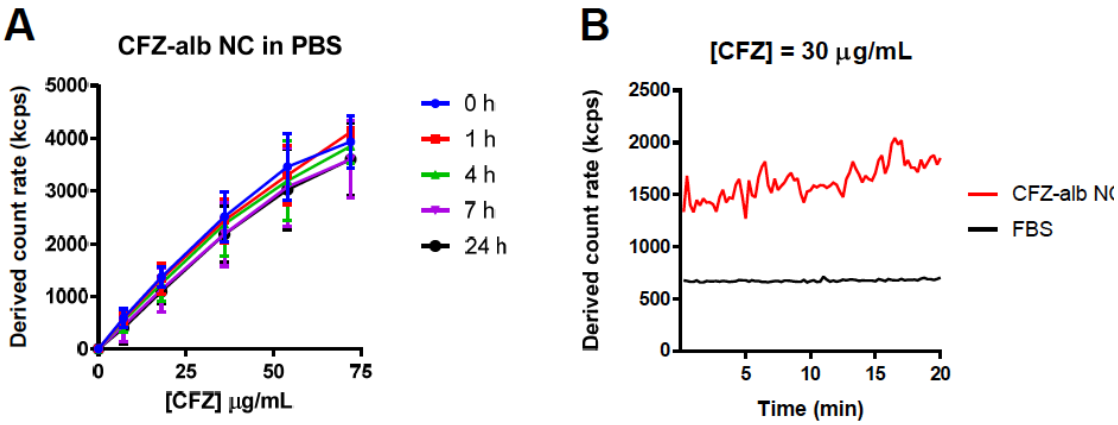

Figure S2. (related to Figure 2). (A) The derived count rates of CFZ-alb NC in PBS maintained linear relationships over the concentrations ranges tested (7.2 to 72 µg/mL CFZ) for 24 h. (B) The derived count rates of CFZ-alb NC (equivalent to 30 µg/mL CFZ, in the presence of undiluted FBS) were obtained by continuous monitoring for the first 20 min. Mean values ± SD.

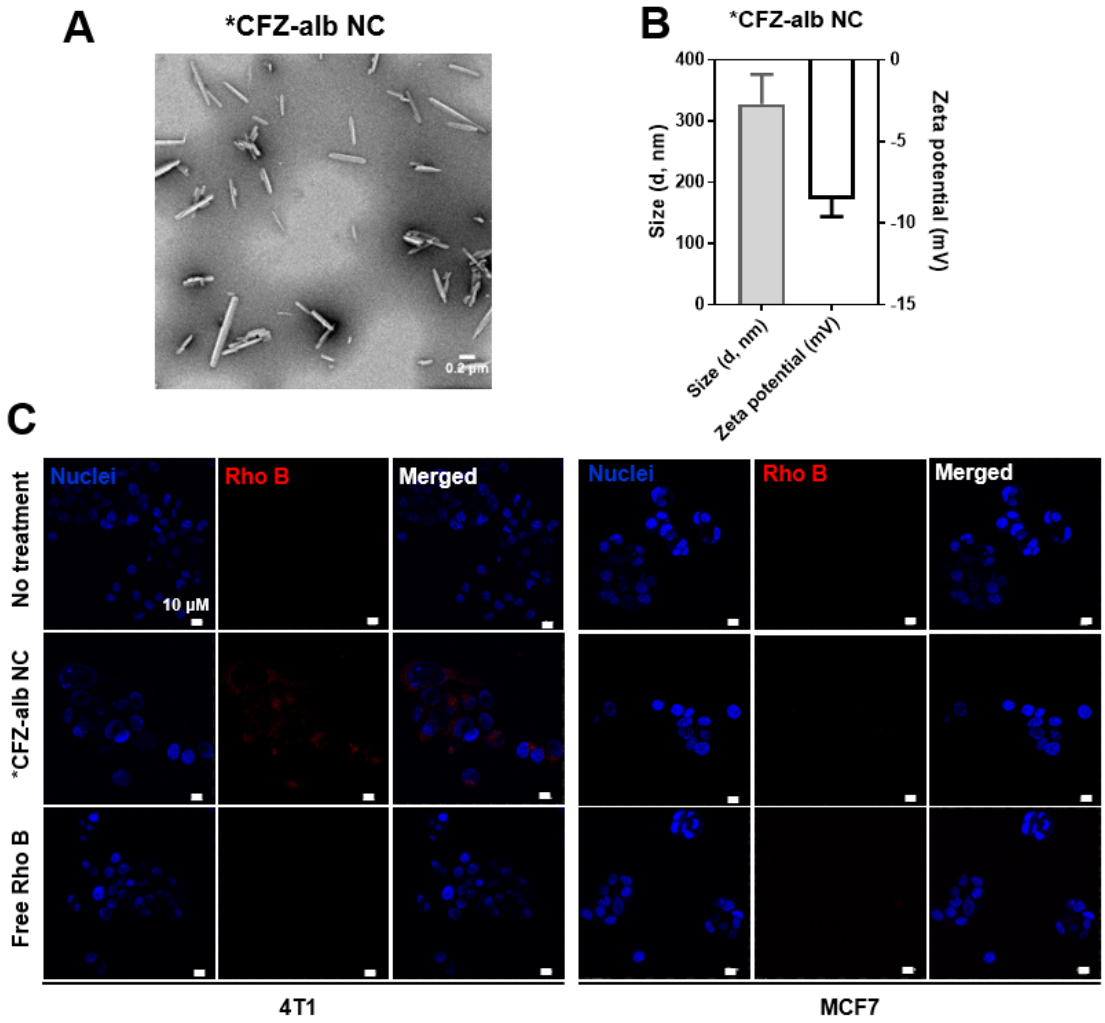

Figure S3. (related to Figure 3). (A) Representative TEM image of rhodamine B-labeled CFZ-alb NC (*CFZ-alb NC) (B) The average size and zeta potential of *CFZ-alb NC, measured by DLS. (C) Cellular uptake of *CFZ-alb NC in breast cancer cell lines (4T1 and MCF7). Representative confocal microscopy images following 2 h incubation with *CFZ-alb NC (30 μg/mL CFZ). Free rhodamine B (Rho B) was used as a negative control. Scale bar = 10 μm.

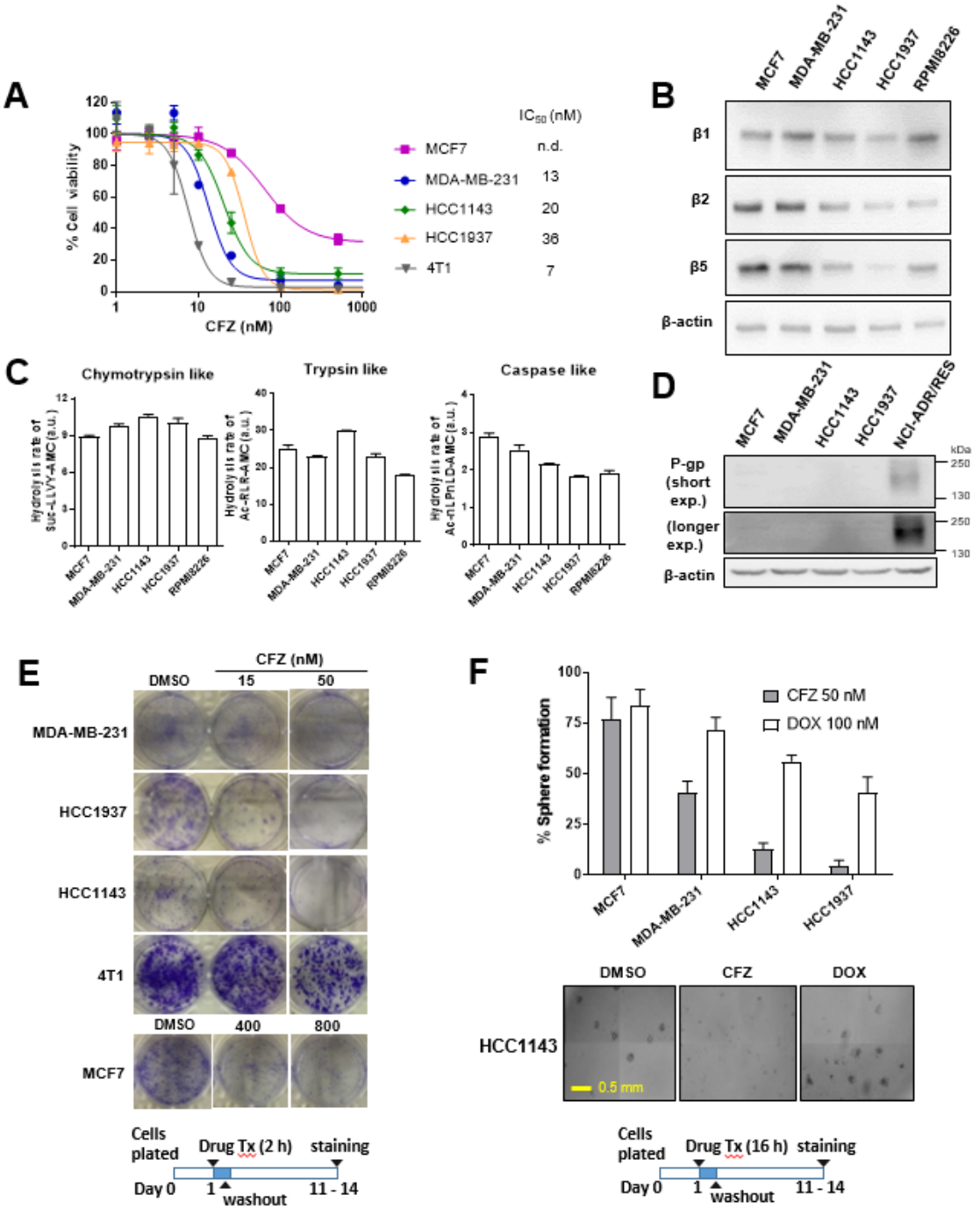

Figure S4. (related to Figure 4) The sensitivity of breast cancer cell lines to CFZ. (A) The cytotoxic effects of CFZ in breast cancer cell lines following continues treatment for 72 h. (IC_{50}, half maximal inhibitory concentration; n.d., not determined) (B and C) The expression of proteasome catalytic subunits (β1, β2, and β5) and proteasomal activities in breast cancer cell lines. Human multiple myeloma RPMI8226 cells were used as a positive control. (D) The expression level of P-glycoprotein (P-gp) in breast cancer cell lines. NCI-ADR/RES cells were used as a positive control. (E and F) The inhibitory effect of CFZ on 2D-colony (E) and 3D spheroid (F) formation in breast cancer cell lines after 2 h and 16 h incubation, respectively, followed by the maintenance in drug-free media for 11 – 14 days. Representative images of the spheroids formed in HCC1143 cells. Mean values ± SD.

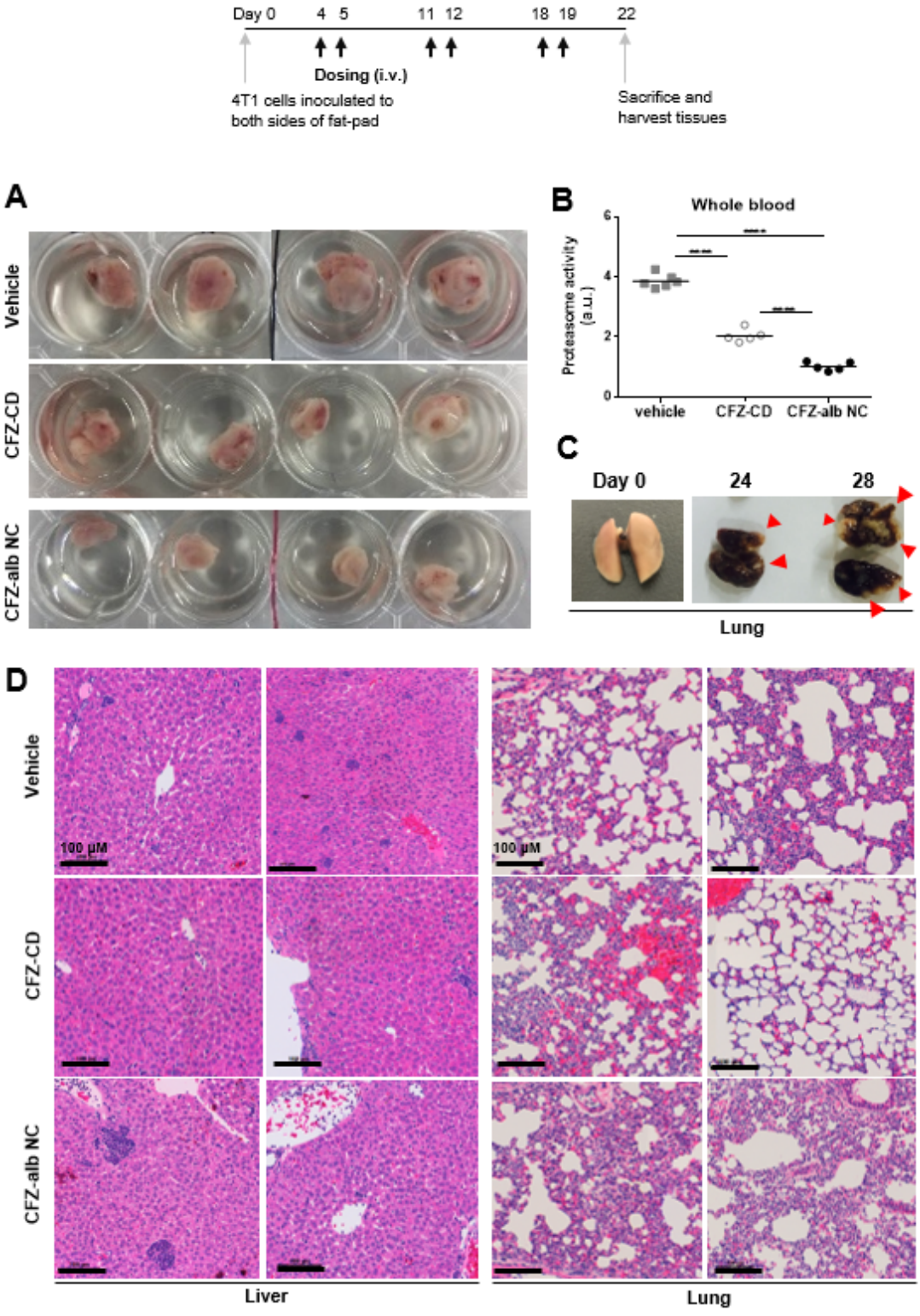

Figure S5. (related to Figure 5) (A) Representative images of tumor harvested on day 22. (3 days following the last injection) (B) The proteasome activity from whole blood collected on day 22. One-way ANOVA followed by Tukey's *post hoc* test. ****$p < 0.0001$ (a.u.; arbitrary units). (C) Representative images of lung harvested on days 24 and 28 after inoculation of 4T1 cells in BALB/c mice. ▲ indicated metastasis lung nodules. (D) Histological examination of liver and lung tissues (H & E staining; representative images, scale bar = 100 μm). Mean values ± SD.

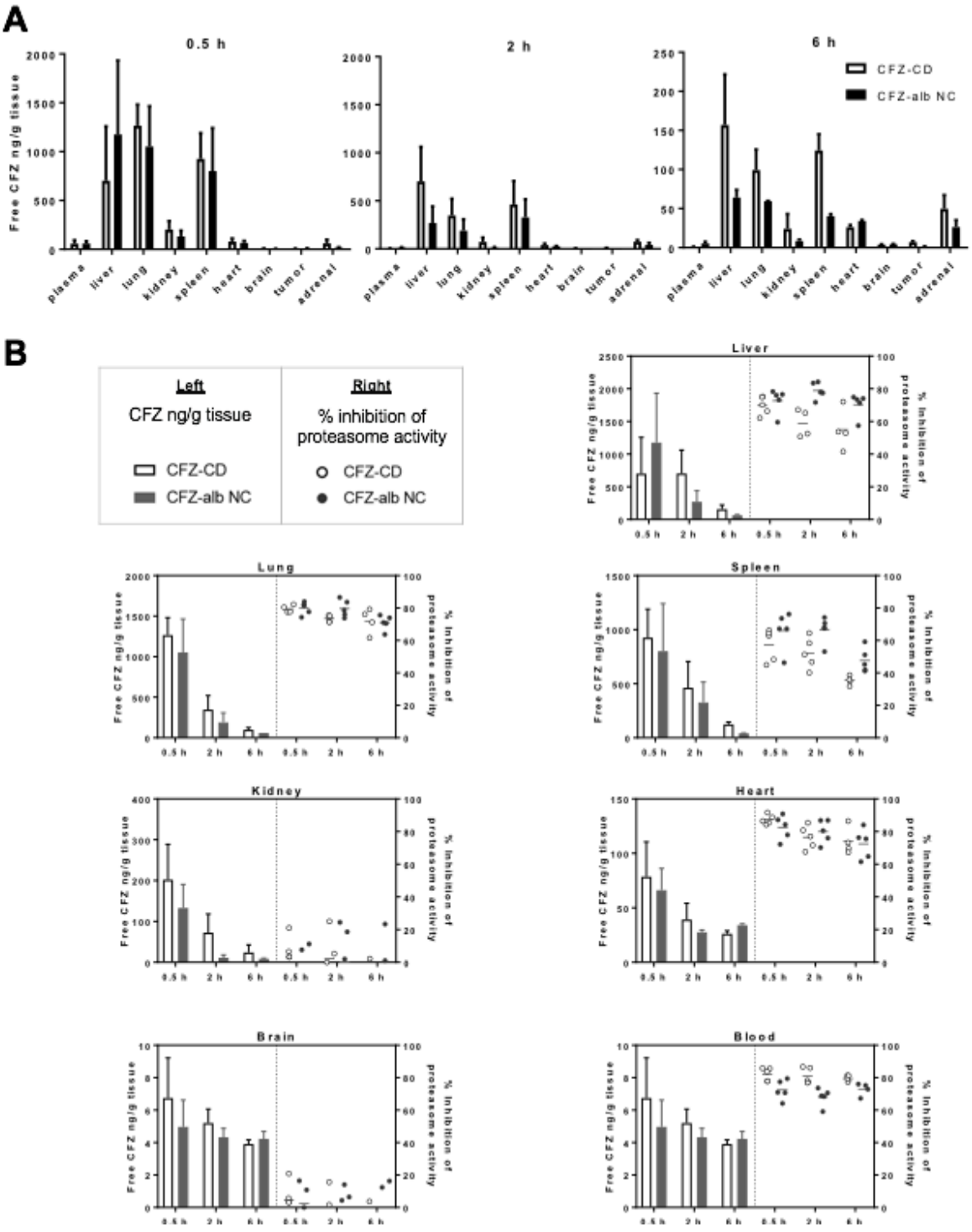

Figure S6. (related to Figure 6) (A) The amount of CFZ per gram tissue in the major organs. (B) The amount of CFZ (left y-axis, shown as a bar graph) and the inhibitory extent of the proteasomal activity (right y-axis, shown as a dot plots) in the respective tissues. Mean values ± SD.

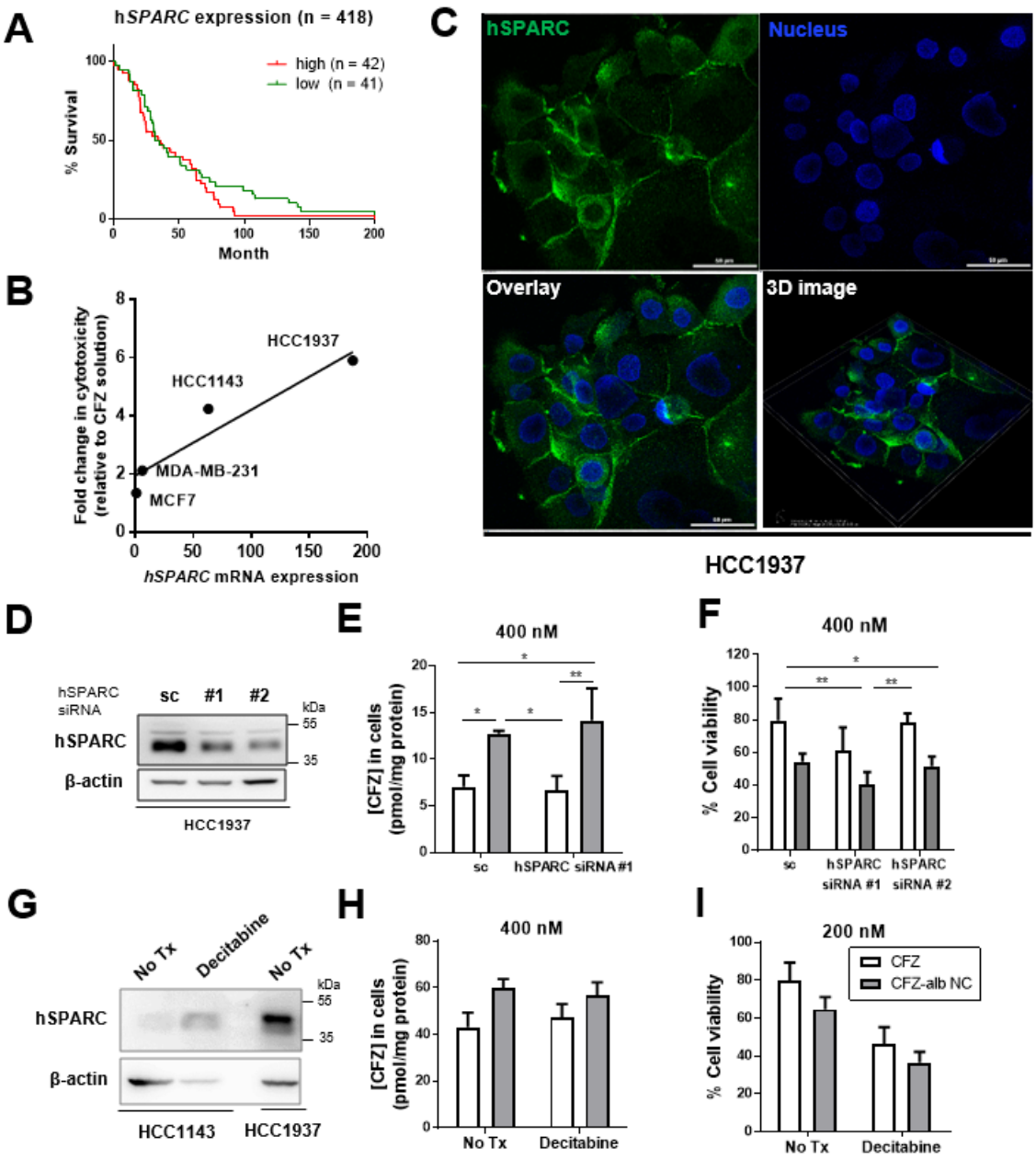

Figure S7. (related to Figure 7). (A) Kaplan-Meier curves depicting the overall survival of breast cancer patients with the low and high expression levels of h*SPARC* (n = 418, extracted from [3]). (B) Correlation between the mRNA expression level of *hSPARC* and the extent of enhanced cytotoxicity of CFZ-alb NC relative to unformulated CFZ solution at the concentration of 400 nM. (C) SPARC expression on the plasma membrane in HCC1937 cells. Green: anti-human SPARC antibody. Blue: nuclei stained with Hoechst 33342. (D) hSPARC expression in HCC1937 cells transfected with scrambled (sc) siRNA (negative control) or two different siRNAs targeting hSPARC. (E & F) The amount of CFZ (E) and cell viability (F) in HCC1937 cells transfected with hSPARC-targeting siRNA following the exposure to CFZ-alb NC or CFZ solution. Two-way ANOVA followed by Tukey's *post hoc* test (H) or Sidak's *post hoc* test (I). (G) hSPARC expression in HCC1143 cells pre-treated with decitabine. (H & I) The amount of CFZ (H) and cell viability (I) in HCC1143 cells which showed a modest upregulation of SPARC following the exposure to CFZ-alb NC or CFZ solution. $*p < 0.0332$, $**p < 0.0021$. Mean values ± SD.

CONCLUSION

With the clinical successes of three FDA-approved proteasome inhibitor (PI) drugs (bortezomib, BTZ; carfilzomib, CFZ; ixazomib, IXZ), the PI therapy is firmly established as a mainstay for the treatment of multiple myeloma (MM) and other hematological malignancies. Yet, there remains much room for further improvement, especially with regards to drug resistance (intrinsic and acquired), poor efficacy against solid cancers and adverse effects (via on-target and off-target interactions). For CFZ, its pharmacokinetic aspects (namely, rapid metabolic inactivation and short circulation time) have also been suspected as a factor limiting its efficacy against solid cancer. To improve upon existing PI drugs, a number of next-generation PIs are currently under clinical and preclinical development. With data accumulating from new PI drug candidates, it has become increasingly evident that the clinical efficacy of PI drugs is impacted not only by their inhibitory potency, but also by the mode, extent and duration of proteasome inhibition. Moving forward, a careful examination of the pharmacokinetic (PK) and pharmacodynamic (PD) profiles of PI drug candidates may provide important insights in bridging the current gap between initial preclinical results and eventual clinical outcomes.

Many of the oncology-based nanoformulations are designed to enhance the drug delivery to tumor tissues, thus broadening the therapeutic window. In this thesis work, both of novel CFZ nanoformulations (polymer micelle-based formulation, CFZ-PM (Chapter I); nanocrystal with albumin coating, CFZ-alb NC (Chapter II)) improved metabolic stability *in vitro*. In the case of CFZ-PM, the improvement observed *in vitro* however did not yield a similar improvement *in vivo* (in terms of plasma PK profiles and anticancer efficacy in a mouse model carrying lung cancer xenografts). The lack of translatability from *in vitro* to *in vivo* may be attributed to multiple factors, but it would be important to keep in mind that *in vitro* results may not predict the *in vivo* performances of nanomedicine-based chemotherapeutics (especially, the stability in circulation and drug distribution at the tissue/cellular levels).

So far, the accumulating body of information suggests that novel approaches including previously unexplored structural scaffolds may address limitations of PIs and further expand the utility

of existing PI drugs harboring peptide scaffold. As an approach to improve bio- and/or physico-chemical properties of peptide-based drugs, macrocyclization (yielding so-called constrained peptides) can be applied to CFZ or next-generation PI drug candidates. Macrocyclization of peptide-based compounds may improve the plasma stability of peptide- or peptidomimetic-based small molecules compared to linear peptides [155][DR Cary et al., J-STAGE, 2017]. In an attempt to develop orally available and metabolically stable PIs, a recent report synthesized the structurally diverse PI-derived macrocyclic peptides containing epoxyketone pharmacophore and the compounds displayed superior *in vivo* metabolic stability with potent proteasome inhibition [156]. Additionally, alternative targets in the ubiquitin-proteasome system (other than the catalytic subunits of the proteasome) present promising therapeutic potential and preclinical evaluation of compounds targeting such targets is underway. In particular, deubiquitinases (DUBs), an essential component in the UPS, have emerged as a novel target in cancer therapy, especially for cancers refractory to existing PI drugs. These efforts may yield therapeutic agents targeting non-proteasomal components of the UPS, used on their own or in combination with PI drugs.

In this thesis work, our efforts of developing CFZ nanoformulations (i.e., polymer micelles and nanocrystals coated with albumin) did not achieve the marked efficacy against lung and breast cancer falling short of our initial expectations. However, other drug delivery systems may still offer further improvements of the pharmacokinetics, biodistribution and pharmacodynamics of CFZ. In exploring other drug delivery systems, it would be important to consider the exposure and release profiles (the extent and kinetics) of the drug in circulation and in tumor tissues. With continuing efforts, it is hoped that next-generation PIs with improved pharmacokinetic and pharmacodynamic profiles will eventually bring therapeutic benefits to patients with MM as well as other types of cancer.

REFERENCES

1. Schmidt, M. and D. Finley, *Regulation of proteasome activity in health and disease.* Biochim Biophys Acta, 2014. **1843**(1): p. 13-25.
2. Dick, T.P., et al., *Contribution of proteasomal beta-subunits to the cleavage of peptide substrates analyzed with yeast mutants.* J Biol Chem, 1998. **273**(40): p. 25637-46.
3. Rabl, J., et al., *Mechanism of gate opening in the 20S proteasome by the proteasomal ATPases.* Mol Cell, 2008. **30**(3): p. 360-8.
4. Huang, X. and V.M. Dixit, *Drugging the undruggables: exploring the ubiquitin system for drug development.* Cell Res, 2016. **26**(4): p. 484-98.
5. Cohen, P. and M. Tcherpakov, *Will the ubiquitin system furnish as many drug targets as protein kinases?* Cell, 2010. **143**(5): p. 686-93.
6. Manasanch, E.E. and R.Z. Orlowski, *Proteasome inhibitors in cancer therapy.* Nat Rev Clin Oncol, 2017. **14**(7): p. 417-433.
7. Nikesitch, N. and S.C. Ling, *Molecular mechanisms in multiple myeloma drug resistance.* J Clin Pathol, 2016. **69**(2): p. 97-101.
8. Buac, D., et al., *From bortezomib to other inhibitors of the proteasome and beyond.* Curr Pharm Des, 2013. **19**(22): p. 4025-38.
9. Roeten, M.S.F., J. Cloos, and G. Jansen, *Positioning of proteasome inhibitors in therapy of solid malignancies.* Cancer Chemother Pharmacol, 2018. **81**(2): p. 227-243.
10. Huang, Z., et al., *Efficacy of therapy with bortezomib in solid tumors: a review based on 32 clinical trials.* Future Oncol, 2014. **10**(10): p. 1795-807.
11. Weinstein, J.N., et al., *An information-intensive approach to the molecular pharmacology of cancer.* Science, 1997. **275**(5298): p. 343-9.
12. Adams, J., et al., *Proteasome inhibitors: a novel class of potent and effective antitumor agents.* Cancer Res, 1999. **59**(11): p. 2615-22.
13. Sanchez-Serrano, I., *Success in translational research: lessons from the development of bortezomib.* Nat Rev Drug Discov, 2006. **5**(2): p. 107-14.
14. Orlowski, M., *The multicatalytic proteinase complex, a major extralysosomal proteolytic system.* Biochemistry, 1990. **29**(45): p. 10289-97.
15. Vinitsky, A., et al., *Inhibition of the chymotrypsin-like activity of the pituitary multicatalytic proteinase complex.* Biochemistry, 1992. **31**(39): p. 9421-8.
16. Mitch, W.E. and A.L. Goldberg, *Mechanisms of muscle wasting. The role of the ubiquitin-proteasome pathway.* N Engl J Med, 1996. **335**(25): p. 1897-905.
17. Adams, J., et al., *Potent and selective inhibitors of the proteasome: dipeptidyl boronic acids.* Bioorg Med Chem Lett, 1998. **8**(4): p. 333-8.
18. Teicher, B.A., et al., *The proteasome inhibitor PS-341 in cancer therapy.* Clin Cancer Res, 1999. **5**(9): p. 2638-45.
19. Groll, M., et al., *Crystal structure of the boronic acid-based proteasome inhibitor bortezomib in complex with the yeast 20S proteasome.* Structure, 2006. **14**(3): p. 451-6.
20. Chen, D., et al., *Bortezomib as the first proteasome inhibitor anticancer drug: current status and future perspectives.* Curr Cancer Drug Targets, 2011. **11**(3): p. 239-53.
21. Hideshima, T., et al., *The proteasome inhibitor PS-341 inhibits growth, induces apoptosis, and overcomes drug resistance in human multiple myeloma cells.* Cancer Res, 2001. **61**(7): p. 3071-6.
22. Nawrocki, S.T., et al., *The proteasome inhibitor bortezomib enhances the activity of docetaxel in orthotopic human pancreatic tumor xenografts.* Mol Cancer Ther, 2004. **3**(1): p. 59-70.
23. Adams, J., *Development of the Proteasome Inhibitor PS-341.* Oncologist, 2002. **7**(1): p. 9-16.
24. Kane, R.C., et al., *Velcade: U.S. FDA approval for the treatment of multiple myeloma progressing on prior therapy.* Oncologist, 2003. **8**(6): p. 508-13.
25. Richardson, P.G., et al., *Bortezomib or high-dose dexamethasone for relapsed multiple myeloma.* N Engl J Med, 2005. **352**(24): p. 2487-98.
26. San Miguel, J.F., et al., *Bortezomib plus melphalan and prednisone for initial treatment of multiple myeloma.* N Engl J Med, 2008. **359**(9): p. 906-17.

27. Teicher, B.A. and K.C. Anderson, *CCR 20th anniversary commentary: In the beginning, there was PS-341.* Clin Cancer Res, 2015. **21**(5): p. 939-41.
28. Kupperman, E., et al., *Evaluation of the proteasome inhibitor MLN9708 in preclinical models of human cancer.* Cancer Res, 2010. **70**(5): p. 1970-80.
29. Chauhan, D., et al., *A novel orally active proteasome inhibitor induces apoptosis in multiple myeloma cells with mechanisms distinct from Bortezomib.* Cancer Cell, 2005. **8**(5): p. 407-19.
30. Zhou, H.J., et al., *Design and Synthesis of an Orally Bioavailable and Selective Peptide Epoxyketone Proteasome Inhibitor (PR-047).* J Med Chem, 2009.
31. Demo, S.D., et al., *Antitumor activity of PR-171, a novel irreversible inhibitor of the proteasome.* Cancer Res, 2007. **67**(13): p. 6383-91.
32. Chauhan, D., et al., *In vitro and in vivo selective antitumor activity of a novel orally bioavailable proteasome inhibitor MLN9708 against multiple myeloma cells.* Clin Cancer Res, 2011. **17**(16): p. 5311-21.
33. Caravita, T., et al., *Bortezomib: efficacy comparisons in solid tumors and hematologic malignancies.* Nat Clin Pract Oncol, 2006. **3**(7): p. 374-87.
34. Dorsey, B.D., et al., *Discovery of a potent, selective, and orally active proteasome inhibitor for the treatment of cancer.* J Med Chem, 2008. **51**(4): p. 1068-72.
35. Zhang, L. and D.E. Mager, *Physiologically-based pharmacokinetic modeling of target-mediated drug disposition of bortezomib in mice.* J Pharmacokinet Pharmacodyn, 2015. **42**(5): p. 541-52.
36. Papandreou, C.N., et al., *Phase I trial of the proteasome inhibitor bortezomib in patients with advanced solid tumors with observations in androgen-independent prostate cancer.* J Clin Oncol, 2004. **22**(11): p. 2108-21.
37. Leveque, D., M.C. Carvalho, and F. Maloisel, *Review. Clinical pharmacokinetics of bortezomib.* In Vivo, 2007. **21**(2): p. 273-8.
38. Uttamsingh, V., et al., *Relative contributions of the five major human cytochromes P450, 1A2, 2C9, 2C19, 2D6, and 3A4, to the hepatic metabolism of the proteasome inhibitor bortezomib.* Drug Metab Dispos, 2005. **33**(11): p. 1723-8.
39. Pekol, T., et al., *Human metabolism of the proteasome inhibitor bortezomib: identification of circulating metabolites.* Drug Metab Dispos, 2005. **33**(6): p. 771-7.
40. Venkatakrishnan, K., et al., *Effect of the CYP3A inhibitor ketoconazole on the pharmacokinetics and pharmacodynamics of bortezomib in patients with advanced solid tumors: a prospective, multicenter, open-label, randomized, two-way crossover drug-drug interaction study.* Clin Ther, 2009. **31 Pt 2**: p. 2444-58.
41. Hellmann, A., et al., *Effect of cytochrome P450 3A4 inducers on the pharmacokinetic, pharmacodynamic and safety profiles of bortezomib in patients with multiple myeloma or non-Hodgkin's lymphoma.* Clin Pharmacokinet, 2011. **50**(12): p. 781-91.
42. Quinn, D.I., et al., *Effect of the cytochrome P450 2C19 inhibitor omeprazole on the pharmacokinetics and safety profile of bortezomib in patients with advanced solid tumours, non-Hodgkin's lymphoma or multiple myeloma.* Clin Pharmacokinet, 2009. **48**(3): p. 199-209.
43. Kaygusuz, I., et al., *Bortezomib in patients with renal impairment.* Hematology, 2011. **16**(4): p. 200-8.
44. Williamson, M.J., et al., *The relationship among tumor architecture, pharmacokinetics, pharmacodynamics, and efficacy of bortezomib in mouse xenograft models.* Mol Cancer Ther, 2009. **8**(12): p. 3234-43.
45. Ashley, J.D., et al., *Liposomal bortezomib nanoparticles via boronic ester prodrug formulation for improved therapeutic efficacy in vivo.* J Med Chem, 2014. **57**(12): p. 5282-92.
46. Shen, S., et al., *Delivery of bortezomib with nanoparticles for basal-like triple-negative breast cancer therapy.* J Control Release, 2015. **208**: p. 14-24.
47. Swami, A., et al., *Engineered nanomedicine for myeloma and bone microenvironment targeting.* Proc Natl Acad Sci U S A, 2014. **111**(28): p. 10287-92.
48. Richardson, P.G., et al., *A phase 2 study of bortezomib in relapsed, refractory myeloma.* N Engl J Med, 2003. **348**(26): p. 2609-17.
49. Vij, R., et al., *An open-label, single-arm, phase 2 (PX-171-004) study of single-agent carfilzomib in bortezomib-naive patients with relapsed and/or refractory multiple myeloma.* Blood, 2012. **119**(24): p. 5661-70.
50. Kumar, S. and S.V. Rajkumar, *Many facets of bortezomib resistance/susceptibility.* Blood, 2008. **112**(6):

p. 2177-8.
51. McConkey, D.J. and K. Zhu, *Mechanisms of proteasome inhibitor action and resistance in cancer.* Drug Resist Updat, 2008. **11**(4-5): p. 164-79.
52. Arastu-Kapur, S., et al., *Nonproteasomal targets of the proteasome inhibitors bortezomib and carfilzomib: a link to clinical adverse events.* Clin Cancer Res, 2011. **17**(9): p. 2734-43.
53. Voortman, J., A. Checinska, and G. Giaccone, *The proteasomal and apoptotic phenotype determine bortezomib sensitivity of non-small cell lung cancer cells.* Mol Cancer, 2007. **6**: p. 73.
54. Moreau, P., et al., *Subcutaneous versus intravenous administration of bortezomib in patients with relapsed multiple myeloma: a randomised, phase 3, non-inferiority study.* Lancet Oncol, 2011. **12**(5): p. 431-40.
55. Bringhen, S., et al., *Efficacy and safety of once-weekly bortezomib in multiple myeloma patients.* Blood, 2010. **116**(23): p. 4745-53.
56. Reeder, C.B., et al., *Once- versus twice-weekly bortezomib induction therapy with CyBorD in newly diagnosed multiple myeloma.* Blood, 2010. **115**(16): p. 3416-7.
57. Herndon, T.M., et al., *U.s. Food and Drug Administration approval: carfilzomib for the treatment of multiple myeloma.* Clin Cancer Res, 2013. **19**(17): p. 4559-63.
58. Meng, L., et al., *Epoxomicin, a potent and selective proteasome inhibitor, exhibits in vivo antiinflammatory activity.* Proc Natl Acad Sci U S A, 1999. **96**(18): p. 10403-8.
59. Elofsson, M., et al., *Towards subunit-specific proteasome inhibitors: synthesis and evaluation of peptide alpha',beta'-epoxyketones.* Chem Biol, 1999. **6**(11): p. 811-22.
60. Kim, K.B., et al., *Proteasome inhibition by the natural products epoxomicin and dihydroeponemycin: insights into specificity and potency.* Bioorg Med Chem Lett, 1999. **9**(23): p. 3335-40.
61. Schrader, J., et al., *The inhibition mechanism of human 20S proteasomes enables next-generation inhibitor design.* Science, 2016. **353**(6299): p. 594-8.
62. Carmony, K., W. Lee, and K.B. Kim, *High-Resolution Snapshots of Proteasome Inhibitors in Action Revise Inhibition Paradigms and Inspire Next-Generation Inhibitor Design.* Chembiochem, 2016. **17**(22): p. 2115-2117.
63. Redic, K., *Carfilzomib: a novel agent for multiple myeloma.* J Pharm Pharmacol, 2013. **65**(8): p. 1095-106.
64. Reece, D.E., et al., *Pharmacokinetic and pharmacodynamic study of two doses of bortezomib in patients with relapsed multiple myeloma.* Cancer Chemother Pharmacol, 2011. **67**(1): p. 57-67.
65. Moreau, P., et al., *Pharmacokinetic, pharmacodynamic and covariate analysis of subcutaneous versus intravenous administration of bortezomib in patients with relapsed multiple myeloma.* Clin Pharmacokinet, 2012. **51**(12): p. 823-9.
66. Alsina, M., et al., *A phase I single-agent study of twice-weekly consecutive-day dosing of the proteasome inhibitor carfilzomib in patients with relapsed or refractory multiple myeloma or lymphoma.* Clin Cancer Res, 2012. **18**(17): p. 4830-40.
67. Wang, Z., et al., *Clinical pharmacokinetics, metabolism, and drug-drug interaction of carfilzomib.* Drug Metab Dispos, 2013. **41**(1): p. 230-7.
68. Papadopoulos, K.P., et al., *A phase I/II study of carfilzomib 2-10-min infusion in patients with advanced solid tumors.* Cancer Chemother Pharmacol, 2013. **72**(4): p. 861-8.
69. Papadopoulos, K.P., et al., *Phase I study of 30-minute infusion of carfilzomib as single agent or in combination with low-dose dexamethasone in patients with relapsed and/or refractory multiple myeloma.* J Clin Oncol, 2015. **33**(7): p. 732-9.
70. Berenson, J.R., et al., *CHAMPION-1: a phase 1/2 study of once-weekly carfilzomib and dexamethasone for relapsed or refractory multiple myeloma.* Blood, 2016. **127**(26): p. 3360-8.
71. Kumar, S.K., et al., *Phase 1 study of weekly dosing with the investigational oral proteasome inhibitor ixazomib in relapsed/refractory multiple myeloma.* Blood, 2014. **124**(7): p. 1047-55.
72. Richardson, P.G., et al., *Phase 1 study of twice-weekly ixazomib, an oral proteasome inhibitor, in relapsed/refractory multiple myeloma patients.* Blood, 2014. **124**(7): p. 1038-46.
73. Gupta, N., et al., *Switching from body surface area-based to fixed dosing for the investigational proteasome inhibitor ixazomib: a population pharmacokinetic analysis.* Br J Clin Pharmacol, 2015. **79**(5): p. 789-800.
74. Gupta, N., et al., *Population Pharmacokinetic Analysis of Ixazomib, an Oral Proteasome Inhibitor, Including Data from the Phase III TOURMALINE-MM1 Study to Inform Labelling.* Clin Pharmacokinet,

2017. **56**(11): p. 1355-1368.

75. Hewings, D.S., et al., *Activity-based probes for the multicatalytic proteasome.* FEBS J, 2017. **284**(10): p. 1540-1554.
76. Kraus, M., et al., *Activity patterns of proteasome subunits reflect bortezomib sensitivity of hematologic malignancies and are variable in primary human leukemia cells.* Leukemia, 2007. **21**(1): p. 84-92.
77. Ruckrich, T., et al., *Characterization of the ubiquitin-proteasome system in bortezomib-adapted cells.* Leukemia, 2009. **23**(6): p. 1098-105.
78. Kammerl, I.E., et al., *Impairment of Immunoproteasome Function by Cigarette Smoke and in Chronic Obstructive Pulmonary Disease.* Am J Respir Crit Care Med, 2016. **193**(11): p. 1230-41.
79. O'Connor, O.A., et al., *A phase 1 dose escalation study of the safety and pharmacokinetics of the novel proteasome inhibitor carfilzomib (PR-171) in patients with hematologic malignancies.* Clin Cancer Res, 2009. **15**(22): p. 7085-91.
80. Stewart, A.K., et al., *Carfilzomib, lenalidomide, and dexamethasone for relapsed multiple myeloma.* N Engl J Med, 2015. **372**(2): p. 142-52.
81. Dimopoulos, M.A., et al., *Carfilzomib or bortezomib in relapsed or refractory multiple myeloma (ENDEAVOR): an interim overall survival analysis of an open-label, randomised, phase 3 trial.* Lancet Oncol, 2017. **18**(10): p. 1327-1337.
82. Yang, J., et al., *Pharmacokinetics, pharmacodynamics, metabolism, distribution, and excretion of carfilzomib in rats.* Drug Metab Dispos, 2011. **39**(10): p. 1873-82.
83. Badros, A.Z., et al., *Carfilzomib in multiple myeloma patients with renal impairment: pharmacokinetics and safety.* Leukemia, 2013. **27**(8): p. 1707-14.
84. Quach, H., et al., *Pharmacokinetics and safety of carfilzomib in patients with relapsed multiple myeloma and end-stage renal disease (ESRD): an open-label, single-arm, phase I study.* Cancer Chemother Pharmacol, 2017. **79**(6): p. 1067-1076.
85. Korde, N., et al., *Treatment With Carfilzomib-Lenalidomide-Dexamethasone With Lenalidomide Extension in Patients With Smoldering or Newly Diagnosed Multiple Myeloma.* JAMA Oncol, 2015. **1**(6): p. 746-54.
86. Moreau, P., et al., *Oral Ixazomib, Lenalidomide, and Dexamethasone for Multiple Myeloma.* N Engl J Med, 2016. **374**(17): p. 1621-34.
87. Kumar, S.K., et al., *Phase 2 trial of ixazomib in patients with relapsed multiple myeloma not refractory to bortezomib.* Blood Cancer J, 2015. **5**: p. e338.
88. Gupta, N., et al., *Effects of Strong CYP3A Inhibition and Induction on the Pharmacokinetics of Ixazomib, an Oral Proteasome Inhibitor: Results of Drug-Drug Interaction Studies in Patients With Advanced Solid Tumors or Lymphoma and a Physiologically Based Pharmacokinetic Analysis.* J Clin Pharmacol, 2018. **58**(2): p. 180-192.
89. Gupta, N., et al., *Pharmacokinetics of ixazomib, an oral proteasome inhibitor, in solid tumour patients with moderate or severe hepatic impairment.* Br J Clin Pharmacol, 2016. **82**(3): p. 728-38.
90. Petrocca, F., et al., *A genome-wide siRNA screen identifies proteasome addiction as a vulnerability of basal-like triple-negative breast cancer cells.* Cancer Cell, 2013. **24**(2): p. 182-96.
91. Bianchi, G., et al., *The proteasome load versus capacity balance determines apoptotic sensitivity of multiple myeloma cells to proteasome inhibition.* Blood, 2009. **113**(13): p. 3040-9.
92. Ling, S.C., et al., *Response of myeloma to the proteasome inhibitor bortezomib is correlated with the unfolded protein response regulator XBP-1.* Haematologica, 2012. **97**(1): p. 64-72.
93. Verbrugge, S.E., et al., *Inactivating PSMB5 mutations and P-glycoprotein (multidrug resistance-associated protein/ATP-binding cassette B1) mediate resistance to proteasome inhibitors: ex vivo efficacy of (immuno)proteasome inhibitors in mononuclear blood cells from patients with rheumatoid arthritis.* J Pharmacol Exp Ther, 2012. **341**(1): p. 174-82.
94. Franke, N.E., et al., *Impaired bortezomib binding to mutant beta5 subunit of the proteasome is the underlying basis for bortezomib resistance in leukemia cells.* Leukemia, 2012. **26**(4): p. 757-68.
95. Suzuki, E., et al., *Molecular mechanisms of bortezomib resistant adenocarcinoma cells.* PLoS One, 2011. **6**(12): p. e27996.
96. Kale, A.J. and B.S. Moore, *Molecular mechanisms of acquired proteasome inhibitor resistance.* J Med Chem, 2012. **55**(23): p. 10317-27.
97. Ao, L., et al., *Development of peptide-based reversing agents for p-glycoprotein-mediated resistance to carfilzomib.* Mol Pharm, 2012. **9**(8): p. 2197-205.

98. Gutman, D., A.A. Morales, and L.H. Boise, *Acquisition of a multidrug-resistant phenotype with a proteasome inhibitor in multiple myeloma.* Leukemia, 2009. **23**(11): p. 2181-3.
99. Ettari, R., et al., *Immunoproteasome-selective and non-selective inhibitors: A promising approach for the treatment of multiple myeloma.* Pharmacol Ther, 2018. **182**: p. 176-192.
100. Miller, Z., W. Lee, and K.B. Kim, *The immunoproteasome as a therapeutic target for hematological malignancies.* Curr Cancer Drug Targets, 2014. **14**(6): p. 537-48.
101. Kisselev, A.F. and M. Groettrup, *Subunit specific inhibitors of proteasomes and their potential for immunomodulation.* Curr Opin Chem Biol, 2014. **23**: p. 16-22.
102. Basler, M., et al., *The immunoproteasome: a novel drug target for autoimmune diseases.* Clin Exp Rheumatol, 2015. **33**(4 Suppl 92): p. S74-9.
103. Micale, N., et al., *Peptide-based proteasome inhibitors in anticancer drug design.* Med Res Rev, 2014. **34**(5): p. 1001-69.
104. Kisselev, A.F., W.A. van der Linden, and H.S. Overkleeft, *Proteasome inhibitors: an expanding army attacking a unique target.* Chem Biol, 2012. **19**(1): p. 99-115.
105. Kazi, A., et al., *Discovery of a novel proteasome inhibitor selective for cancer cells over non-transformed cells.* Cell Cycle, 2009. **8**(12): p. 1940-51.
106. Lawrence, H.R., et al., *Synthesis and biological evaluation of naphthoquinone analogs as a novel class of proteasome inhibitors.* Bioorg Med Chem, 2010. **18**(15): p. 5576-92.
107. Kazi, A., et al., *Discovery of PI-1840, a novel noncovalent and rapidly reversible proteasome inhibitor with anti-tumor activity.* J Biol Chem, 2014. **289**(17): p. 11906-15.
108. Miller, Z., et al., *Proteasome inhibitors with pyrazole scaffolds from structure-based virtual screening.* J Med Chem, 2015. **58**(4): p. 2036-41.
109. Blackburn, C., et al., *Characterization of a new series of non-covalent proteasome inhibitors with exquisite potency and selectivity for the 20S beta5-subunit.* Biochem J, 2010. **430**(3): p. 461-76.
110. Ge, Y., et al., *Design, synthesis and biological evaluation of novel non-peptide boronic acid derivatives as proteasome inhibitors.* Eur J Med Chem, 2017. **128**: p. 180-191.
111. Otvos, L., Jr. and J.D. Wade, *Current challenges in peptide-based drug discovery.* Front Chem, 2014. **2**: p. 62.
112. Hare, J.I., et al., *Challenges and strategies in anti-cancer nanomedicine development: An industry perspective.* Adv Drug Deliv Rev, 2017. **108**: p. 25-38.
113. Frasco, M.F., et al., *Transferrin surface-modified PLGA nanoparticles-mediated delivery of a proteasome inhibitor to human pancreatic cancer cells.* J Biomed Mater Res A, 2015. **103**(4): p. 1476-84.
114. Su, J., et al., *Catechol polymers for pH-responsive, targeted drug delivery to cancer cells.* J Am Chem Soc, 2011. **133**(31): p. 11850-3.
115. Wang, M., et al., *Tumor extracellular acidity activated "off-on" release of bortezomib from a biocompatible dendrimer.* Biomater Sci, 2015. **3**(3): p. 480-9.
116. Xu, W., et al., *Acid-labile boronate-bridged dextran-bortezomib conjugate with up-regulated hypoxic tumor suppression.* Chem Commun (Camb), 2015. **51**(31): p. 6812-5.
117. Zuccari, G., et al., *Tumor vascular targeted liposomal-bortezomib minimizes side effects and increases therapeutic activity in human neuroblastoma.* J Control Release, 2015. **211**: p. 44-52.
118. Shen, J., et al., *The use of hollow mesoporous silica nanospheres to encapsulate bortezomib and improve efficacy for non-small cell lung cancer therapy.* Biomaterials, 2014. **35**(1): p. 316-26.
119. Mahmoudian, M., H. Valizadeh, and P. Zakeri-Milani, *Bortezomib-loaded solid lipid nanoparticles: preparation, characterization, and intestinal permeability investigation.* Drug Dev Ind Pharm, 2018. **44**(10): p. 1598-1605.
120. Reichel, D., et al., *Tethered polymer nanoassemblies for sustained carfilzomib release and prolonged suppression of proteasome activity.* Ther Deliv, 2016. **7**(10): p. 665-681.
121. Ashley, J.D., et al., *Dual Carfilzomib and Doxorubicin-Loaded Liposomal Nanoparticles for Synergistic Efficacy in Multiple Myeloma.* Mol Cancer Ther, 2016. **15**(7): p. 1452-9.
122. Kang, T., et al., *Nanoparticles Coated with Neutrophil Membranes Can Effectively Treat Cancer Metastasis.* ACS Nano, 2017. **11**(2): p. 1397-1411.
123. Argyriou, A.A., G. Iconomou, and H.P. Kalofonos, *Bortezomib-induced peripheral neuropathy in multiple myeloma: a comprehensive review of the literature.* Blood, 2008. **112**(5): p. 1593-9.
124. Stewart, A.K., et al., *Carfilzomib, lenalidomide, and dexamethasone for relapsed multiple myeloma.* N.

Engl. J. Med., 2015. **372**(2): p. 142-52.

125. Dimopoulos, M.A., et al., *Carfilzomib and dexamethasone versus bortezomib and dexamethasone for patients with relapsed or refractory multiple myeloma (ENDEAVOR): a randomised, phase 3, open-label, multicentre study.* Lancet Oncol, 2016. **17**(1): p. 27-38.
126. Mark, T.M., et al., *High-Dose Carfilzomib and Dexamethasone As First-Line Treatment in Symptomatic Multiple Myeloma.* Blood, 2015. **126**(23): p. 4258-4258.
127. Kim, K.B. and C.M. Crews, *From epoxomicin to carfilzomib: chemistry, biology, and medical outcomes.* Nat. Prod. Rep., 2013. **30**(5): p. 600-4.
128. Yang, J., et al., *Pharmacokinetics, pharmacodynamics, metabolism, distribution, and excretion of carfilzomib in rats.* Drug Metab. Dispos., 2011. **39**(10): p. 1873-82.
129. Deshaies, R.J., *Proteotoxic crisis, the ubiquitin-proteasome system, and cancer therapy.* BMC Biol., 2014. **12**: p. 94.
130. Papadopoulos, K.P., et al., *A phase I/II study of carfilzomib 2-10-min infusion in patients with advanced solid tumors.* Cancer Chemother. Pharmacol., 2013. **72**(4): p. 861-8.
131. Matsumura, Y. and H. Maeda, *A new concept for macromolecular therapeutics in cancer chemotherapy: mechanism of tumoritropic accumulation of proteins and the antitumor agent smancs.* Cancer Res., 1986. **46**(12 Pt 1): p. 6387-92.
132. Biswas, S., et al., *Recent advances in polymeric micelles for anti-cancer drug delivery.* Eur. J. Pharm. Sci., 2016. **83**: p. 184-202.
133. Ao, L., et al., *Polymer micelle formulations of proteasome inhibitor carfilzomib for improved metabolic stability and anticancer efficacy in human multiple myeloma and lung cancer cell lines.* J. Pharmacol. Exp. Ther., 2015. **355**(2): p. 168-73.
134. Jones, M. and J. Leroux, *Polymeric micelles - a new generation of colloidal drug carriers.* Eur. J. Pharm. Biopharm., 1999. **48**(2): p. 101-11.
135. Ashley, J.D., et al., *Liposomal carfilzomib nanoparticles effectively target multiple myeloma cells and demonstrate enhanced efficacy in vivo.* J. Controlled Release, 2014. **196**: p. 113-21.
136. Lee, S.J., et al., *Clinical activity of carfilzomib correlates with inhibition of multiple proteasome subunits: application of a novel pharmacodynamic assay.* Br J Haematol, 2016. **173**(6): p. 884-95.
137. Tanaka, K. and A. Ichihara, *Half-life of proteasomes (multiprotease complexes) in rat liver.* Biochem Biophys Res Commun, 1989. **159**(3): p. 1309-15.
138. Cuervo, A.M., et al., *Degradation of proteasomes by lysosomes in rat liver.* Eur J Biochem, 1995. **227**(3): p. 792-800.
139. Hendil, K.B., *The 19 S multicatalytic "prosome" proteinase is a constitutive enzyme in HeLa cells.* Biochem Int, 1988. **17**(3): p. 471-7.
140. Hayter, J.R., et al., *The subunit structure and dynamics of the 20S proteasome in chicken skeletal muscle.* Mol Cell Proteomics, 2005. **4**(9): p. 1370-81.
141. Murata, S., H. Yashiroda, and K. Tanaka, *Molecular mechanisms of proteasome assembly.* Nat Rev Mol Cell Biol, 2009. **10**(2): p. 104-15.
142. Park, J.E., et al., *A FRET-based approach for identification of proteasome catalytic subunit composition.* Molecular bioSystems 2014. **10**(2): p. 196-200.
143. Hanahan, D. and R.A. Weinberg, *Hallmarks of cancer: the next generation.* Cell, 2011. **144**(5): p. 646-74.
144. Solimini, N.L., J. Luo, and S.J. Elledge, *Non-oncogene addiction and the stress phenotype of cancer cells.* Cell, 2007. **130**(6): p. 986-8.
145. Petrocca, F., et al., *A genome-wide siRNA screen identifies proteasome addiction as a vulnerability of basal-like triple-negative breast cancer cells.* Cancer Cell, 2013. **24**(2): p. 182-96.
146. Adams, J., et al., *Proteasome inhibitors: a novel class of potent and effective antitumor agents.* Cancer Res., 1999. **59**(11): p. 2615-22.
147. Maeda, H., H. Nakamura, and J. Fang, *The EPR effect for macromolecular drug delivery to solid tumors: Improvement of tumor uptake, lowering of systemic toxicity, and distinct tumor imaging in vivo.* Adv. Drug Delivery Rev., 2013. **65**(1): p. 71-9.
148. Cabral, H., et al., *Accumulation of sub-100 nm polymeric micelles in poorly permeable tumours depends on size.* Nat. Nanotechnol., 2011. **6**(12): p. 815-23.
149. Prabhakar, U., et al., *Challenges and key considerations of the enhanced permeability and retention effect for nanomedicine drug delivery in oncology.* Cancer Res., 2013. **73**(8): p. 2412-7.

150. Bae, Y.H. and K. Park, *Targeted drug delivery to tumors: myths, reality and possibility.* J. Controlled Release, 2011. **153**(3): p. 198-205.
151. Lammers, T., et al., *Image-guided and passively tumour-targeted polymeric nanomedicines for radiochemotherapy.* Br. J. Cancer, 2008. **99**(6): p. 900-10.
152. Stapleton, S., D. Jaffray, and M. Milosevic, *Radiation effects on the tumor microenvironment: Implications for nanomedicine delivery.* Adv. Drug Delivery Rev., 2016.
153. Theek, B., et al., *Sonoporation enhances liposome accumulation and penetration in tumors with low EPR.* J. Controlled Release, 2016. **231**: p. 77-85.
154. Mikhail, A.S. and C. Allen, *Poly(ethylene glycol)-b-poly(epsilon-caprolactone) micelles containing chemically conjugated and physically entrapped docetaxel: synthesis, characterization, and the influence of the drug on micelle morphology.* Biomacromolecules, 2010. **11**(5): p. 1273-80.
155. Cary, D.R., et al., *Constrained Peptides in Drug Discovery and Development.* Journal of Synthetic Organic Chemistry, Japan, 2017. **75**(11): p. 1171-1178.
156. Li, D., et al., *Development of Macrocyclic Peptides Containing Epoxyketone with Oral Availability as Proteasome Inhibitors.* J Med Chem, 2018. **61**(20): p. 9177-9204.

Chapter I

1. Argyriou AA, Iconomou G, Kalofonos HP. Bortezomib-induced peripheral neuropathy in multiple myeloma: a comprehensive review of the literature. Blood. 2008. **112**(5): p. 1593-9.
2. Stewart AK, Rajkumar SV, Dimopoulos MA, Masszi T, Spicka I, Oriol A, et al. Carfilzomib, lenalidomide, and dexamethasone for relapsed multiple myeloma. N Engl J Med. 2015. **372**(2): p. 142-52.
3. Dimopoulos MA, Moreau P, Palumbo A, Joshua D, Pour L, Hajek R, et al. Carfilzomib and dexamethasone versus bortezomib and dexamethasone for patients with relapsed or refractory multiple myeloma (ENDEAVOR): a randomised, phase 3, open-label, multicentre study. Lancet Oncol. 2016. **17**(1): p. 27-38.
4. Mark TM, Yadlapati S, Neglyad L, Bourke J, Jayabalan D, Rossi AC, et al. High-Dose Carfilzomib and Dexamethasone As First-Line Treatment in Symptomatic Multiple Myeloma. Blood. 2015. **126**(23): p. 4258.
5. Kim KB, Crews CM. From epoxomicin to carfilzomib: chemistry, biology, and medical outcomes. Nat Prod Rep. 2013. **30**(5): p. 600-4.
6. Yang J, Wang Z, Fang Y, Jiang J, Zhao F, Wong H, et al. Pharmacokinetics, pharmacodynamics, metabolism, distribution, and excretion of carfilzomib in rats. Drug Metab Dispos. 2011. **39**(10): p. 1873-82.
7. Deshaies RJ. Proteotoxic crisis, the ubiquitin-proteasome system, and cancer therapy. BMC Biol. 2014. 12: p. 94.
8. Papadopoulos KP, Burris HA, 3rd, Gordon M, Lee P, Sausville EA, Rosen PJ, et al. A phase I/II study of carfilzomib 2-10-min infusion in patients with advanced solid tumors. Cancer Chemother Pharmacol. 2013. **72**(4): p. 861-8.
9. Matsumura Y, Maeda H. A new concept for macromolecular therapeutics in cancer chemotherapy: mechanism of tumoritropic accumulation of proteins and the antitumor agent smancs. Cancer Res. 1986. **46**(12 Pt 1): p. 6387-92.
10. Biswas S, Kumari P, Lakhani PM, Ghosh B. Recent advances in polymeric micelles for anti-cancer drug delivery. Eur J Pharm Sci. 2016. **83**: p. 184-202.
11. Ao L, Reichel D, Hu D, Jeong H, Kim KB, Bae Y, et al. Polymer micelle formulations of proteasome inhibitor carfilzomib for improved metabolic stability and anticancer efficacy in human multiple myeloma and lung cancer cell lines. J Pharmacol Exp Ther. 2015. **355**(2): p. 168-73.
12. Jones M, Leroux J. Polymeric micelles - a new generation of colloidal drug carriers. Eur J Pharm Biopharm. 1999. **48**(2): p. 101-11.
13. Ashley JD, Stefanick JF, Schroeder VA, Suckow MA, Alves NJ, Suzuki R, et al. Liposomal carfilzomib nanoparticles effectively target multiple myeloma cells and demonstrate enhanced efficacy in vivo. J Controlled Release. 2014. **196**: p. 113-21.
14. Demo SD, Kirk CJ, Aujay MA, Buchholz TJ, Dajee M, Ho MN, et al. Antitumor activity of PR-171, a novel irreversible inhibitor of the proteasome. Cancer research. 2007. **67**(13): p. 6383-91.
15. Lee SJ, Levitsky K, Parlati F, Bennett MK, Arastu-Kapur S, Kellerman L, et al. Clinical activity of

carfilzomib correlates with inhibition of multiple proteasome subunits: application of a novel pharmacodynamic assay. British journal of haematology. 2016. **173**(6): p. 884-95.

16. Tanaka K, Ichihara A. Half-life of proteasomes (multiprotease complexes) in rat liver. Biochemical and biophysical research communications. 1989. **159**(3): p. 1309-15.
17. Cuervo AM, Palmer A, Rivett AJ, Knecht E. Degradation of proteasomes by lysosomes in rat liver. European journal of biochemistry. 1995. **227**(3): p. 792-800.
18. Hendil KB. The 19 S multicatalytic "prosome" proteinase is a constitutive enzyme in HeLa cells. Biochemistry international. 1988. **17**(3): p. 471-7.
19. Hayter JR, Doherty MK, Whitehead C, McCormack H, Gaskell SJ, Beynon RJ. The subunit structure and dynamics of the 20S proteasome in chicken skeletal muscle. Molecular & cellular proteomics : MCP. 2005. **4**(9): p. 1370-81.
20. Murata S, Yashiroda H, Tanaka K. Molecular mechanisms of proteasome assembly. Nat Rev Mol Cell Biol. 2009. **10**(2): p. 104-15.
21. Park JE, Wu Y, Carmony KC, Miller Z, Sharma LK, Lee DM, et al. A FRET-based approach for identification of proteasome catalytic subunit composition. Molecular bioSystems 2014. **10**(2): p. 196-200.
22. Hanahan D, Weinberg RA. Hallmarks of cancer: the next generation. Cell. 2011. **144**(5): p. 646-74.
23. Solimini NL, Luo J, Elledge SJ. Non-oncogene addiction and the stress phenotype of cancer cells. Cell. 2007. **130**(6): p. 986-8.
24. Petrocca F, Altschuler G, Tan SM, Mendillo ML, Yan H, Jerry DJ, et al. A genome-wide siRNA screen identifies proteasome addiction as a vulnerability of basal-like triple-negative breast cancer cells. Cancer Cell. 2013. **24**(2): p. 182-96.
25. Adams J, Palombella VJ, Sausville EA, Johnson J, Destree A, Lazarus DD, et al. Proteasome inhibitors: a novel class of potent and effective antitumor agents. Cancer Res. 1999. **59**(11): p. 2615-22.
26. Maeda H, Nakamura H, Fang J. The EPR effect for macromolecular drug delivery to solid tumors: Improvement of tumor uptake, lowering of systemic toxicity, and distinct tumor imaging in vivo. Adv Drug Delivery Rev. 2013. **65**(1): p. 71-9.
27. Cabral H, Matsumoto Y, Mizuno K, Chen Q, Murakami M, Kimura M, et al. Accumulation of sub-100 nm polymeric micelles in poorly permeable tumours depends on size. Nat Nanotechnol. 2011. **6**(12): p. 815-23.
28. Prabhakar U, Maeda H, Jain RK, Sevick-Muraca EM, Zamboni W, Farokhzad OC, et al. Challenges and key considerations of the enhanced permeability and retention effect for nanomedicine drug delivery in oncology. Cancer Res. 2013. **73**(8): p. 2412-7.
29. Bae YH, Park K. Targeted drug delivery to tumors: myths, reality and possibility. J Controlled Release. 2011. **153**(3): p. 198-205.
30. Lammers T, Subr V, Peschke P, Kuhnlein R, Hennink WE, Ulbrich K, et al. Image-guided and passively tumour-targeted polymeric nanomedicines for radiochemotherapy. Br J Cancer. 2008. **99**(6): p. 900-10.
31. Stapleton S, Jaffray D, Milosevic M. Radiation effects on the tumor microenvironment: Implications for nanomedicine delivery. Adv Drug Delivery Rev. 2016.
32. Theek B, Baues M, Ojha T, Mockel D, Veettil SK, Steitz J, et al. Sonoporation enhances liposome accumulation and penetration in tumors with low EPR. J Controlled Release. 2016. **231**: p. 77-85.
33. Mikhail AS, Allen C. Poly(ethylene glycol)-b-poly(epsilon-caprolactone) micelles containing chemically conjugated and physically entrapped docetaxel: synthesis, characterization, and the influence of the drug on micelle morphology. Biomacromolecules. 2010. **11**(5): p. 1273-80.

Chapter II

1. Ghoncheh, M., Z. Pournamdar, and H. Salehiniya, *Incidence and Mortality and Epidemiology of Breast Cancer in the World.* Asian Pac J Cancer Prev, 2016. **17**(S3): p. 43-6.
2. Ferlay, J., et al., *Cancer incidence and mortality worldwide: sources, methods and major patterns in GLOBOCAN 2012.* Int J Cancer, 2015. **136**(5): p. E359-86.
3. Foulkes, W.D., I.E. Smith, and J.S. Reis-Filho, *Triple-negative breast cancer.* N Engl J Med, 2010. **363**(20): p. 1938-48.
4. Kalimutho, M., et al., *Targeted Therapies for Triple-Negative Breast Cancer: Combating a Stubborn Disease.* Trends Pharmacol Sci, 2015. **36**(12): p. 822-846.
5. Petrocca, F., et al., *A genome-wide siRNA screen identifies proteasome addiction as a vulnerability of*

basal-like triple-negative breast cancer cells. Cancer Cell, 2013. **24**(2): p. 182-96.

6. Weyburne, E.S., et al., *Inhibition of the Proteasome beta2 Site Sensitizes Triple-Negative Breast Cancer Cells to beta5 Inhibitors and Suppresses Nrf1 Activation.* Cell Chem Biol, 2017. **24**(2): p. 218-230.
7. Huang, Z., et al., *Efficacy of therapy with bortezomib in solid tumors: a review based on 32 clinical trials.* Future Oncol, 2014. **10**(10): p. 1795-807.
8. Williamson, M.J., et al., *The relationship among tumor architecture, pharmacokinetics, pharmacodynamics, and efficacy of bortezomib in mouse xenograft models.* Mol Cancer Ther, 2009. **8**(12): p. 3234-43.
9. Vij, R., et al., *An open-label, single-arm, phase 2 study of single-agent carfilzomib in patients with relapsed and/or refractory multiple myeloma who have been previously treated with bortezomib.* Br J Haematol, 2012. **158**(6): p. 739-48.
10. Ashley, J.D., et al., *Liposomal carfilzomib nanoparticles effectively target multiple myeloma cells and demonstrate enhanced efficacy in vivo.* J Control Release, 2014. **196**: p. 113-21.
11. Papadopoulos, K.P., et al., *A phase I/II study of carfilzomib 2-10-min infusion in patients with advanced solid tumors.* Cancer Chemother Pharmacol, 2013. **72**(4): p. 861-8.
12. Ashley, J.D., et al., *Dual Carfilzomib and Doxorubicin-Loaded Liposomal Nanoparticles for Synergistic Efficacy in Multiple Myeloma.* Mol Cancer Ther, 2016. **15**(7): p. 1452-9.
13. Park, J.E., et al., *Polymer micelle formulation for the proteasome inhibitor drug carfilzomib: Anticancer efficacy and pharmacokinetic studies in mice.* PLoS One, 2017. **12**(3): p. e0173247.
14. Reichel, D., et al., *Tethered polymer nanoassemblies for sustained carfilzomib release and prolonged suppression of proteasome activity.* Ther Deliv, 2016. **7**(10): p. 665-681.
15. Kang, T., et al., *Nanoparticles Coated with Neutrophil Membranes Can Effectively Treat Cancer Metastasis.* ACS Nano, 2017. **11**(2): p. 1397-1411.
16. Muller, R.H., S. Gohla, and C.M. Keck, *State of the art of nanocrystals--special features, production, nanotoxicology aspects and intracellular delivery.* Eur J Pharm Biopharm, 2011. **78**(1): p. 1-9.
17. Liu, F., et al., *Targeted cancer therapy with novel high drug-loading nanocrystals.* J Pharm Sci, 2010. **99**(8): p. 3542-51.
18. Lu, Y., Y. Li, and W. Wu, *Injected nanocrystals for targeted drug delivery.* Acta Pharm Sin B, 2016. **6**(2): p. 106-13.
19. Peng, Q., et al., *Preformed albumin corona, a protective coating for nanoparticles based drug delivery system.* Biomaterials, 2013. **34**(33): p. 8521-30.
20. Sleep, D., J. Cameron, and L.R. Evans, *Albumin as a versatile platform for drug half-life extension.* Biochim Biophys Acta, 2013. **1830**(12): p. 5526-34.
21. Park, J., et al., *A Comparative In Vivo Study of Albumin-Coated Paclitaxel Nanocrystals and Abraxane.* Small, 2018. **14**(16): p. e1703670.
22. Stehle, G., et al., *Plasma protein (albumin) catabolism by the tumor itself--implications for tumor metabolism and the genesis of cachexia.* Crit Rev Oncol Hematol, 1997. **26**(2): p. 77-100.
23. Desai, N., et al., *Increased antitumor activity, intratumor paclitaxel concentrations, and endothelial cell transport of cremophor-free, albumin-bound paclitaxel, ABI-007, compared with cremophor-based paclitaxel.* Clin Cancer Res, 2006. **12**(4): p. 1317-24.
24. Guarneri, V., M.V. Dieci, and P. Conte, *Enhancing intracellular taxane delivery: current role and perspectives of nanoparticle albumin-bound paclitaxel in the treatment of advanced breast cancer.* Expert Opin Pharmacother, 2012. **13**(3): p. 395-406.
25. Brufsky, A., *nab-Paclitaxel for the treatment of breast cancer: an update across treatment settings.* Exp Hematol Oncol, 2017. **6**: p. 7.
26. Kudarha, R.R. and K.K. Sawant, *Albumin based versatile multifunctional nanocarriers for cancer therapy: Fabrication, surface modification, multimodal therapeutics and imaging approaches.* Mater Sci Eng C Mater Biol Appl, 2017. **81**: p. 607-626.
27. Gad, S.F., et al., *Enhancing Docetaxel Delivery to Multidrug-Resistant Cancer Cells with Albumin-Coated Nanocrystals.* Mol Pharm, 2018.
28. Park, J., B. Sun, and Y. Yeo, *Albumin-coated nanocrystals for carrier-free delivery of paclitaxel.* J Control Release, 2017. **263**: p. 90-101.
29. Anhalt, K., et al., *Development of a new method to assess nanocrystal dissolution based on light scattering.* Pharm Res, 2012. **29**(10): p. 2887-901.
30. Min, J.S., et al., *Quantitative determination of carfilzomib in mouse plasma by liquid chromatography-*

tandem mass spectrometry and its application to a pharmacokinetic study. J Pharm Biomed Anal, 2017. **146**: p. 341-346.

31. Ciriello, G., et al., *Comprehensive Molecular Portraits of Invasive Lobular Breast Cancer.* Cell, 2015. **163**(2): p. 506-19.
32. Cancer Genome Atlas, N., *Comprehensive molecular portraits of human breast tumours.* Nature, 2012. **490**(7418): p. 61-70.
33. Pawar, V.K., et al., *Pluronic F-127 Stabilised Docetaxel Nanocrystals Improve Apoptosis by Mitochondrial Depolarization in Breast Cancer Cells: Pharmacokinetics and Toxicity Assessment.* J Biomed Nanotechnol, 2015. **11**(10): p. 1747-63.
34. Yuan, F., et al., *Vascular permeability in a human tumor xenograft: molecular size dependence and cutoff size.* Cancer Res, 1995. **55**(17): p. 3752-6.
35. Hobbs, S.K., et al., *Regulation of transport pathways in tumor vessels: role of tumor type and microenvironment.* Proc Natl Acad Sci U S A, 1998. **95**(8): p. 4607-12.
36. Jain, R.K., *Determinants of tumor blood flow: a review.* Cancer Res, 1988. **48**(10): p. 2641-58.
37. Stylianopoulos, T. and R.K. Jain, *Design considerations for nanotherapeutics in oncology.* Nanomedicine, 2015. **11**(8): p. 1893-907.
38. Wilhelm, S., et al., *Analysis of nanoparticle delivery to tumours.* Nature Reviews Materials, 2016. **1**: p. 16014.
39. Toy, R., et al., *Shaping cancer nanomedicine: the effect of particle shape on the in vivo journey of nanoparticles.* Nanomedicine (Lond), 2014. **9**(1): p. 121-34.
40. Riches, A.C., et al., *Blood volume determination in the mouse.* J Physiol, 1973. **228**(2): p. 279-84.
41. Yang, J., et al., *Pharmacokinetics, pharmacodynamics, metabolism, distribution, and excretion of carfilzomib in rats.* Drug Metab Dispos, 2011. **39**(10): p. 1873-82.
42. Chen, Y. and T. Li, *Cellular Uptake Mechanism of Paclitaxel Nanocrystals Determined by Confocal Imaging and Kinetic Measurement.* AAPS J, 2015. **17**(5): p. 1126-34.
43. Zhao, R., et al., *Hybrid nanocrystals: achieving concurrent therapeutic and bioimaging functionalities toward solid tumors.* Mol Pharm, 2011. **8**(5): p. 1985-91.
44. Verbrugge, S.E., et al., *Inactivating PSMB5 mutations and P-glycoprotein (multidrug resistance-associated protein/ATP-binding cassette B1) mediate resistance to proteasome inhibitors: ex vivo efficacy of (immuno)proteasome inhibitors in mononuclear blood cells from patients with rheumatoid arthritis.* J Pharmacol Exp Ther, 2012. **341**(1): p. 174-82.
45. Bielecka, Z.F., et al., *Three-dimensional cell culture model utilization in cancer stem cell research.* Biol Rev Camb Philos Soc, 2017. **92**(3): p. 1505-1520.
46. Dean, M., T. Fojo, and S. Bates, *Tumour stem cells and drug resistance.* Nat Rev Cancer, 2005. **5**(4): p. 275-84.
47. Alsina, M., et al., *A phase I single-agent study of twice-weekly consecutive-day dosing of the proteasome inhibitor carfilzomib in patients with relapsed or refractory multiple myeloma or lymphoma.* Clin Cancer Res, 2012. **18**(17): p. 4830-40.
48. Wang, Z., et al., *Clinical pharmacokinetics, metabolism, and drug-drug interaction of carfilzomib.* Drug Metab Dispos, 2013. **41**(1): p. 230-7.
49. Kocaturk, B. and H.H. Versteeg, *Orthotopic injection of breast cancer cells into the mammary fat pad of mice to study tumor growth.* J Vis Exp, 2015(96).
50. Jakubowiak, A.J., *Evolution of carfilzomib dose and schedule in patients with multiple myeloma: a historical overview.* Cancer Treat Rev, 2014. **40**(6): p. 781-90.
51. Kuhn, D.J., et al., *Potent activity of carfilzomib, a novel, irreversible inhibitor of the ubiquitin-proteasome pathway, against preclinical models of multiple myeloma.* Blood, 2007. **110**(9): p. 3281-90.
52. Schrader, J., et al., *The inhibition mechanism of human 20S proteasomes enables next-generation inhibitor design.* Science, 2016. **353**(6299): p. 594-8.
53. Tanaka, K. and A. Ichihara, *Half-life of proteasomes (multiprotease complexes) in rat liver.* Biochem Biophys Res Commun, 1989. **159**(3): p. 1309-15.
54. Davies, B. and T. Morris, *Physiological parameters in laboratory animals and humans.* Pharm Res, 1993. **10**(7): p. 1093-5.
55. Sigfridsson, K., et al., *Nanocrystal formulations of a poorly soluble drug. 2. Evaluation of nanocrystal liver uptake and distribution after intravenous administration to mice.* Int J Pharm, 2017. **524**(1-2): p. 248-256.

56. Fuhrmann, K., M.A. Gauthier, and J.C. Leroux, *Targeting of injectable drug nanocrystals.* Mol Pharm, 2014. **11**(6): p. 1762-71.
57. Gao, W., et al., *Impact of surfactant treatment of paclitaxel nanocrystals on biodistribution and tumor accumulation in tumor-bearing mice.* J Control Release, 2016. **237**: p. 168-76.
58. Demo, S.D., et al., *Antitumor activity of PR-171, a novel irreversible inhibitor of the proteasome.* Cancer Res, 2007. **67**(13): p. 6383-91.
59. Stella, V.J. and Q. He, *Cyclodextrins.* Toxicol Pathol, 2008. **36**(1): p. 30-42.
60. Perry, C.S., et al., *The binding interaction of synthetic ozonide antimalarials with natural and modified beta-cyclodextrins.* J Pharm Sci, 2006. **95**(1): p. 146-58.
61. Hoang, B., et al., *Docetaxel-carboxymethylcellulose nanoparticles target cells via a SPARC and albumin dependent mechanism.* Biomaterials, 2015. **59**: p. 66-76.
62. Desai, N., et al., *SPARC Expression Correlates with Tumor Response to Albumin-Bound Paclitaxel in Head and Neck Cancer Patients.* Transl Oncol, 2009. **2**(2): p. 59-64.
63. Shao, H., et al., *Improved response to nab-paclitaxel compared with cremophor-solubilized paclitaxel is independent of secreted protein acidic and rich in cysteine expression in non-small cell lung cancer.* J Thorac Oncol, 2011. **6**(6): p. 998-1005.
64. Desai, N.P., et al., *Improved effectiveness of nanoparticle albumin-bound (nab) paclitaxel versus polysorbate-based docetaxel in multiple xenografts as a function of HER2 and SPARC status.* Anticancer Drugs, 2008. **19**(9): p. 899-909.
65. Neesse, A., et al., *SPARC independent drug delivery and antitumour effects of nab-paclitaxel in genetically engineered mice.* Gut, 2014. **63**(6): p. 974-83.
66. Kim, H., et al., *SPARC-Independent Delivery of Nab-Paclitaxel without Depleting Tumor Stroma in Patient-Derived Pancreatic Cancer Xenografts.* Mol Cancer Ther, 2016. **15**(4): p. 680-8.
67. Nagaraju, G.P., et al., *Molecular mechanisms underlying the divergent roles of SPARC in human carcinogenesis.* Carcinogenesis, 2014. **35**(5): p. 967-73.
68. Tai, I.T. and M.J. Tang, *SPARC in cancer biology: its role in cancer progression and potential for therapy.* Drug Resist Updat, 2008. **11**(6): p. 231-46.
69. Hyun, H., et al., *Surface modification of polymer nanoparticles with native albumin for enhancing drug delivery to solid tumors.* Biomaterials, 2018. **180**: p. 206-224.

S1. John, J.M., S. Sivakami, and P.M. Dongre, *Elucidation of structural and functional properties of albumin bound to gold nanoparticles.* J Biomol Struct Dyn, 2016: p. 1-38.
S2. Park, J., B. Sun, and Y. Yeo, *Albumin-coated nanocrystals for carrier-free delivery of paclitaxel.* J Control Release, 2017. **263**: p. 90-101.
S3. Ciriello, G., et al., *Comprehensive Molecular Portraits of Invasive Lobular Breast Cancer.* Cell, 2015. **163**(2): p. 506-19.

요약 (국문 초록)

현재 임상에서 사용되고 있는 2 세대 프로테아좀 저해제인 carfilzomib (CFZ)은 1 세대 프로테아좀 저해제인 bortezomib 과 더불어 다발성 골수종 치료에 매우 획기적인 치료효과를 나타내고 있다. CFZ 은 bortezomib 보다 향상된 항암 효과 뿐만 아니라, 구조적으로 epoxyketone pharmacophore 를 가지고 있어 타겟인 프로테아좀에 보다 선택적으로 반응하여 개선된 안전성 프로파일을 나타낸다. 하지만 수용성이 매우 낮고 1 시간 이내에 체내에서 대부분 소실되는 경향을 보인다는 제한점이 있다. 이는 CFZ 의 펩타이드 backbone 과 epoxyketone 구조가 대사 반응에 취약하여, 체내 대사가 빠른 시간 내에 일어나기 때문에 짧은 반감기의 약물동태학적 특성을 보이는 것으로 사료된다. 이러한 제한점을 극복하기 위해 나노제형을 도입한다면 CFZ 의 약물동태학적 문제점을 해결하고 더 나아가 약물동력학적 특성도 개선할 수 있어 고형암 환자에게 적용 가능성의 향상을 또한 예상하는 바, 본 연구에서는 CFZ 의 새로운 나노제형을 개발하고 고형암 세포주와 실험 동물 모델을 사용하여 항암 효능을 평가 하였다.

이전의 연구에서는 생분해성 폴리머인 폴리에틸렌글리콜과 폴리카프로락톤으로 구성된 폴리머마이셀에 CFZ 을 loading 하였을 경우 in vitro 실험계에서 대사 안정성이 향상되었음 이미 보고 한 바가 있다. 이에 본 논문연구에서는 선행 연구되었던 CFZ 을 포함하는 폴리머마이셀 나노제형(CFZ-PM)의 항암 효능의 향상 여부를 인간 폐암 세포주 H460 가 이식된 마우스 실험 동물 모델에서 평가하여 보았다. CFZ-PM 를 투약한 마우스에서 종양 증식 억제효과가 나타나기는 하였지만, 임상적으로 사용되는 사이클로 덱스트린 기반의 CFZ 제제 (CFZ-CD)보다 우수한 효과를 나타내지는 않았다. 이는 CFZ-PM 의 혈장 약물동태학 프로파일이 CFZ-CD 과 유사하였고, CFZ-PM 이 이종 이식 마우스에서 자란 폐암 조직에 대한 CFZ 의 접근성이 증가하지 못하여 폐암 조직에 존재하는 프로테아좀을 일부만 억제하는 효과를 보였기 때문으로 사료된다. 이러한 결과를 바탕으로, 보다 제제

안정성이 높고 효과적으로 CFZ 을 암조직으로 전달 하기 위해 새로운 나노제형의 CFZ 을 준비하였다.

친수성이 약한 CFZ 은 쉽게 결정화되는 특징을 갖고 있어 체내 안정성이 높은 나노크리스탈 제제로 제형화가 가능하리라는 판단 하에 CFZ 을 나노크리스탈 제제로 개발하였다. 그리고 CFZ 나노크리스탈 제형의 표면은 알부민으로 코팅하여 암세포 및 암세포 주변에 위치한 알부민 결합 단백질과의 상호 작용을 통해 종양에 대한 약물 전달을 향상시킬 전략을 세웠다. 알부민이 코팅 된 CFZ 의 나노크리스탈 제제 (CFZ-alb NC)는 280nm 크기로서 약 80%의 높은 약물 loading content 를 나타내었다. CFZ-alb NC 은 in vitro 와 in vivo 실험계에서 향상된 대사 안정성을 보였을 뿐만 아니라, CFZ solution 과 비교하였을 경우 사람의 여러 유방암 세포주에서 향상된 세포 침투 능력 및 세포 독성 효과를 나타냈다. 또한 CFZ-alb NC 을 마우스의 유방암 세포주인 4T1 가 이식된 BALB/C 마우스 orthotopic 유방암 실험 동물 모델에 투약 하였을 경우 부작용이 없이 CFZ-CD 보다 더 향상된 항암 효과를 나타냈다. 이는 CFZ-alb NC 에 코팅된 알부민이 유방암 조직에 과발현 되어있는 알부민 결합 단백질인 SPARC 가 관여하는 전달 메커니즘에 기반함을 검증하였다. 이 연구를 통해 유방암 치료에 적용 가능한 CFZ-alb NC 나노입자 제제화의 잠재력을 입증하였다.

주요어: 프로테아좀 저해제, carfilzomib, 나노제형, 폴리머마이셀, 나노크리스탈, 알부민, 고형암

학번 : 2016-30511

APPENDIX

Park Curriculum Vitae

JI EUN PARK

jieun.park@snu.ac.kr
College of Pharmacy
Seoul National University (SNU)
1 Gwanak-ro, Gwanak-gu, Bldg 21 Rm 310
Seoul, S. Korea 08826
Tel) 82-2-880-7878

jieun.park.ra@riken.jp
RIKEN Cluster for Science,
Technology and Innovation Hub
1-7-22 Suehiro-cho, Tsurumi, Yokohama,
Kanagawa 230-0045, Japan
Tel) 81-45-503-9211

EDUCATION

2002/03 – 2006/02	B.S. in Pharmacy College of Pharmacy, Sookmyung Women's University, Seoul, S. Korea
2006/03 – 2009/08	M.S. in Pharmacy Division of Medicinal Chemistry and Pharmacognosy, College of Pharmacy, Sookmyung Women's University, Seoul, S. Korea Thesis: *Design and synthesis of D-ring removed estradiol analogues as selective estrogen receptor modulators* Advisor: Hee Do Kim, PhD
2013/01 – 2015/06	M.S. in Pharmaceutical Sciences Division of Drug Discovery, College of Pharmacy, University of Kentucky, USA Thesis: *Development of a FRET-based strategy to identify individual proteasome subtypes and evaluating efficacy of carfilzomib as an anticancer agent in liver cancer cells* Advisors: Kyung Bo Kim, Ph.D.
2016/03 – 2019/02	Graduate Student, Ph.D. candidate Division of Pharmaceutics, College of Pharmacy, Seoul National University, Seoul, S. Korea Thesis: *Pharmacokinetics and pharmacodynamics of novel nanoformulations for the proteasome inhibitor drug carfilzomib: Expanding its therapeutic utility against solid cancers* Advisor: Wooin Lee, Ph.D.

PROFESSIONAL EXPERIENCE

2007/06 – 2009/02	Pharmacist & Research Scientist Department of Pharmacy, CHA Medical Center, Seoul, S. Korea
2011/12 – 2012/11	Research Scientist Pharmaceutical Sciences, College of Pharmacy, University of Kentucky, USA (Advisors: Kyung Bo Kim, Ph.D. & Wooin Lee, Ph.D.)
2015/08 – 2016/02	Research Scientist College of Pharmacy, Seoul National University, Seoul, S. Korea (Advisor: Wooin Lee, Ph.D.)
2018/01 – 2018/02	Short-term research exchange student Department of Industrial and Physical Pharmacy, College of Pharmacy, Purdue University, USA (Advisor: Yoon Yeo, Ph.D.)
2018/07 – present	Visiting Scholar (Pre-doctoral Fellow, the Nagai Foundation Tokyo) Sugiyama Laboratory, RIKEN Baton Zone Program, RIKEN Cluster for Science, Technology and Innovation Hub, Yokohama, Japan (Advisor: Yuichi Sugiyama, Ph.D.)
2019/01 – present	Post-doctoral Position Pharmacokinetic, Dynamics and Metabolism AP-Japan, Sanofi, Tokyo, Japan

PUBLICATIONS

(5 first-authored publications; 11 co-authored publications)

1. Chang M, Park S, Kim J, Jang M, Park J, **Park JE**, Park H, Suh Y, Jeong Y, Park Y, and Kim HD. Silicon switch approach in TRPV1 antagonist MK-056 and its analogues. BioorgMed Chem 18(1):111-116 (**2010**)
2. **Park JE**, Ao L, Miller Z, Kim K, Wu Y, Jang ER, Lee E, Kim KB, and Lee W. *PSMB9* codon 60 polymorphisms have no impact on the activity of the immunoproteasome catalytic subunit β1i expressed in multiple types of solid cancer. PLoS One 8(9):e73732 (**2013**)
3. **Park JE**, Wu Y, Carmony K.C, Miller Z, Sharma L.K, Lee D, Kim DY, Lee W, and Kim KB. A FRET-based approach for identification of proteasome catalytic subunit composition. Mol BioSyst 10(2):196-200 (**2014**)
4. Carmony K.C, Sharma L.K, Lee D, **Park JE**, Lee W, and Kim KB. Elucidating the catalytic subunit composition of distinct proteasome subtypes: A crosslinking approach employing bifunctional activity-based probes. ChemBioChem 16(2):284-292 (**2015**)
5. Min H-Y, Lee S-C, Woo JK, Jung HJ, Park KH, Jeong HM, Hyun SY, Cho J, Lee W, **Park JE**, Kwon SJ, Lee H, Ni X, Shin YK, Johnson FM, Duvic M, and Lee H-Y. Essential role of DNA methyltransferase 1–mediated transcription of Insulin-like Growth Factor 2 in resistance to histone deacetylase inhibitors. Clinical Cancer Research 23(5):1299-1311 (**2016**)
6. Chun S-E, Thakkar N, **Park JE**, Han S, Ryu G, Oh Y, Hahn H, Maeng SH, Lim Y-R, Han BW, and Lee W. The N-terminal region of organic anion transporting polypeptide 1B3 (OATP1B3) plays an essential role in regulating its membrane trafficking. Biochem Pharmacol 131:98-105 (**2017**)
7. **Park JE**, Chun S-E, Reichel D, Min JS, Lee S-C, Han S, Ryoo G, Oh Y, Park S-H, Ryu H-M, Kim KB, Lee H-Y, Bae SK, Bae Y, and Lee W. Polymer micelle formulation for the proteasome inhibitor drug carfilzomib: Anticancer efficacy and pharmacokinetic studies in mice. PLoS One 12(3):e0173247 (**2017**)
8. Min JS, Kim J, Kim JH, Kim D, Zheng YF, **Park JE,** Lee W, and Bae SK. Quantitative determination of carfilzomib in mouse plasma by liquid chromatography–tandem mass spectrometry and its application to a pharmacokinetic study. J Pharm Biomed Anal 146:341-346 (**2017**)
9. Hyung S, Pyeon W, **Park JE**, Song Y-K, and Chung S-J. The conditional stimulation of rat organic cation transporter 2, but not its human ortholog, by mesoridazine: the possibility of the involvement of the high-affinity binding site of the transporter in the stimulation. J Pharm Pharmacol 69(11):1513-1523 (**2017**)
10. **Park JE**, Ryoo G, and Lee W. Alternative splicing: Expanding diversity in major ABC and SLC drug transporters. AAPS J 19(6):1643-1655 (**2017**)
11. Oh Y, Jeong Y-S, Kim M-S, Min JS, Ryoo G, **Park JE**, Jun Y, Song Y-K, Chun S-E, Han S, Bae SK, Chung S-J, and Lee W. Inhibition of organic anion transporting polypeptide 1B1 and 1B3 by betulinic acid: Effects of pre-incubation and albumin in the media. J Pharm Sci S0022-3549(18):30093-5 (**2018)**
12. Gad S, Park J, **Park JE**, Feith G, Tous S, Lee W, and Y Yeo. Enhancing docetaxel delivery to multidrug-resistant cancer cells with albumin-coated nanocrystals. Mol Pharm (**2018)**
13. Park J, **Park JE**, Hedrick VE, Wood KV, Bonham C, Lee W, and Yeo Y. A comparative in vivo study of albumin-coated paclitaxel nanocrystals and abraxane. Small 14(16):e1703670 (**2018**)
14. **Park JE**, Miller Z, Jun Y, Lee W, and Kim KB. Next-generation proteasome inhibitors for cancer therapy. Transl Res (18):30044-6 (**2018**)
15. Hyun H, Park J, Willis K, **Park JE**, Lyle T, Lee W, and Yeo Y. Surface modification of polymer nanoparticles with native albumin for enhancing drug delivery to solid tumors. Biomaterials 180:206-224 **(2018)**
16. Song Y-K, **Park JE**, Oh Y, Hyung S, Jeong Y-S, Kim M-S, Lee W and Chung S-J. Suppression of canine ABCB1 in MDCKII cells unmasks human ABCG2-mediate efflux of olaparib. J Pharm Exp Ther 368(1):79-87 (**2019**)

Under review

- **Park JE**, Park J, Jun Y, Oh Y, Ryoo G, Jeong Y-S, Min JS, Jo JH, Song MG, Kang KW, Bae SK, Yeo Y, and Lee W. Expanding therapeutic utility of carfilzomib for breast cancer therapy by novel albumin-coated nanocrystal formulation. Submitted to J Control Release (Under revision)
- Lee MJ, Miller Z, **Park JE,** Bhattarai D, Lee W, and Kim KB. H727 cells are inherently resistant to the proteasome activity for cell survival and growth. Submitted to Scientific Reports (Under review)
- Lee MJ, Bhattarai D, Yoo ZS; Miller Z; **Park JE**, Lee W, Driscoll, J, and Kim KB. Development of novel epoxyketone-based proteasome inhibitors as a strategy to overcome cancer resistance to carfilzomib and bortezomib. Submitted to J Med Chem (Under review)
- Kwon OS, Lee H, Kong HJ, **Park JE**, Lee W, Kang S, Kim M, Kim W, and Cha HJ. Computational drug repositioning of bortezomib to reverse metastatic effect of GALNT14 in lung cancer. J Clin Investig (Under review)

PRESENTATIONS

Podium

1. Azaisoflavones, D-ring removed estradiols, and phytoestrogens from *Psoralea corylifolia* as novel SERMs. The 2009 Winter Research Presentation of Sookmyung Research Center for Women Diseases, Seoul, S. Korea (Jan 2009)
2. Development of an innovative fluorescence resonance energy transfer (FRET)-based approach to identify different proteasome subtypes. Annual Symposium on Drug Discovery & Development, University of Kentucky, USA (Sep 2013)
3. Albumin-coated nanocrystal formulation of the proteasome inhibitor drug carfilzomib for breast cancer therapy. 2017 Annual Meeting and International Conference of the Korean Society of Pharmaceutical Sciences and Technology, Seoul, S. Korea (Dec 2017, *a recipient of the Best Oral Presentation Award*)

Poster

1. **Park JE,** Jung BI, Song YS and Kim HD. 17 β-Estradiol analogues as selective estrogen receptor modulators. The 2008 Fall International Convention of the Pharmaceutical Society of Korea, Seoul, S. Korea (Oct 2008)
2. **Park JE**, Jung BI, Yeo H, Lee S, Kim D, Yim M, Jeon R, Ryu JH, Song YS and Kim HD. D-ring removed estradiol analogues as selective estrogen receptor modulators. The 2009 Spring International Convention of the Pharmaceutical Society of Korea, Daejeon, S. Korea (May 2009)
3. **Park JE**, Yeo H, Jung BI, Chang H, Ryu JH, Song YS and Kim HD. D-ring removed 17 β-estradiol analogues as selective estrogen receptor modulator. The 5th Pharmaceutical Society of Korea Medicinal Chemistry Workshop, Cheonan, S. Korea (June 2009, *a recipient of the Best Poster Presentation Award*)
4. **Park JE**, Kim K, Wu Y, Miller Z, Lee N, Kim KB and Lee W. Commonly occurring codon 60 R/H polymorphism of the *PSMB9* gene does not influence the catalytic activity of the immunoproteasome. Annual Symposium on Drug Discovery & Development, University of Kentucky, USA (Sep 2012)
5. **Park JE,** Wu Y, Carmony K.C, Miller Z, Sharma L.K, Lee D, Kim DY, Lee W and Kim KB. A FRET-Based strategy to identify individual proteasome subtypes. 2014 Rho Chi Research Day, College of Pharmacy, University of Kentucky, USA (April 2014)
6. **Park JE,** Wu Y, Carmony K.C, Miller Z, Sharma L.K, Lee D, Kim DY, Lee W and Kim KB**.** Development of an innovative fluorescence resonance energy transfer (FRET)-based approach to identify different proteasome subtypes. The 46th Pharmaceutics Graduate Students Research Meeting, University of Illinois at Chicago, USA (June 2014)
7. **Park JE**, Carmony K.C, Lee W, and Kim KB. Anticancer effects of carfilzomib, a second-generation proteasome inhibitor drug, against hepatic cancer cell lines and liver cancer stem cells. 2015 Annual Meeting of the Korean Society of Applied Pharmacology, Seoul, S. Korea (Oct 2015)
8. **Park JE**, Ao L, Chun S-E, Reichel D, Hu D, Han S, Ryoo G, Oh Y, Park S-H, Min JS, Ryu H-M, Bae SK, Lee H-Y, Kim KB, Bae Y, and Lee W. Polymer micelle formulation of proteasome inhibitor carfilzomib as a potential strategy to improve metabolic stability and anti-cancer efficacy in human multiple myeloma and lung cancer. The 11th International ISSX Meeting, Busan, S. Korea (June 2016)
9. **Park JE,** Ryoo G, Kang KB, Sung SH, and Lee W. Identification of proteasome inhibitors with a novel non-peptide scaffold from a library of naturally occurring triterpenoids. The 1st Workshop for Japan-Korea Young Scientists on Pharmaceutics, Kyoto, Japan (June 2016, *a recipient of the Travel Award*)
10. **Park JE**, Chun S-E, Reichel D, Min JS, Lee S-C, Han S, Ryoo G, Oh Y, Park S-H, Ryu H-M, Lee H-Y, Bae SK, Bae Y, and Lee W. Polymer micelle formulation for the proteasome inhibitor drug carfilzomib: Anticancer efficacy and pharmacokinetic studies in mice. 2016 Annual Meeting and International Conference of the Korean society of Pharmaceutical Sciences and Technology, Seoul, S. Korea (Dec 2016, *a recipient of the Best Poster Award*)
11. **Park JE**, Chun S-E, Reichel D, Park J, Min JS, Ryoo G, Oh Y, Bae SK, Bae Y, and Lee W. Novel polymer micelle and nanocrystal formulations for the proteasome inhibitor drug carfilzomib: Pharmacokinetic and pharmacodynamic studies in human lung and breast cancer models. Annual Meeting at Experimental Biology 2017, Chicago, USA (April 2017)
12. **Park JE,** Park J, Jun Y, Oh Y, Ryoo G, Jeong Y-S, Min JS, Bae SK, Yeo Y, and Lee W. Albumin-coated nanocrystal formulation of the proteasome inhibitor drug carfilzomib for breast cancer therapy. The 2nd Workshop for Korea-Japan Young Scientists on Pharmaceutics, Seoul, S. Korea (June 2018)
13. **Park JE,** Park J, Jun Y, Oh Y, Ryoo G, Jeong Y-S, Min JS, Bae SK, Yeo Y, and Lee W. Albumin-coated nanocrystal formulation of the proteasome inhibitor drug carfilzomib for breast cancer therapy. 2018 International Meeting on 22nd MDO and 33rd JSSX in Kanazawa, Japan (Oct 2018)

AWARDS AND DISTINCTIONS

2002- 2005	Merit-based Scholarship, College of Pharmacy, Sookmyung Women's Univ., Seoul, S. Korea
	Sookmyung Leader Group Scholarship, Sookmyung Women's Univ., Seoul, S. Korea
	Alumnae Scholarship, An alumni association of Sookmyung, Seoul, S. Korea
2009	The Best Poster Presentation Award
	The 5th Pharmaceutical Society of Korea Medicinal Chemistry Workshop, Cheonan, S. Korea
2016	The Best Poster Award
	2016 Annual Meeting and International Conference of the Korean society of Pharmaceutical Sciences and Technology, Seoul, S. Korea
2016	Travel Award
	The 1st Workshop for Japan-Korea Young Scientists on Pharmaceutics, Kyoto, Japan
2017	Alumnae Scholarship, Seoul National University Alumni Association, Seoul, S. Korea
2017	The Best Presentation Award
	The 2017 Annual Meeting and International Conference of the Korean society of Pharmaceutical Sciences and Technology, Seoul, S. Korea
2018	SNU Short-term Study Abroad Scholarship, Seoul National University, Seoul, S. Korea
2018	Pre-Doctoral Fellowship, The Nagai Foundation Tokyo, Tokyo, Japan

WORKSHOP PARTICIPATION

2017	Simcyp Workshop "Model-informed drug development: Incorporating population variability into mechanistic prediction of PK and modeling" Busan, S. Korea (5-day workshop)
2018	1st Korean Pharmacokinetics Bootcamp Workshop, Seoul, S. Korea (1.5-day workshop)
2018	7th RIKEN Sugiyama Lab PK Summer Boot Camp 2018, RIKEN Yokohama campus, Japan (2-day workshop)